EFFECTS OF ESTROGEN DEFICIENCY ON THE OSTEOCYTE LACUNAR-CANALICULAR NETWORK

by

Divya Sharma

A dissertation submitted to the Graduate Faculty in Biomedical Engineering in fulfillment of the requirements for the degree of Doctor of Philosophy,
The City University of New York

2012

This manuscript has been read and accepted for the
Graduate Faculty in Engineering in satisfaction of the
dissertation requirement for the degree of Doctor of Philosophy.

Dr. Susannah P. Fritton

Date

Chair of Examining Committee

Dr. Mumtaz Kassir

Date

Executive Officer

Dr. Stephen B. Doty

Dr. Stephen C. Cowin

Dr. Mitchell B. Schaffler

Dr. Luis Cardoso

Supervision Committee

THE CITY UNIVERSITY OF NEW YORK

ABSTRACT

EFFECTS OF ESTROGEN DEFICIENCY ON THE OSTEOCYTE LACUNAR-CANALICULAR NETWORK

by

Divya Sharma

Adviser: Dr. Susannah P. Fritton

Postmenopausal bone loss is associated with estrogen deficiency, increased bone remodeling, and altered osteocyte viability. Osteocytes are mechanosensory cells that may alter their surroundings in response to mechanical or environmental changes. To better understand the effects of estrogen loss on bone degradation, osteocyte viability, and bone remodeling that may alter the osteocyte mechanical environment, studies were designed. The ovariectomized (OVX) rat was used as a model for postmenopausal osteoporosis. Firstly, changes were assessed in the osteocyte lacunar-canalicular network using high-resolution microscopy techniques by quantifying several aspects of the osteocyte microenvironment. Confocal microscopy analyses showed that OVX rats have a larger effective lacunar-canalicular porosity surrounding osteocytes from proximal tibial metaphysis, due to increased effective canalicular size. Electron microscopy demonstrated nanostructural matrix-mineral level differences surrounding the osteocyte in OVX rats. Nanostructural changes in the osteocyte microenvironment suggest that lacunar-canalicular walls are becoming more permeable in estrogen-deficient rats, which could affect interstitial fluid flow around osteocytes during mechanical loading. The second study determined effects of estrogen loss on osteocyte apoptosis and tested two potential candidates of bone degradation, matrix metalloproteinases MMP-2 and -3. A temporal increase in osteocyte apoptosis was seen in OVX rats. The MMP analysis demonstrated that significant differences

were not found in MMP-2 and MMP-3 presence between SHAM and OVX. These results indicate that MMP-2 and MMP-3 are not primary candidates of bone degradation that may create the nanostructural matrix changes observed in the osteocyte lacunar-canalicular environment in estrogen-deficient rats. Finally newly formed bone and differences in mineralization of the OVX tissue were assessed using fluorescent bone labels and nanoindentation. Mineral apposition and bone formation rates increased in OVX rats at endocortical surface, but no changes were seen in mineralizing surface on periosteal surface. A non-significant trend of increasing percent mineralizing vascular pores was also seen in OVX rats. The nanoindentation analysis showed that elastic modulus and hardness were unaltered due to estrogen deficiency. These results suggest that nanostructural matrix-mineral level changes in the estrogen-deficient state are alterations occurring locally on the osteocyte lacunar-canalicular surfaces. These results provide evidence that osteocytes may be modulating the lacunar-canalicular spaces during estrogen deficiency.

ACKNOWLEDGEMENTS

I would like to sincerely thank everyone who made my graduate (and undergraduate) school experience, the best years (10 years!) of my life.

I would first like to thank my supervisor, Dr. Susannah P. Fritton for the overabundant support, help in correcting my writing and speech, and encouragement that she has given me these past six years. My time in the Biomechanics Laboratory and Bone and Joint Laboratory at the City College of New York and the Mineralized Tissue Laboratory at the Hospital for Special Surgery has been very rewarding and I owe gratitude to Dr. Susannah P. Fritton, Dr. Stephen B. Doty and Dr. Mitchell B. Schaffler who made this an incredible experience by cultivating great working environments. I would also like to thank my other committee members, Dr. Stephen C. Cowin for his expert advice and suggestions, and Dr. Luis Cardoso, for his support, suggestions, and jokes throughout my academic life.

The projects in this dissertation would not have been possible without technical assistance. Thank you to Orla O'Shea, Janane Diouri, Rachael Sibson, Tony Labissiere, and Damien Laudier for training me in histology, immunohistochemistry, and electron microscopy techniques and for always answering my numerous questions. To Dr. James. C. Fritton, Dr. Devendra Bajaj, Dr. Adrian Mann, and Dr. Bedabibhas Mohanty, at the University of Medicine and Dentistry of New Jersey and Rutgers University, for their help in sample preparation and training with nanoindentation.

To the undergraduate and graduate students who contributed to the work presented in this dissertation including Paolo Palacio-Mancheno, Jessica Levy, Adriana Larriera, Andrew Moon, Deboleena Kanjilal, this work would have never been completed without your help. Very special thanks to Kelly Emerton and Cesare Ciani for being my first mentors who taught me *in vitro* and

in vivo skills. To Melissa Ramcharan, Dr. Richard Able, Zeynep Dereli Korkut, Zeynep Seref, Dr. Oran Kennedy, Rishi Mathura, Dr. Limary Cancel, and Dr. Danielle Berardi, thank you for always being there to help me in all of the big and small problems I ever had.

I would like to acknowledge my family for their love and support and for being there for me during stressful times. Thank you to my parents Mr. Inder Kumar Sharma and Mrs. Vimlesh Sharma, and my siblings Dr. Tarunmitra Sharma and Dr. Alka Sharma for always being with me. You are my pillars of strength. Finally, thank you to Sapan Shah for understanding me better than anyone and for being unconditionally supportive and loving.

Lastly, I would also like to acknowledge the funding sources. The studies in this disseratation were supported by a grant from the National Institutes of Health: NIAMS AR052866.

TABLE OF CONTENTS

LIST OF TABLES

LIST OF FIGURES

CHAPTER 1

INTRODUCTION

1. BONE FUNCTION AND STRUCTURE

Bones provide mechanical support to the skeleton, giving the body its form, the ability to move, and protecting the internal organs. Apart from structural functions, bone also performs critical metabolic functions, including maintaining pH and calcium concentration and production of blood by bone marrow. Despite a stable appearance, bone undergoes continuous evolution to adapt to the demands of the body [1]. Throughout life bone modifies itself by laying down new bone and resorbing old bone tissue.

Understanding the composition of bone is the first step to making efforts to decipher bone-related pathological conditions. Bone is composed of collagen, hydroxyapatite (HA) mineral, proteoglycans (PG) and non-collagenous proteins [1-3]. The collective interaction of these components gives bone its properties of being hard and stiff and able to sustain heavy loads. The organization of these materials is of importance as well, as any alterations to the arrangement may lead to pathological conditions.

Bone is divided into two types: cancellous (spongy or trabecular) bone and cortical (compact) bone [1]. Trabecular bone contributes to the larger porosity of the skeleton, ranging from 75-95% porous, and is found mainly in the vertebrae, flat bones, and ends of the long bones of the skeleton in the confinement of the cortical bone shell [2]. Cortical bone is found in the cortex of the shaft of long bones, forming the outer shell and making a dense structure with a porosity that is approximately 5-10% [2] (Fig. 1.1). Both types of bone have internal pores that contain fluid. A medullary canal that holds the bone marrow is located in the interior of long bones, and the inner surface of cortical bone is called the endosteal surface. All bones also have a periosteum that is the external smooth surface, which consists of connective tissues and cells that help bone to change its architecture [1].

Fig. 1.1: Hierarchical structure of bone tissue showing the different levels of porosities [http://www.octc.kctcs.edu/gcaplan/anat/images/Image269.gif]

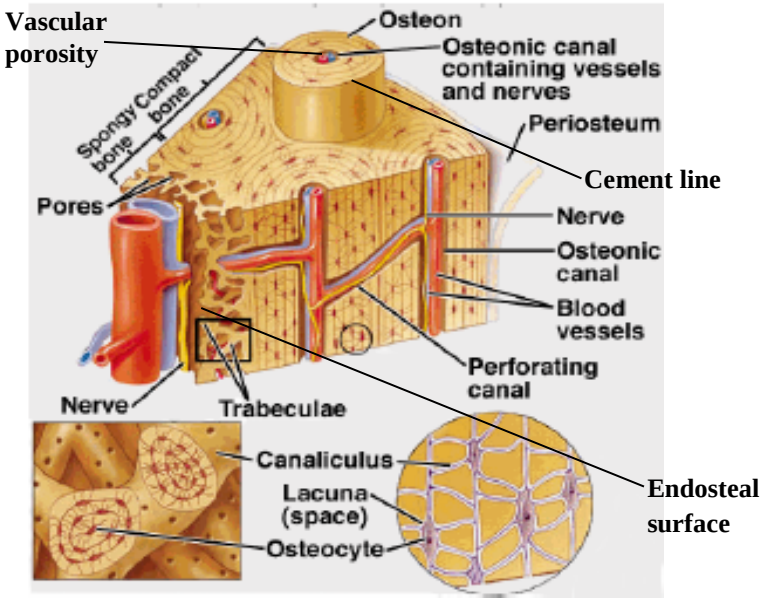

Bone tissue has several levels of porosities that enable transport of soluble molecules vital for bone tissue health. The largest porosity is found within the primary and secondary osteons, which contains vascular canals that house the bone blood vessels. Primary osteons are made when new bone is formed with the blood vessel in the middle, and secondary osteons are formed later in life where mineralized bone is excavated to form new osteons [1]. Secondary osteons (~200 μm) are the quasi-cylindrical elements in bone [1], with the Haversian canal (~25-75 μm) present in the middle of each osteon (Fig. 1.1) [2]. The outside boundary of a secondary osteon is the cement line. The Haversian canal is usually aligned with the long axis of the bone, and Volkmann's canals (~20 μm) run transverse, connecting the Haversian canals [2]. These canals have blood vessels to sustain bone nourishment. Additional bone pores are the osteocyte lacunae (10-20 μm) and canaliculi (0.1-0.7 μm), which span a large surface area of the bone, giving the three-dimensional network that enables transport of fluid and waste products (Fig. 1.1)

[1,4]. Understanding normal bone organization and porosity helps in understanding the changes that occur when bone is altered in conditions like osteoporosis.

1.1 BONE CELLS AND THEIR FUNCTION: FOCUS ON OSTEOCYTES

The coordinated events of four different cells, osteoblasts, osteoclasts, bone lining cells and osteocytes, keep bone healthy and functional. Osteoblasts, osteocytes, and bone lining cells come from the same cell lineage, called the 'osteoblastic lineage.' Osteoclasts, on the other hand, are a part of the hematopoietic cell lineage.

Osteoblasts and osteoclasts together take care of two aspects of bone remodeling: bone formation and resorption (discussed in detail in Section 1.2). Osteoblasts lay down organic matrix, forming osteoid. Osteoblasts that are active on the outer bone surfaces change the external morphology of the bone and those that are active on inner surfaces create bone density changes. Bone lining cells are resting cells found on inactive surfaces and are believed to be derived from the same lineage as the osteoblasts. The fate of these cells is interesting as they can revert back to becoming stem cells or pre-osteoblasts if needed [2].

Osteocytes are the non-proliferative cells encased in the bone matrix and are the most abundant cells present in bone [1]. The lacunar-canalicular porosity houses the osteocyte cell body and processes (Fig. 1.2) [1,4]. The spacing between the osteocyte cell body and the lacunar wall is ~1 um [4]. Osteocyte processes extend into the canaliculi, and the space between the cell process and canalicular wall (~50-100 nm) is filled with a pericellular matrix made of proteoglycans [4,5]. These processes exhibit tortuosity, traveling from lacunae to the periosteal and endosteal bone surfaces (Fig. 1.2). Osteocytes are osteoblasts that have no differentiation capabilities left and over time are covered by bone matrix. Osteocyte processes are

interconnected via gap junctions that transmit signals from osteocytes that reside in the mineralized matrix to osteoblasts and osteoclasts residing on the different surfaces of bone [6]. Osteocytes are ideally positioned in the bone matrix to sense mechanical loads and can then translate that signal into biomolecular signals by triggering osteoclasts or osteoblasts to resorb and form bone; this is why osteocytes are believed to be the mechanosensory cells of bone [7]. Section 1.4 will discuss theoretical models of fluid flow in the lacunar-canalicular network that show how osteocytes are thought to transduce mechanical loads to biomechanical signals.

Fig. 1.2 Osteocyte lacunar-canalicular network
[http://www.udel.edu/PR/UDaily/2008/nov/Lacunar-canalicular-syslg.jpg]

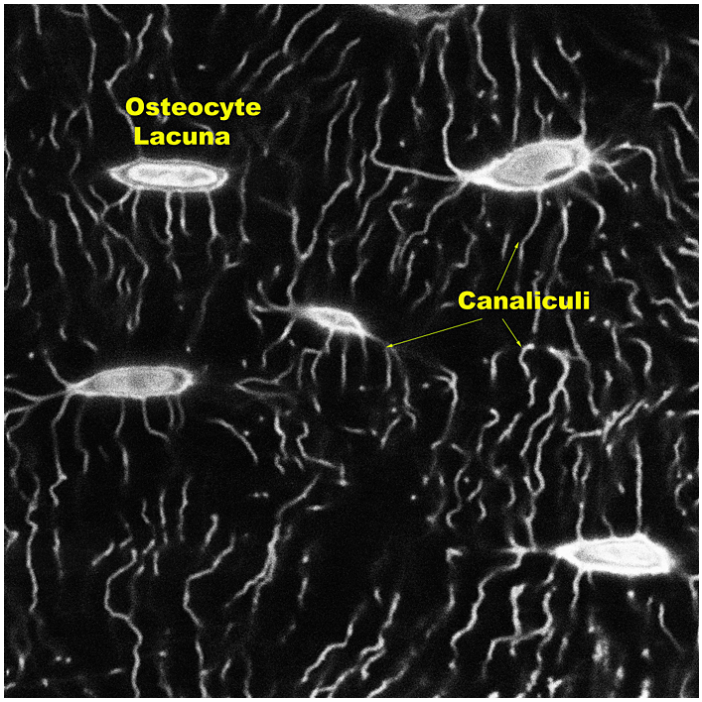

1.2 BONE REMODELING

Modeling and remodeling are two ways bone changes its architecture. Growing bones go through a process called modeling, which shapes and reshapes the bone and stops at sexual

maturity. Modeling creates changes to the cortex, marrow cavity, and overall shape of the long bones [1]. When there is bone resorption and formation after the skeleton has matured, it is called remodeling. Remodeling can remove trabecular bone, increase cortical porosity, increase/decrease cortical width, and has the potential to alter bone strength [1]. This process is initiated by bone resorption from the osteoclasts and is followed by bone formation by the osteoblasts. In diseased states like osteoporosis, this remodeling process becomes unbalanced and a net loss of bone occurs, which leads to a decreased bone mass.

Bone is a constantly changing tissue and its architectural changes are controlled by the forces it experiences and by the circulating hormones in the body [8]. Frost's Mechanostat Theory proposed that bones adapt to mechanical loads and then cellular and biological components interact to change the skeletal mass and architecture to sustain the needs of the skeleton [8]. Hormones such as estrogen alter the bone remodeling process by increasing the resorption process, which creates a net bone loss [8].

Targeted bone remodeling has been demonstrated to occur after microdamage, whereas non-targeted remodeling has been shown to occur in conditions such as disuse, estrogen loss, and lactation [9,10]. Osteocytes are now known to be the key player in this process. Examples of how osteocytes can send feedback signals are seen in microdamage studies that have suggested that osteocytes can recruit osteoclasts to damaged regions [11]. Verborgt et al. [11] demonstrated that osteocytes undergo apoptosis in areas of bone that are damaged. These cells then died by apoptosis and the same location was then subsequently resorbed. Apoptosis inhibition studies demonstrated that this resorption can be inhibited in the absence of osteocyte apoptosis, thus suggesting that osteocyte apoptosis can control the activation and response to remove microdamage [12]. Contrary to targeted remodeling, stochastic remodeling (non-targeted

remodeling) is thought to occur randomly in bone, as seen in conditions such as estrogen loss, glucocorticoid treatment, disuse, and during lactation [13-15]. However, a recent study by Emerton et al. [16] showed that osteocyte apoptosis after estrogen loss occurred in a highly specific manner in a mouse ovariectomy model, where apoptosis was highest in regions that subsequently underwent resorption. Studies in Chapter 3 measure osteocyte apoptosis in the rat ovariectomy model and more on osteocyte apoptosis is discussed in Section 4.

1.3 BONE POROSITIES AND INTERSTITIAL FLUID FLOW

A prerequisite of metabolism in any living tissue is the sufficient supply of nutrients and removal of waste products, which is enabled by interstitial fluid flow through bone porosities. Because bone is a mineralized tissue, diffusion alone may not be enough to provide nutrients and to maintain bone health [17]. Many studies present the importance of this interstitial fluid flow in transport and promotion of cell viability and tissue health, making it a major mechanical tool that enables the development of an optimal skeleton structure [6,7,18].

The three different levels of cortical bone porosities that span the three-dimensional bone tissue space contain interstitial fluid. These porosities are the vascular porosity, lacunar-canalicular porosity, and collagen-apatite porosity:

1) The vascular porosity is the largest bone porosity, consisting of primary and/or secondary osteonal canals (Fig. 1.1). This porosity is at a low pressure, around 40-60 mmHg, similar to the blood pressure in bone [2].
2) The lacunar-canalicular porosity is postulated to be the site where bone mechanotransduction takes place. The lacunar-canalicular porosity is at higher pressures for a longer time due to mechanical loading in daily activities [19,20]. Hence, there is an

interactive relationship between the vascular porosity and lacunar-canalicular porosity via exchange of fluid from the lacunar-canalicular porosity to the vascular porosity due to the pressure differences [19] (Fig. 1).

3) The collagen-apatite porosity is associated with spaces between collagen and crystals of apatite. Most researchers believe that there is no fluid movement in this porosity because water is bound to ionic crystals [21].

Similar to cortical bone, cancellous bone also consists of three levels of porosity: the marrow space surrounding the trabeculae, the lacunar-canalicular porosity, and the collagen-apatite porosity.

Fluid flow through these porosities is essential for tissue survival because it helps carry vital molecular information to cells like osteoclasts and osteoblasts to enable bone repair process, and to help remove waste products. Osteocytes are deeply embedded inside the bone tissue, and an efficient solute transport mechanism becomes extremely important for their survival [22]. Therefore, it becomes important to know what size molecules can reach these cells. Bone exhibits a molecular sieving phenomenon created by the hierarchical levels of fluid spaces through which interstitial fluid flows, carrying many different solutes, ions, and waste products from the vascular porosity to the lacunar-canalicular porosity [23]. Studies using different sized tracers have established transport of molecules by fluid movement in the absence of mechanical loading. Studies using larger sized tracers (6-12 nm) have determined the size of the largest molecule that can pass through the pericellular matrix surrounding the osteocyte processes [22]. It is now assumed that the pericellular fiber matrix is larger than 6 nm but smaller than 12 nm, and is postulated to be around 7 nm [19,23]. Alterations in the osteocyte lacunar-canalicular network will make the osteocyte microenvironment more permeable (as seen in Chapter 2) to

larger sized molecules and could also alter bone mechanotransduction. In the next section, theoretical models of fluid flow and bone mechanotransduction are described in detail.

1.4 BONE CELL MECHANOSENSITIVITY AND MECHANOTRANSDUCTION

Bone experiences mechanical loading *in vivo* due to daily physiological activities. Fluid flows to and from the vascular porosity and lacunar-canalicular porosity during daily activities, which enhances the net transport in bone. Load-induced fluid flow has been used by researchers to study whether more solute can be transported to osteocytes that are embedded deep within the mineralized matrix. *In vivo* load-induced tracer studies have shown that more of the tracer is transported by convection into the bone tissue when loaded compared to controls [24,25].

In vitro studies of fluid shear stress applied to bone cells have shown that mechanically stimulated cells release signaling molecules. Fluid flow applied to osteocytes and osteoblasts has stimulated release of signaling molecules such as PGE_2, PGI_2, ATP, Ca^{2+}, and NO [26-30]. Pulsatile fluid flow applied to osteocyte cultures *in vitro* causes the release of PGE_2 and PGI_2 and intracellular calcium [27,28,30]. Exposing osteocytes to fluid shear stresses also causes the release of ATP [30]. Furthermore, to establish whether osteocytes may be stimulated at the cell body or at its process *in vivo*, site-dependent experiments have shown that osteocytes respond more when the stimulus is applied at the cell process than the cell body [31]. These studies provide insight about osteocyte mechanosensitivity, indicating that fluid flow imparted by loading regulates signaling events from osteocytes that are important for bone tissue survival. Understanding the influence of fluid flow in the osteocyte lacunar-canalicular network is important for predicting osteocyte response in normal and disease states that may help predict impaired osteocyte mechanosensitivity [32].

In recent years, electron microscopy (EM) imaging has revealed the intricate structure of the osteocytes, their processes and attachments. Studies show that osteocyte processes have a central actin filament bundle [33]. They also show that the osteocyte processes are connected to the canalicular wall by tethering fibers, at a spacing of 40 nm, running across the whole length of the process [33]. The annular spacing between the osteocyte process and the canalicular wall is filled with pericellular matrix and there are also conical protrusions emanating from the canalicular wall, which are canalicular protrusions that infrequently touch the osteocyte process [34]. β3 integrin staining has been demonstrated on the cell body and β1 staining on the cell process [34]. These integrins are also thought to be situated on top of the canalicular protrusions, which may enable signal transduction (Fig. 1.3).

Fig. 1.3 Top: EM images of the canaliculi in which the osteocyte process extends, with a zoomed in image of the tethering elements and the conical protrusions extending from the wall and making contact with the cell process. **Bottom:** a theoretical model of the osteocyte process, tethering elements, and the drag experienced when interstitial fluid passes through the pericellular matrix. Adapted from Wang et al. [36]

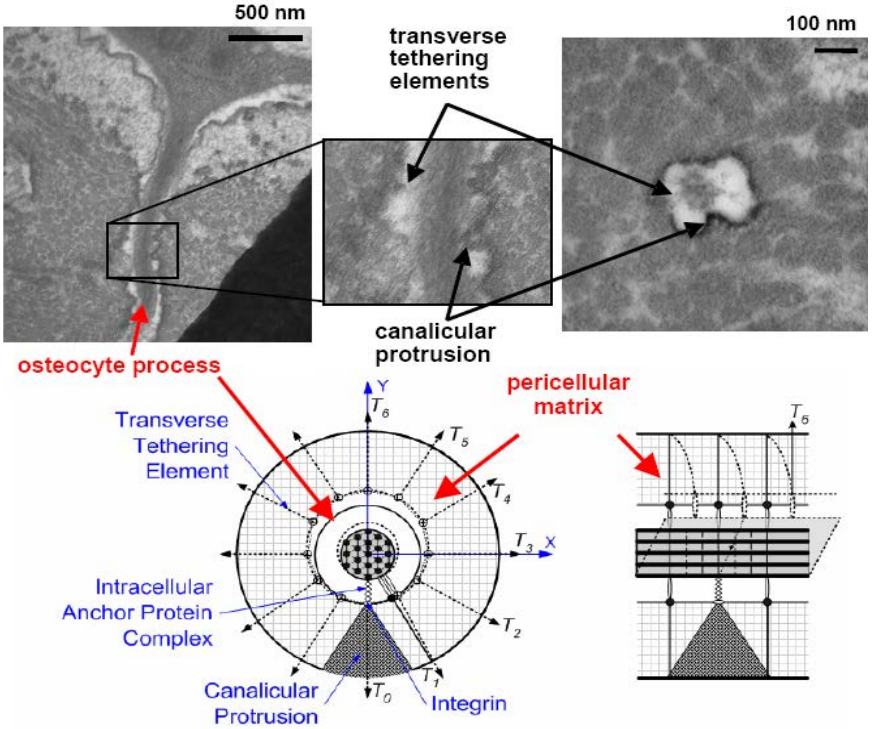

Taking these ultrastructural details of the surroundings of the osteocyte, a strain amplification and integrin based mechanotransduction model was developed. Han et al. [35] proposed a hydrodynamic model of strain amplification showing that 1 Hz loading at 20 MPa (0.1% strain) generated a strain equivalent to 0.5% at the cellular level. By adding an integrin attachment on the conical protrusion, Wang et al. [36] advanced this model, and showed that the same loading conditions generated an even higher (6%) strain at the cellular level, which corroborates *in vitro* studies that show at least 5000 microstrain is needed to obtain a cellular response [37]. This model showed how initiation of bone mechanotransduction would occur with the help of an integrin-based intracellular attachment site that could initiate signaling by load-induced interstitial fluid flow. Tethering complexes attach the osteocyte process membrane surface to the central actin filament bundle by cross-linking molecules. Due to bone deformation actin filaments slide axially, which then allows stress concentrations and large axial strains to develop near the integrin attachment sites when fluid flows in the canaliculus [22,34,36]. This is how osteocytes are postulated to sense mechanical loads. Thus, architectural alterations to the osteocytic network and in the osteocyte annular spaces of the canaliculi have the potential to impair mechanotransduction by creating diminished loads to be transmitted to the osteocytes, altering the cell's ability to respond to the mechanical stimulus.

Osteocytes may sense the fluid flow in vivo by strains experienced by tethering attachment sites as fluid flows through the canaliculus as mentioned above, or by receptor proteins like ERalpha, which may be triggered by shear stresses caused by the fluid flow over the osteocyte processes [38]. Another mechanism that is postulated to initiate bone mechanotransduction involves the primary cilia, which may act as a mechanosensor when the cilium deflection produces large deformation and strains at its base [39]. Bending of the primary

cilia has been shown to cause intracellular calcium release in kidney cells [40]. However, the specific role of the cilium in physiological conditions is still not completely understood.

1.5 BONE ADAPTATION TO MECHANICAL LOADING

Throughout life, bone architecture is continually optimized by altered loads by a process called bone adaptation [41]. Bone adaptation occurs when the bone cells detect mechanical signals and translate these signals into appropriate changes that can alter the bone architecture [42]. The process of cellular mechanotransduction starts with converting the mechanical forces into mechanical signals, such as fluid shear stresses and strains that initiate a response by bone cells [27-31], then creating biochemical responses by cells that send signaling molecules to other cells nearby [41], which then results in an action that either creates bone or resorbs it [41].

Lanyon and Rubin [43] showed that bone adaptation in the avian ulna was related to the peak strain that was applied. Studies since then have shown that bone responds to high magnitude strain, with short duration exercises, with rest-inserted periods being more beneficial to elicit a response, because extended loading durations diminished effects of loading [44,45]. Increased bone volume fraction by thickening trabeculae and increased mineral apposition rates have been observed in loaded rabbit bones compared to the contralateral unloaded limb [46]. Studies using rat ovariectomy (OVX) models show that increased and high impact exercise cause bone growth and bone formation and has a positive effect on the rat skeleton by creating increasing bone mass and strength, compared to a non-exercised OVX counterpart [47,48]. Voluntary exercise in rats has also shown to prevent osteocyte death, which has been associated with increased biomechanical properties of bone [49]. Furthermore, osteoporotic bone tissue has been shown to gain bone mass by exercise; however, the amount of bone gained is not

proportional to that of age-matched control animals [47,48]. This may occur by the action of hormones, which have been proposed to enhance or inhibit the effects of mechanical loading at some level within the bone cell mechanotransduction machinery [8]. Where and how this inhibition takes place is still unknown.

2. OSTEOPOROSIS AND EFFECTS OF REDUCED ESTROGEN LEVELS ON BONE

Osteoporosis is a disease characterized by the presence of fragile bones that are more likely to fracture due to loss of bone mass and structural deterioration of bone tissue. Osteoporosis currently affects 44 million Americans, 55% of the population who are 50 years and older [50]. Amongst this number, 10 million have osteoporosis, while 34 million have low bone mass, which puts them at risk of developing osteoporosis. Out of these 10 million, 8 million are females and two million are males [50]. Thus, even though osteoporosis is a predominantly female oriented disease, males are also affected. While most females start losing bone rapidly at the onset of menopause due to the reduction of estrogen levels, men also experience bone loss, usually a decade later than females. Osteoporotic fractures usually occur in the hip, spine and wrist, and sometimes require not only hospitalization but also long periods of care associated with high medical expenses [50,51]. At the end of treatment there is very little benefit, as the underlying problem still exists; there is still less bone at the site of injury to sustain mechanical loads of the body. Hence, preventative methods of bone loss need to be developed. Anabolic drugs or applied loading regimes may counteract this bone loss; however, bone quality and mechanical strength need to be optimized at the same time for the proper functioning of the tissue [51].

Estrogen is a major sex hormone that has been shown to influence growth, remodeling, and homeostasis of the skeleton [9,10,16]. The influence of estrogen on the normal remodeling process helps maintain an optimal level for minerals in fluids of the body. Loss of estrogen causes an imbalance in bone formation and resorption, by decreased osteoblastogenesis and increased osteoclastogenesis [52]. Studies administering estrogen hormone in *in vitro* cell cultures have shown that estrogens increase the lifespan of osteoblasts and reduce activities of osteoclasts [53]. Inflammatory cytokines, such as Interleukin-1 and -6 (IL-1 and IL-6), tumor necrosis factor-α (TNF-α), and macrophage colony stimulating factor (M-CSF), enhance the formation and activation of osteoclasts, which results in increased bone resorption [54]. Osteocytes can also antagonize osteoblasts by producing sclerostin [55].

2.1 RAT OVARIECTOMY (OVX) MODEL OF OSTEOPOROSIS

An animal model of postmenopausal bone loss must closely mimic the ovarian hormone deficiency that occurs in human females. Ovariectomy (OVX) is the most widely used model to study bone loss due to estrogen loss. This method involves the removal of the ovaries of female animals. Control rats typically undergo sham surgery, without the removal of ovaries. Extensive research has been done to study rat skeletal growth and bone loss in the ovariectomized rat. This rat model of osteoporosis does not develop fractures; it is called a model of osteopenia rather than osteoporosis [56].

Because basic bone turnover and growth occur similarly in rats and humans, the rat OVX model is widely used to examine bone changes due to reduced estrogen levels. OVX bone loss occurs in both cancellous and cortical compartments. The more prominently researched sites of cancellous bone loss are the proximal tibia, lumbar vertebra, and the distal femur. Osteopenic

changes are most evident at the central metaphyseal cancellous areas of long bones [56,57]. Rats ovariectomized at 3 months demonstrate a rapid initial phase of bone loss in the proximal tibia, which occurs up to 3 months post-OVX and is followed by a relative stabilization of bone volume between 3–9 months post-OVX [57-59]. Mineralizing surfaces and bone formation rates are also greater in OVX rats in this model compared to controls [57-59]. Similar trends of bone loss in the proximal tibial metaphysis have been observed in rats ovariectomized at later time points (e.g., 3.5 months and 8 months of age), in which OVX rats have a decreased cancellous bone volume ratio 1 and 9 months after OVX surgery, respectively, compared to controls [60,61]. Thus, a net loss of bone in OVX rats occurs, with certain areas of bone that are perhaps formed while others resorbed. The rat skeleton does not continuously grow; the proximal tibial epiphyseal growth cartilage thins, ossifies, halts endochondral ossification and closes. Longitudinal bone growth of the tibia declines by 20 to 26 weeks of age [62,63]. Thus, the OVX rat model shows increased endochondral resorption and increased cancellous bone turnover with resorption exceeding formation, which leads to a net bone loss (Fig. 1.4) [64,65].

Fig. 1.4 Cancellous bone loss in the proximal tibial metaphysis 1 month after ovariectomy (OVX) surgery at the age of 3 months. Adapted from [66].

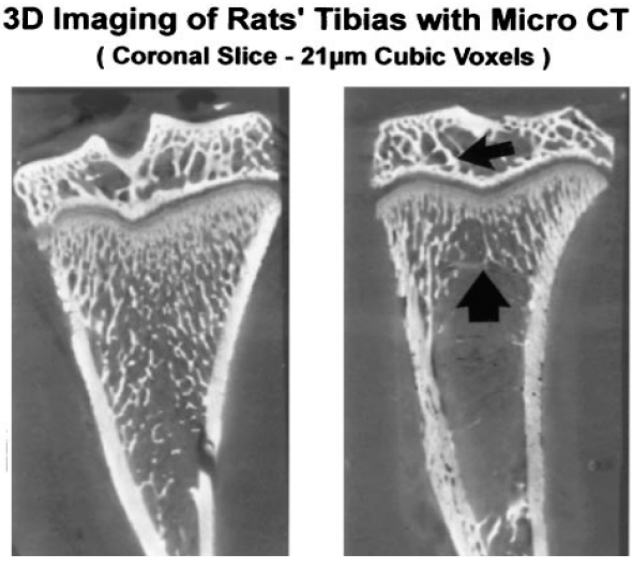

2.2 MICRO- AND NANO-STRUCTURAL MATRIX AND MINERAL CHANGES DUE TO ESTROGEN DEFICIENCY

Contradictory results exist in the literature regarding mineral content present in osteoporotic samples at the micro and nano level. Some studies show decreased mineral content in bone tissue due to estrogen deficiency [67-69], or find no changes in mineral content [70,71], while others have shown an increase in mineral content [72,73]. An increase in mineral heterogeneity is often noted due to increased bone turnover [68]. These discrepancies in mineral content may arise due to variations in anatomical sites and animal models used for these studies. Similar contradictions exist in regards to the osteoporotic bone crystal characteristics (Table 1.1).

Table 1.1: Techniques used to assess mineral content in humans and other animal models of osteoporosis

Reference	Species	Site analyzed	What is measured?	Results	What is used?
Boyde et al. 1998 [72]	Human	Iliac crest	Distribution of mineral density	Increased mineral density	Backscattered EM
Cheng et al. 2009 [69]	Fischer rats	Trabecular bone, vertebra	Mineral content (g/cm^3)	Decreased mineral content	microCT
Gadeleta et al. 2000 [67]	Cynomolgus monkeys	Trabecular bone, vertebra	Mineral:matrix ratio (mineral content) Crystallinity	Lower mineral content, larger apatite crystals	FTIR
Li & Aspden et al. 1997 [70]	Human	Proximal femur (neck region)	Trabecular and cortical bone, mineral content (g/cm^3)	No change in mineral content	Ash bone weight
McNamara et al. 2006 [73]	Wistar rats	Individual trabecular bone, proximal tibia	Mineral content (g/cm^3)	Increased mineral content	microCT
Guo & Goldstein et al. 2000 [71]	Sprague Dawley Rats	Trabecular bone	Elastic modulus, Hardness	No change	Nanoindentation

Collagen and noncollagenous proteins are also altered due to estrogen deficiency. Alterations in collagen composition have also been shown in osteoporotic patients [74]. TEM analysis has indicated structural changes in bone fibril architecture in OVX rats, showing irregular and disturbed collagen fibril arrangement compared to a more organized arrangement seen in controls [75]. Shrinkage of the D-spacing in collagen fibril periodicity has also been seen in OVX bone [76]. Modification in the concentrations of noncollagenous proteins or changes in their molecular orientation have also been shown in osteoporotic bone [77]. Thus, the native state of matrix proteins in bone tissue may be compromised in osteoporotic tissue. Studies conducted for this thesis also show matrix-mineral changes occurring in the OVX rat model as described in Chapter 2.

2.3 BONE MATRIX CHANGES BY MATRIX METALLOPROTEINASES (MMPs)

MMPs regulate many biological functions that influence several physiological and pathological processes, including aspects of embryonic development, tissue morphogenesis, wound repair, inflammatory diseases, and cancer [78,79]. It has been observed that MMPs are expressed in repair or remodeling processes and in diseased or inflamed tissues [78,79]. Murine mutation or ablation models of growth plate development that target MMPs have shown skeletal abnormalities, indicating the critical role that MMPs play in these animal models and in skeletal maturation [81]. Many of these MMPs are crucial for bone growth and development and are also regulated by estrogen withdrawal.

MMPs are likely candidates of bone degradation, especially of increases in bone porosity because they are seen to be localized around osteocyte lacunae in several studies of bone defects, knockout models and disuse studies [78,79,82]. Osteocytes and osteoblasts synthesize MMP-2, -

3, -13, -14 [78-84]. The two MMPs studied in this thesis are MMP-2 and MMP-3. MMP-2 is a gelatinase that cleaves denatured collagen I, collagen type IV and other ECM molecules (Table 1.2). Serum MMP-2 levels have been shown to be significantly higher in postmenopausal women with osteoporosis and significantly increased in 50-69 year old women [85]. OVX rats exhibited significantly increased MMP-2 levels in cancellous bone as assessed by gel zymography. Although this is an interesting finding, gel zymography requires homogenization of bone tissue, which makes it impossible to identify which cells may be regulating MMP-2 levels *in vivo* [84]. An MMP-2 knockout mouse shows a disrupted canalicular structure, which leads to empty

Table 1.2: Relevant MMPs of interest in bone growth, development and homeostasis, with the indicative substrates they cleave and phenotypic changes observed. (In blue are MMPs involved with osteocytes in growth and development of knockout mice, in red is the osteocyte MMP activity seen in disuse)

MMP	Protein	Cleaves	Secreted By/bound to	Observations
MMP-1	Collagenase 1	Collagen type I, II, III	Osteoblasts Osteoclasts **Osteocytes**	Endochondral bone formation Removal of osteoid Found upregulated in disuse [121]
MMP-2	Gelatinase A	Denatured collagen and type IV	Osteoblasts **Osteocytes**	Null mice had osteoporotic symptoms with apparent decreases in bone mineral density (BMD), present empty lacunae, disruption of canalicular network [82]
MMP-3	Stromelysin 1	Proteoglycans, types III, IV, V collagens (non-helical), casein and fibronectin	Osteoclast **Osteocytes**	Found in osteocytes close to remodeling surfaces of human neonatal ribs [86]
MMP-13	Collagenase 3	Collagen type I, II, III	Osteoblast Osteoclast **Osteocytes**	Endochondral bone formation Removal of osteoid Increased expression in estrogen deficient environment (in vitro) [79]
MMP-14	MT1-MMP (Membrane-type – MMP)	Collagen type I, II, III, fibrin, aggrecan, fibronectin, vitronectin, laminin-1, -5	Osteoblasts Osteoclasts **Osteocytes**	Skeletal disorders-osteopenia, dwarfism MMP-14 deficient mice showed lack of or smaller canaliculi [79]

lacunae as the animal reaches an older age [82]. Compared to wild type mice, MMP-2 knockouts exhibit lower bone mineral density (BMD), with decreases in mineralization in trabecular and cortical bone compartments [82]. A loss of continuity of the canalicular network visualized by Bodian staining of the canals in the long bones and calvaria of MMP-2 knockout animals indicates that irregularity of canals may be the cause of the empty lacunae observed [82]. MMP-2 seems to play a role in osteocyte cell process extension and making of the canaliculi and the absence of MMP-2 leads to bone loss [82]. MMP-3, on the other hand, has been found in osteocytes close to remodeling surfaces of human neonatal ribs [86] (Table 1.2). Another study showed an up-regulation of MMP-3 synthesis in osteoblasts following estrogen withdrawal [87]. An *in vivo* model inhibiting osteoblastic MMPs prevented bone loss created by estrogen deficiency, with a significant decrease in bone resorption [88]. There also is a substrate specificity with MMP-2 and -3 and those that are present in the pericellular space around osteocytes, some of which include osteopontin, perlecan, fibronectin, vitronectin, aggrecan and bone sialoprotein [34,89-91].

The hypothesis that MMPs may contribute to bone loss during osteoporosis should be examined since there have not been many studies focusing on whether MMPs play a role in bone degradation around the osteocytic network. Because osteocytes have been shown to focally produce MMPs, this may indicate the osteocyte's ability to regulate its environment. A disruption of cell connections after estrogen withdrawal may contribute to the etiology of osteopenia through the compromised state of native tissue.

3. THE OSTEOCYTE'S ROLE IN BONE REMODELING, APOPTOSIS, AND INTERSTITIAL FLUID FLOW

Osteocytes coordinate the bone remodeling process by controlling other bone cell types such as osteoblasts and osteoclasts. Osteocytes have the capacity to stimulate osteoclast differentiation by producing cytokines like RANKL. Expression of RANKL has been localized in osteocytes [55,92], and recent studies indicate that selective genetic ablation of RANKL in osteocytes results in impaired resorption during development and decreases remodeling in response to mechanical unloading [92]. Sclerostin (SOST) is an inhibitory protein produced by osteocytes that antagonizes osteoblasts and has been shown to play an essential role in regulating bone's response to mechanical unloading because its expression is upregulated in patients with disuse-induced bone loss [93]. Osteocyte apoptosis following estrogen withdrawal has also been shown to trigger osteoclasts that resorb areas exhibiting increased apoptosis [16]. The precise mechanism by which this happens is still unknown.

Apoptosis is a programmed cell death that occurs in several tissues of the body during growth and development [94]. Apoptosis is the most common method by which many tissues get rid of damaged cells without causing local inflammation from leakage of cell contents as seen during necrosis [94]. Apoptosis is identified by morphological alterations in the nuclear envelope such as DNA laddering and formation of leaky vesicles. Apoptosis is initiated by two pathways: intrinsic and extrinsic. The intrinsic apoptosis pathway is triggered from within the cell by signals sent during growth or severe cell stress, such as when DNA is damaged. The extrinsic pathway is activated when a pro-apoptotic protein binds to a pro-apoptotic receptor (Fig. 1.5). The extrinsic and intrinsic pathways merge at the point of the caspase pathway [95]. Caspase signaling is initiated by the activation of the initiator caspases (2, 8, 9, 10), which in turn activate the downstream effector caspases (3, 6 and 7) (Fig. 1.5). Caspase 3, in particular, is the last effector caspase in the cascade, which causes cell death once it has been activated or cleaved

[95]. The caspase-3 pathway is the most ideal and definite way to detect cell apoptosis and it has been used in several studies as an endpoint for apoptotic cell death. Terminal deoxynucleotidyl transferase dUTP nick end labeling (TUNEL) is also used for detecting apoptosis by visualizing DNA fragments by tagging the terminal end of nucleic acids [97]. This method has been used in several studies to identify osteocyte apoptosis [96-98]. We chose to study cell death by detecting apoptotic cells using cleaved caspase-3 antibody, as discussed in Chapter 3.

Fig. 1.5: The intrinsic and extrinsic caspase pathway showing activated caspase-3 as the last effector caspase protease.

[http://scielo.isciii.es/img/revistas/diges/v102n1/punto_vista_f3.jpg]

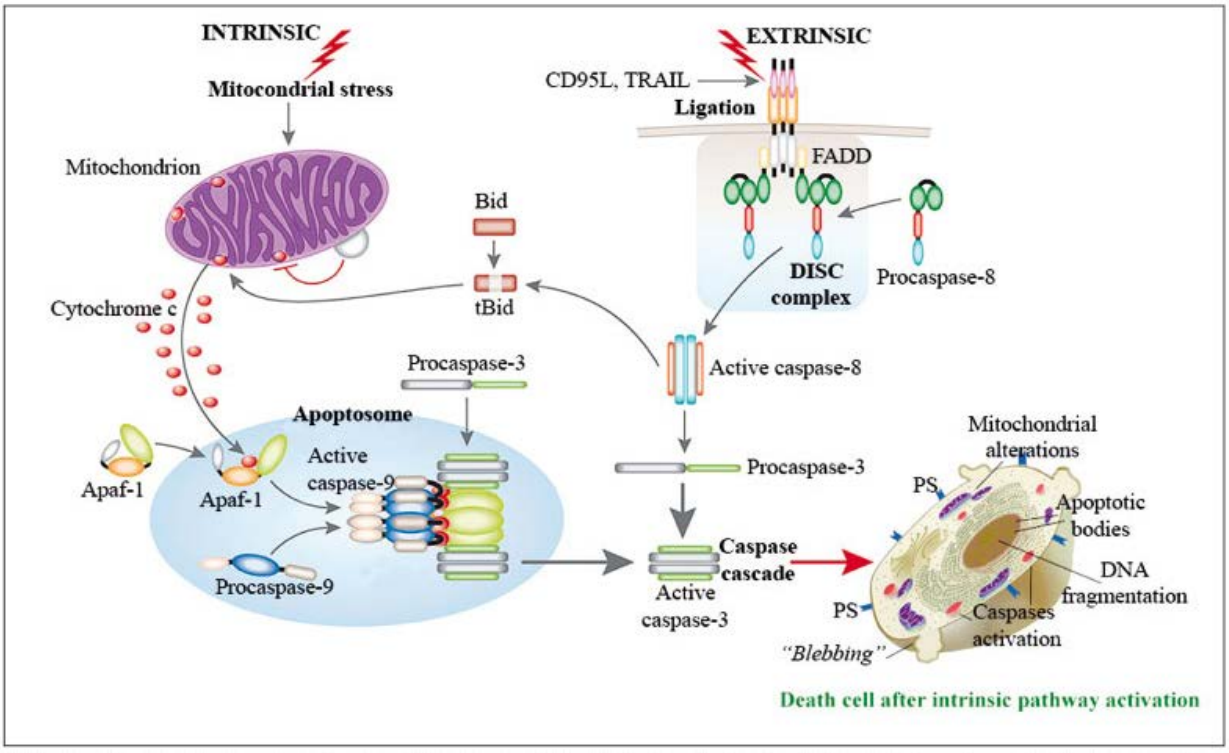

Osteocyte apoptosis has been documented in conditions of microdamage, aging, disuse, and estrogen deficiency [16,96-101]. Microdamage studies have shown osteocytes to initiate bone remodeling. Osteocytes located near the sites of microdamage undergo apoptosis, which

has been correlated with increased bone remodeling due to enhanced RANKL production and an increase in osteoclast formation [11,12]. Cardoso et al. [12] established a correlation between osteocyte apoptosis and osteoclast resorption, and gave evidence that apoptosis is indeed necessary for microdamage removal, as inhibiting fatigue-induced osteocyte apoptosis prevented activation of osteoclast resorption. With aging there is also an increase in osteocyte apoptosis, along with an increase in empty and hypermineralized lacunae [99]. Osteocytes also seem to die by apoptosis in the absence of loading [100,101]. Tatsumi et al. [102] showed that viable osteocytes are necessary to send preventative signals against bone loss, and are also necessary for the bone to feel unloading. With reduction of estrogen, osteocyte apoptosis has been shown to occur in human cancellous and cortical bone and OVX rat bone [97,98], and this osteocyte apoptosis response was blocked by the addition of estrogen [98]. Emerton et al. [16] also showed that regions that exhibited higher osteocyte apoptosis were also resorbed thereafter, showing a non-random effect due to loss of estrogen. However, it is still unclear how estrogen withdrawal might trigger osteocyte apoptosis.

There is also evidence from the literature suggesting that age-related osteocyte loss is caused by accumulation of reactive oxygen species (ROS) in cells. ROS include molecules like hydrogen peroxide (H_2O_2), oxygen (O_2) and nitric oxide (NO), which induce oxidative damage to cells by altering molecular pathways and changing end results of these pathways [103]. Aging causes an increase in anti-oxidative processes that increase damaged lipids, proteins, and DNA [104-106]. The amount of oxidative stress a cell experiences is determined by the balance between ROS production and antioxidant defense [106]. *In vitro* experiments have shown that ROS stimulate osteoclastogenesis [107]. An increase in ROS in the bone marrow of OVX mice led to increased inflammatory cytokines [106,108] that have been shown to increase

osteoclastogenesis. Bone loss in OVX rats has been shown to be prevented by administering antioxidants [107]. Estrogen is a known antioxidant, which prevents cell death as seen by experiments that introduce estrogen to H_2O_2-induced oxidative damaged tissue [107]. The loss of estrogen thus decreases the cells' defense against oxidative stress in bone. Increase in ROS content in connection with osteocyte apoptosis seen after estrogen loss has not yet been tested, but may be a mechanism of how osteocytes die following estrogen withdrawal.

Microstructural alterations caused by microfractures or estrogen withdrawal also have the potential to alter cell viability by disrupting the lacunar-canalicular network and diminishing fluid flow. It has been suggested that estrogen might have the ability to alter in some way the equilibrium strain set point of bone such that the response of actual strain is not felt by the bone cells in the absence of estrogen [109]. If estrogen loss has a direct effect on osteocytes, the three most likely possibilities of how cell viability may be altered are the loss of protective estrogen's antioxidant effect [109], a reduced number of ERalpha receptors, or by a diminished number of tethering elements caused by microstructural alterations. Chapter 2 suggests the possibility of disrupted connections of osteocytes due to nanostructural alterations in the osteocyte lacunar-canalicular environment of estrogen-deficient rats, which has the capability of altering the bone mechanotransduction. The plethora of studies suggesting that osteocytes dictate several bone remodeling processes makes them likely candidates that may be controlling degradation of their immediate lacunar-canalicular surfaces during estrogen deficiency.

4. CAN OSTEOCYTES REGULATE THEIR MICROENVIRONMENT?

Recent evidence suggests that osteocytes are metabolically active cells that produce soluble factors like dentin matrix protein-1 (DMP-1), sclerostin (SOST), fibroblast growth factor

(FGF-23), and receptor activator of nuclear factor kappa-β ligand (RANKL) [53,92,110-112], suggesting that osteocytes can regulate a broad range of functions. Osteocytes are also postulated to resorb calcified matrix around the lacuna and canaliculi, suggesting their role in bone remodeling. Enlarged lacunae have been reported in conditions like primary and secondary hyperparathyroidism, increased levels of parathyroid hormone (PTH) and prolonged immobilization [113,114]. Acid phosphatase has also been seen around osteocyte lacunae, suggesting their probable capacity to resorb [113]. Lane et al. [115] have shown that glucocorticoid-treated mice not only have enlarged lacunae but also localized altered material properties, with a reduced mineral to matrix ratio determined by Raman microspectroscopy, and hypomineralized bone surrounding the lacunae. Recently, Bonewald et al. [14] have also shown that during lactation there is an increase in lacunar and canalicular size. This lytic function of osteocytes is thought to be how osteocytes either maintain systemic mineral homeostasis or initiate bone remodeling processes. Of note is the fact that the space between the mineralized bone matrix and the osteocyte cell process contains non-collagenous proteins and proteoglycans, which allow calcium ions to bind to these proteins, which are in direct contact with bone fluid [116].

Osteocytes have shown to have the capability of depositing matrix and mineralizing ability. Jande and Belanger [117,118] proposed that osteocytes could physiologically synthesize and then remove bone matrix components. In histological sections of cortical bone from rats subjected to chronic PTH treatment, Tazawa et al. [119] observed osteocyte lacunae containing a matrix positive to hematoxylin or toluidine blue, suggesting a regeneration of the bone matrix around the osteocyte after the lacuna was enlarged by the PTH treatment. In a TEM study to assess the distribution of osteopontin, McKee and Nanci [120] showed that this protein is found

around the osteocytes and their processes. Interestingly, multiple bands of osteopontin were seen around some osteocytes, similar to reversal/cement lines seen in osteonal porosity [114]. A similar observation was seen in lactating mice as well, with fluorescent labels indicating new mineral being laid down [14]. Thus, these observations suggest that osteocytes may be able to regulate their immediate surroundings.

Osteocytes take the center stage as the bone mechanosensory cells and are known to be sensitive to interstitial fluid flow. An estrogen-reduced microenvironment may affect the osteocyte's ability to sense fluid forces. The focus of this thesis was to investigate the changes occurring in the osteocytic microenvironment with reduced levels of estrogen, and to predict the mechanism for changes that may be occurring. In Chapter 2, we used the rat OVX model of osteoporosis and high-resolution microscopy techniques to assess several aspects of the osteocyte lacunar-canalicular network. Confocal microscopy was used to assess changes in lacunar-canalicular porosity, lacunar and canalicular size, and the number of canaliculi per lacuna; and scanning and transmission electron microscopy were used to assess canalicular diameter and structural aspects of the peri-lacunar-canalicular matrix. In Chapter 3, we quantified temporal and spatial patterns of osteocyte apoptosis in estrogen-deficient rats and quantified temporal changes in MMP-2 and MMP-3, which were tested as potential candidates causing the nanostructural alterations of bone matrix changes around osteocytes. In chapter 4, we assessed mineral changes at the whole-bone level using fluorescent labels to determine mineral apposition and bone formation rates, and used nanoindentation to identify material property changes that could indicate alterations in mineral content around the osteocyte lacunar-canalicular network. Chapter 5 provides a summary of all the studies and suggests future work

that would further help establish the relationship between estrogen deficiency and osteocyte mechanotransduction.

CHAPTER 2

ALTERATIONS IN THE OSTEOCYTE LACUNAR-CANALICULAR MICROENVIRONMENT DUE TO ESTROGEN DEFICIENCY

Sharma D, Ciani C, Marin PA, Levy JD, Doty SB, Fritton SP. Alterations in the osteocyte lacunar-canalicular microenvironment due to estrogen deficiency. Bone. 2012; doi:10.1016/j.bone.2012.05.014

Abstract

While reduced estrogen levels have been shown to increase bone turnover and induce bone loss, there has been little analysis of the effects of diminished estrogen levels on the lacunar-canalicular porosity that houses the osteocytes. Alterations in the osteocyte lacunar-canalicular microenvironment may affect the osteocyte's ability to sense and translate mechanical signals, possibly contributing to bone degradation during osteoporosis. To investigate whether reduced estrogen levels affect the osteocyte microenvironment, this study used high-resolution microscopy techniques to assess the lacunar-canalicular microstructure in the rat ovariectomy (OVX) model of postmenopausal osteoporosis. Confocal microscopy analyses indicated that OVX rats had a larger effective lacunar-canalicular porosity surrounding osteocytes in both cortical and cancellous bone from the proximal tibial metaphysis, with little change in cortical bone from the diaphysis or cancellous bone from the epiphysis. The increase in the effective lacunar-canalicular porosity in the tibial metaphysis was not due to changes in osteocyte lacunar density, lacunar size, or the number of canaliculi per lacuna. Instead, the effective canalicular size measured using a small molecular weight tracer was larger in OVX rats compared to controls. Further analysis using scanning and transmission electron microscopy demonstrated that the larger effective canalicular size in the estrogen-deficient state was due to nanostructural matrix-mineral level differences like loose collagen surrounding osteocyte canaliculi. These matrix-mineral differences were also found in osteocyte lacunae in OVX, but the small surface changes did not significantly increase the effective lacunar size. The alterations in the lacunar-canalicular surface mineral or matrix environment appear to make OVX bone tissue more permeable to small molecules, potentially altering interstitial fluid flow around osteocytes during mechanical loading.

1. Introduction

Bone's lacunar-canalicular porosity is formed by a three-dimensional network of lacunae and small canals that house the osteocytes and their cytoplasmic processes and allows communication between neighboring osteocytes, osteoblasts, bone lining cells, and the vascular porosity. A pericellular fiber matrix surrounds the osteocyte processes, which have been shown to be tethered to the canalicular wall [1]. With their distribution throughout the bone matrix and their high degree of interconnectivity, osteocytes are in an ideal position to sense mechanical deformations and translate them into biochemical signals to enable bone resorption and formation [2, 3].

Mobile exchangeable interstitial fluid external to the osteocytes fills the lacunar-canalicular porosity and is thought to play an important role in bone maintenance [4]. When cyclic mechanical loading is applied to bone, interstitial fluid flows around the osteocytes in the lacunar-canalicular porosity and drains into and out of the larger pores surrounding the blood vessels and nerves in the vascular porosity. The movement of interstitial fluid in the canalicular network affects bone cells in two ways: it is believed to activate osteocytes via deformation of transmembrane links between the cell process cytoskeleton and the canalicular wall [5,6], and it is involved in mass transport favoring the passage of nutrients and signaling molecules and the removal of waste products from the osteocytes [7-11].

Reduction of estrogen levels has been shown to increase bone turnover, induce bone loss, and increase osteocyte apoptosis [12-14]. Modification of bone macroarchitecture via a decrease in bone volume fraction is frequently reported in ovariectomized rats [13,15-17], yet there is little analysis in the literature related to changes in the lacunar-canalicular porosity that houses the osteocytes. Reduced estrogen levels have been shown to increase osteocyte apoptosis, which

may reduce the communication between neighboring osteocytes [14,18-20]. Alterations in bone mineral content and collagen fibrils have been documented in ovariectomized rats [21,22], but whether these changes at the nanostructural level affect the interstitial fluid pathways is not known. Alterations in the geometry or the interconnectedness of the lacunar-canalicular network may affect interstitial fluid movement and could alter the transduction of mechanical forces to the osteocyte [23,24].

Because changes in the osteocyte lacunar-canalicular microenvironment have the potential to impair mechanotransduction that is vital for bone health, the goal of this study was to determine whether the osteocyte microenvironment is altered after loss of ovarian function. Using the rat ovariectomy model of osteoporosis, this project utilized high-resolution microscopy techniques to assess several aspects of the osteocyte lacunar-canalicular network. Confocal microscopy was used to assess changes in lacunar-canalicular porosity, lacunar and canalicular size, and the number of canaliculi per lacuna; and scanning and transmission electron microscopy were used to assess canalicular diameter and structural aspects of the peri-lacunar-canalicular matrix.

2. Materials and methods

2.1. Animal model and experimental design

The ovariectomized (OVX) rat was used as a model for postmenopausal osteoporosis [12]. Twenty-week-old rats were used to avoid the early, rapid growth stage that produces significant bone turnover in the proximal tibia [25,26]. Bone changes were assessed 6 weeks after loss of ovarian function, a duration shown previously to produce significant bone loss in the

proximal tibia [27,28]. All procedures were approved by the Institutional Animal Care and Use Committee at the Hospital for Special Surgery.

A total of 35 female Sprague Dawley rats (Harlan Laboratories) were used in the analyses. Eighteen rats underwent OVX at 20 weeks of age and were fed ad libitum for one week after surgery. The OVX rats were then pair-fed to the average food intake of control rats (20 g standard rat chow per day). The control groups included age-matched (CTRL, n=11) and sham-operated (SHAM, n=6). SHAM surgery was identical to OVX except the ovaries were not removed. At 26 weeks of age all rats were sacrificed, and uterine horn weights were recorded to assess the effectiveness of OVX versus SHAM.

The work was divided into three analyses that examined the osteocyte lacunar-canalicular network, with focus on cortical and cancellous bone from the proximal tibia. A subset of rats was used for each analysis: 2D confocal study: OVX, n=6, CTRL, n= 6; SEM study: OVX, n=6, CTRL, n=5; TEM and 3D confocal study: OVX, n=6, SHAM, n=6.

2.2 Sample preparation for the confocal microscopy, SEM, and TEM analyses

For the confocal microscopy analyses, harvested tibiae were placed immediately into either a fixative used routinely for electron microscopy (0.5% gluteraldehyde, 2% paraformaldehyde in 0.05M cacodylate-sodium buffer, pH 7.4) or 10% phosphate buffered formalin solution at room temperature. Transverse cortical bone sections (300-400 μm) were cut with a diamond blade saw (Buehler) from the tibial mid-diaphysis and from the metaphysis 2-3 mm distal to the growth plate and then fixed for 24 h at room temperature. The remainder of the proximal tibia, used to analyze cancellous bone from the metaphysis and epiphysis, was fixed for 48 h at room temperature. After fixation, the cortical sections were ground down to a final

thickness of 30-50 μm using Carbimet paper discs (800 and 1200 grit; Buehler) and dehydrated in a series of ascending graded ethanol (EtOH) solutions. The proximal tibia samples containing cancellous bone were also dehydrated in a series of ascending graded EtOH solutions. To label the lacunar-canalicular porosity all the samples were stained using a protocol developed in our lab [29]. Briefly, the cortical sections and cancellous samples were stained while gently mixed in a rotator for 4 hours in a 1% filtered FITC solution (fluorescein isothiocyanate isomer I from Sigma, product #F7250). The cancellous samples were then embedded in PMMA and sagittal or frontal sections (400-500 μm) were cut from the plastic blocks with a diamond blade saw. Cancellous sections were ground down to a final thickness of 40-70 μm using Carbimet paper discs (600 and 1200 grit; Buehler), and dried in ascending graded EtOH solutions. Finally, all the cortical and cancellous sections were placed on slides and coverslipped with mounting media (Richard-Allan Scientific).

For the SEM analyses, ~5 mm thick sections were cut from the proximal end of the tibial metaphysis using a diamond blade saw. The specimens were then cut longitudinally to expose cancellous and cortical bone surfaces. After sonication for 40 min in a 20 ml aqueous solution (2% dimethyl sulfoxide, 2% Triton 100X, and 2% detergent) to remove cellular debris, the samples were rinsed in running water and sonicated for 30 additional minutes in fresh water. Samples were then dehydrated in 100% EtOH overnight, mounted on a sticky stub, and coated with palladium (300 Å coat thickness).

For the TEM analyses, 1-2 mm sections were cut from the proximal tibial metaphysis 2 mm distal to the growth plate and fixed in 0.5% gluteraldehyde, 2% paraformaldehyde in 0.05M cacodylate-sodium buffer, pH 7.4 for 24 h at room temperature. After fixation undemineralized tibial samples were treated with 0.5% reduced osmium tetroxide (EM Sciences) and 1.5 %

anhydrous potassium ferricyanide in distilled water, and then dehydrated in a series of ascending EtOH solution. Final dehydration was done with propylene oxide, and samples were then placed overnight in a mixture of Epon resin (Embed-812, Electron Microscopy Sciences) and propylene oxide (1:1 and then 3:1 overnight) at room temperature. Finally, the samples were embedded in a 1:1 mixture of Epon resin and nadic methyl anhydride, using 0.5 ml of 2,4,6-Tri(dimethylaminomethyl)phenol (DMP-30) catalyst. Thin (80 nm) sections of cancellous bone were cut using an Ultracut microtome with an ultra-diamond knife and mounted on single-slot Formvar-coated grids.

2.3 Quantification of osteocyte lacunar-canalicular porosity and lacunar area using 2D confocal microscopy

The osteocyte lacunar-canalicular porosity was first quantified using 2D confocal microscopy scans (Leica TCS SP2). A 40x oil immersion lens with a 1.25 numerical aperture was used with the pinhole set at 1 Airy unit. A wavelength excitation of 488 nm was used to illuminate FITC.

2.3.1 Quantification of osteocyte lacunar-canalicular porosity of cortical bone cross-sections

To quantify the lacunar-canalicular porosity of cortical bone from the tibial diaphysis and metaphysis, confocal images spanning an entire cross-section were taken at a resolution of 2048 x 2048 pixels with a field of view of 375 µm x 375 µm (650 gain, -5 offset). For each region a high-resolution confocal image of an entire cross-section was obtained by creating a montage of the field-of-view images using Photoshop 7.0 (Adobe Systems) (Fig. 2.1). Each cross-section image was then transformed to grayscale and thresholded using Otsu's method (ImageJ, National Institutes of Health). Otsu’s method is a widely used global thresholding algorithm that extracts

objects from their background. The algorithm assumes that an image is composed of two classes of pixels, object and background, and then computes an optimal threshold value that minimizes the intra-class variance [30]. To ensure that all images were captured similarly, imaging was performed at the same z-depth from the specimen surface and the same gains were applied. This ensured that there would not be large intensity differences between images. The thresholding produced a binary image with the porous areas stained with FITC represented by white pixels, and the impermeable area of the mineralized matrix represented by black pixels. After first marking the vascular pores (including resorption canals if present), the lacunar-canalicular porosity was calculated as the difference between the pixels representing the total FITC-stained regions and the pixels occupied by the vascular pores and resorption canals, divided by the cross-sectional cortical area. The endosteal and periosteal surfaces were excluded for all measurements to avoid the accumulation of FITC at these surfaces. For the cortical metaphysis sections, an additional analysis was also performed to assess the lacunar-canalicular porosity in the regions of trabecular remnants as well as the lamellar regions found in this portion of the tibia (these regions are created during normal long bone growth when marrow space between cancellous struts is filled in with new lamellar bone [31]).

2.3.2 Quantification of osteocyte lacunar-canalicular porosity of cancellous bone

To quantify the lacunar-canalicular porosity of cancellous bone from the proximal tibia, fourteen randomly selected areas were analyzed for each rat, seven from the metaphysis and seven from the epiphysis (Fig. 2.2). Confocal images were taken at a resolution of 2048 x 2048 pixels with a field view of 375 µm x 375 µm (515 gain, 1.5 offset). The images were transformed to grayscale and thresholded using Otsu's method, with the threshold values determined for each image in a region containing canaliculi. The lacunar-canalicular porosity

was quantified as the percentage of white pixels (FITC-stained space) contained in the cancellous bone area examined, excluding marrow space.

2.3.3 Quantification of osteocyte lacunar area

To quantify lacunar area, lacunar pores in the 2D confocal images were marked using ImageJ, and the average area taken up by each lacuna (including the osteocyte body) was measured. Multiple bone sectors, each containing three to seven lacunae, were analyzed for cortical and cancellous bone from the tibial metaphysis. For the cortical metaphysis, both the trabecular remnant and lamellar regions were analyzed using six bone sectors for each region. For the cancellous metaphysis region, seven bone sectors were analyzed for each rat. Thus for each anatomical region approximately 20 lacunae were analyzed per rat. The lacunar areas were averaged first for each rat and then for each group.

2.4 Qualitative assessment of bone mineral using backscattered electron microscopy

To further assess the bone microstructure in regions that appeared impermeable to FITC as viewed using confocal microscopy, a randomly chosen subset from the 2D confocal microscopy study (OVX, n=3 and CTRL, n=3) was imaged using scanning electron microscopy (SEM) in backscattered mode (FEI Quanta 600). Slide coverslips from cortical cross-sections from the tibial diaphysis and metaphysis were removed after being immersed in 100% xylene. Sections were then gently polished with 1200 grit sandpaper to eliminate mounting media and xylene residues, mounted on a microscope stud holder, and visualized with SEM in backscattered mode. Cross-sectional images of the entire cortical mid-diaphysis and metaphysis were obtained and compared to confocal microscopy images of the same sections.

2.5 Quantification of canalicular diameter using 2D confocal microscopy, SEM, and TEM

Canalicular diameter was measured for cortical and cancellous bone from the proximal tibial metaphysis using 2D confocal images, SEM images, and TEM images. For the confocal analysis of cortical and cancellous bone from the metaphysis, at least 20 canaliculi were identified and 4 diameter measurements were made over the length of each canaliculus, resulting in approximately 80 measurements per rat per region. For the SEM analysis, canalicular diameters were measured using the built-in microscope software (FEI Quanta 600) on images taken at 10^4 magnification. At least 40 canalicular diameters were measured per rat for the two regions analyzed (cortical and cancellous metaphysis). Measurements were made on the smallest dimension of the canalicular opening (Fig. 2.3a, b). For the TEM analysis, canalicular diameters from cancellous bone were measured using the built-in microscope software (Olympus 5.1) on TEM images taken at 19000 x magnification (JOEL 100CX-II). Only circular cross-sections of canalicular diameters were measured (Fig. 2.3c), and at least 60 canalicular diameters were measured per rat.

2.6 Quantification of osteocyte lacunar density, number of canaliculi per lacuna, and lacunar and canalicular volume using 3D confocal microscopy

Additional 3D confocal microscopy analyses were performed on cortical bone from the proximal tibial metaphysis, a region found to undergo changes in the 2D confocal analysis. A Leica TCS SP2 microscope was used with a 63x oil immersion lens (1.4 numerical aperture). The pinhole was set at 1 Airy unit, and a wavelength excitation of 488 nm was used to illuminate FITC. A linear intensity compensation for gain was applied to compensate for loss in laser intensity at increasing depth into the sample, and each image was averaged four times to minimize noise. The counter was blinded for all analyses.

2.6.1 3D quantification of osteocyte lacunar density

To calculate volumetric osteocyte lacunar density (N.Lc/BV), confocal images were taken at a resolution of 1024 x 1024 pixels with a field of view of 150 µm x 150 µm and a 1 µm z-step between images for a scan depth of 25 µm. The 3D z-stack images were loaded in ImageJ and lacunae were point-counted directly through the z-stack using the cell counter tool. Partially sectioned lacunae at the top surface of the z-stack were included, while partially sectioned lacunae at the bottom surface or image sides were excluded. The number of lacunae (N.Lc) was divided by the analyzed bone volume (BV) and averaged for three z-stacks per rat to obtain the volumetric osteocyte lacunar density. If the average tissue volume surrounding one osteocyte lacuna is represented by a cube, the length (L) of one side of the cube can be calculated as $\sqrt[3]{1/(\text{N.Lc/BV})}$ (Fig. 2.4a). Because L was found to be approximately 25 µm for the SHAM group (Table 2.2), the next set of confocal scans was taken with this dimension to quantify the number of canaliculi per osteocyte lacuna.

2.6.2 3D quantification of the number of canaliculi per osteocyte lacuna

To calculate the number of canaliculi per osteocyte lacuna, confocal images of single lacunae were taken at a resolution of 1024 x 1024 pixels with a field of view of 25 µm x 25 µm and a 244 nm z-step for a scan depth of 25 µm, with an osteocyte lacuna in the middle of the scan (Fig. 2.4b). All z-stacks were reconstructed using Volocity (Perkin Elmer), and the number of canaliculi penetrating each of the six faces of the cubic volume (considered secondary canaliculi), were then point-counted for three z-stacks per rat and averaged (Fig. 2.4c). The same confocal z-stacks were then cropped close enough to visualize each osteocyte lacuna, and primary canaliculi, considered to be all unbranched, single processes directly connecting to the lacuna, were also point-counted for three z-stacks per rat and averaged (Fig. 2.4d).

2.6.3 3D quantification of osteocyte lacunar and canalicular volumes

The same confocal z-stacks that were used to quantify the number of canaliculi were also used to quantify osteocyte lacunar volumes. Images were thresholded in ImageJ using Otsu's method and were imported into Mimics 3D reconstruction software (Materialise) where segmentation tools were used to isolate lacunar volumes (Fig. 2.4e).

To calculate canalicular volumes, confocal images consisting of only canaliculi between two osteocytes were obtained at a resolution of 2048 x 2048 pixels with a field of view of 10 µm x 10 µm and a 122 nm z-step for a scan depth of 10 µm (Fig. 2.4f). Scanned images were thresholded in ImageJ using Otsu's method and imported into Mimics, which enabled creation of 3D volumes to calculate canalicular volume.

A parametric analysis was performed to assess the effects of threshold on the volume z-stack measurements. First, a parametric analysis was performed for lacunar volume z-stacks using the Otsu threshold, along with a 25% higher and 25% lower threshold. There was less than a 10% difference in lacunar volume for the three thresholds (data not shown). Second, for the canalicular volume measurements, Otsu thresholding was applied using two approaches: (1) thresholding image-by-image within the z-stack and (2) using an average threshold for all images within the z-stack. Both approaches resulted in the same outcome (data not shown), and thus the second approach, using a global Otsu threshold for each z-stack, was utilized using ImageJ.

2.7 Statistical analyses

For the 2D confocal microscopy study, lacunar-canalicular porosity measurements were analyzed using two-way repeated-measures ANOVA with Bonferroni post-hoc t-tests for the two factors: treatment (OVX and CTRL) and location (cortical bone: diaphysis and metaphysis and

cancellous bone: metaphysis and epiphysis). Two-way repeated-measures ANOVA was also used to analyze the lacunar area and canalicular diameter measured using 2D confocal microscopy for the different anatomical regions: cortical metaphysis (trabecular remnant and lamellar regions) and cancellous metaphysis. For the SEM and TEM studies, unpaired, two-tailed t-tests were performed to compare canalicular diameter in OVX and control groups. Unpaired, two-tailed t-tests were also used to assess differences between the SHAM and OVX groups for the 3D confocal microscopy measurements (volumetric osteocyte lacunar density, side length (L) of cubic volume of bone surrounding an osteocyte, the number of primary and secondary canaliculi, osteocyte lacunar volume, and canalicular volume). Finally, unpaired, two-tailed t-tests were used to compare animal and uterine horn weights between OVX and controls. All the statistical analyses were performed with the Prism 5 statistics software package (GraphPad Software Inc.). The normality of all data sets was confirmed before using parametric tests, and the significance level was set at $p < 0.05$.

3. Results

3.1 Effectiveness of ovariectomy

The effectiveness of ovariectomy was verified by the reduced weight of the uterine horns in the OVX rats (0.19 ± 0.03g) compared to SHAM (0.58 ± 0.13g). Despite pair-feeding, at 26 weeks of age the OVX rats weighed more than the age-matched and sham-operated control rats: OVX (n=18): 314 ± 27 g; controls (n=17): 279 ± 36 g.

3.2 Confocal microscopy measurements and observations: osteocyte lacunar-canalicular porosity, canalicular and lacunar size, and number of canaliculi per lacuna

The high-resolution 2D confocal microscopy measurements, which measured effective penetration by a small molecular tracer, showed that ovariectomized rats had an increased effective lacunar-canalicular porosity in the cortical and cancellous bone of the tibial metaphysis compared to controls, with no significant differences in the cortical bone of the diaphysis or cancellous bone of the epiphysis (Fig. 2.5). Cancellous bone of the metaphysis showed the largest increase in lacunar-canalicular porosity in OVX compared to CTRL (+56%), and the cortical metaphysis also had significantly higher lacunar-canalicular porosity (+16%) compared to CTRL.

Qualitative comparisons of cortical bone sections imaged with both confocal microscopy and backscattered electron imaging demonstrated that areas with an absent or disconnected canalicular network, where the FITC tracer could not penetrate, had a higher mineralization density, whereas areas with lower mineralization densities had a higher canalicular density (Fig. 2.6). Cortical bone in the rat tibial metaphysis of both OVX and controls demonstrated trabecular remnants surrounded by lamellar regions (Fig. 2.6a-c). The increase in the effective lacunar-canalicular porosity in the cortical bone of the tibial metaphysis in the OVX group was due to a 24% increase in effective lacunar-canalicular porosity in the lamellar regions; the trabecular remnants of the cortical metaphysis had no change in lacunar-canalicular porosity due to OVX.

Regions found to have an increased effective lacunar-canalicular porosity after OVX demonstrated larger effective canalicular diameter and no change in lacunar area as measured with 2D confocal microscopy (Table 2.1). In cancellous bone from the tibial metaphysis, the effective canalicular diameter measured using 2D confocal microscopy was larger (+48%) in OVX compared to CTRL. In the lamellar regions of cortical bone from the metaphysis, the

effective canalicular diameter was also significantly larger (+26%) in OVX compared to CTRL, while there were no differences in canalicular diameter in the trabecular remnants in the cortical metaphysis. OVX did not significantly change osteocyte lacunar area in cortical or cancellous bone of the tibial metaphysis (Table 2.1).

The high-resolution 3D confocal microscopy measurements of cortical bone from the tibial metaphysis showed a 34% increase in effective canalicular volume in OVX compared to SHAM (Fig. 2.7). In addition, no significant differences between SHAM and OVX were found for osteocyte lacunar density, side length of cubic volume surrounding one lacuna, lacunar volume, and number of primary and secondary canaliculi per lacuna (Table 2.2).

3.3 SEM and TEM measurements and observations: changes in lacunar-canalicular interfaces

The SEM and TEM measurements did not demonstrate significant differences in canalicular diameter due to OVX; however, morphological alterations at the lacunar-canalicular interfaces were evident. While the canalicular diameter measured from SEM images of cancellous bone from the metaphysis was similar in both groups (CTRL: 335 ± 32 nm; OVX: 341 ± 32 nm), loose collagen fiber arrangements that diffusely covered the canalicular openings and masked their edges were seen in OVX compared to CTRL (Fig. 2.3a, b). These fibers made it difficult to find canalicular openings that could be measured in the SEM images and prevented measurement of canalicular diameter in the cortical metaphysis samples. While the canalicular diameter measured from TEM images of cancellous bone from the metaphysis was also not significantly different between groups (SHAM: 228 ± 11 nm; OVX: 242 ± 22 nm), morphological differences were observed in lacunae and canaliculi of OVX rats. The SHAM group demonstrated smooth lacunar and canalicular boundaries, while loose collagen fibers were

observed invading the lacunar and canalicular spaces of the OVX group, throughout the areas analyzed (Fig. 2.8). Matrix debris and collagen fragments were also observed in the pericellular spaces of lacunae of OVX rats.

4. Discussion

Using high-resolution analyses, this study has demonstrated alterations in the osteocyte microenvironment in the rat OVX model of postmenopausal osteoporosis. Confocal microscopy analyses demonstrated that OVX increased the effective lacunar-canalicular porosity surrounding osteocytes in cortical and cancellous bone from the rat tibia metaphysis, with the increase in porosity largely explained by increased effective canalicular porosity, as measured by penetration of a small molecular weight dye. No significant changes were found in osteocyte lacunar density, lacunar size, or the number of canaliculi per lacuna. TEM and SEM analyses demonstrated that the larger effective canalicular size in the estrogen-deficient state was due to nanostructural matrix-mineral level differences around the osteocyte canaliculi. These matrix-mineral differences were also found in osteocyte lacunae in OVX, but the small surface changes did not significantly increase the effective lacunar size. The nanostructural changes of the osteocyte lacunar-canalicular microenvironment suggest that the lacunar-canalicular walls in the OVX rats became more permeable, which could affect interstitial fluid flow around osteocytes during mechanical loading.

Because estrogen deficiency leads to increased bone turnover, it is important to assess whether the lacunar-canalicular differences seen in OVX rats were related to the maturation of osteocytes in newly laid down bone. Osteocytes observed in the TEM analyses were slender cells with reduced cytoplasm and diminished quantity of endoplasmic reticulum, Golgi complex, and

mitochondria. Such characteristics are typical of mature osteocytes rather than newly formed osteocytes [32,33]. In addition, the nanostructural matrix changes observed in the EM analyses of osteocyte lacunae and canaliculi were found uniformly throughout the cancellous bone of the OVX rats, and only rarely in osteocytes in the SHAM group. The osteocyte morphology and distribution of changes of the lacunar-canalicular surfaces in OVX lead us to believe that the osteocyte lacunar-canalicular changes documented in this study were not simply changes due to new bone laid down post-OVX. In future studies, histomorphometric analysis of fluorochrome label-based bone dynamics will facilitate the identification of newly formed bone regions that arise due to remodeling changes associated with estrogen-deficiency, and quantitative backscattered electron imaging can be used to assess mineral heterogeneity.

Contradictory results exist in the literature regarding mineral content present in osteoporotic samples at the micro and nano level. Some studies show decreased mineral content in bone tissue due to estrogen deficiency [34-36], or find no changes in mineral content [37], while others have shown an increase in mineral content [38,39]. An increase in mineral heterogeneity is often noted due to increased bone turnover [40]. Alterations in collagen composition have also been shown in osteoporotic patients [41]. TEM analysis has indicated structural changes in bone fibril architecture in OVX rats, showing irregular and disturbed collagen fibril arrangement compared to a more organized arrangement seen in controls [21]. Shrinkage of the D-spacing in collagen fibril periodicity has also been seen in OVX bone [21,42]. Modification in the concentrations of noncollagenous proteins or changes in their molecular orientation have also been shown in osteoporotic bone [43]. Defects in mineralization, changes in matrix fiber architecture or cross-linking may also be explored in future studies analyzing changes in bone architecture due to reduced estrogen levels.

The lack of response to loss of ovarian function in the tibial diaphysis and epiphysis, and the active response in the metaphysis is similar to bone macroporosity changes reported in the literature, where the proximal metaphysis of the rat tibia has demonstrated significant cancellous bone loss as measured by bone volume fraction, with little change in the diaphysis or epiphysis [15,16,27]. It is possible that there is a link between osteocyte-level changes in estrogen-deficient bone and osteoclast removal of bone, as some studies have suggested [44-46]. Ikeda et al. [44] showed osteocytes in the metaphyseal trabecular bone of OVX rats expressed osteopontin mRNA, which tended to be resorbed after estrogen withdrawal. Furthermore, osteocyte mRNA expression differed in the metaphyseal compartment compared to the epiphysis. Emerton et al. [45] showed that when osteocyte apoptosis was suppressed, it prevented OVX-induced osteoclast resorption, thus demonstrating a direct link between osteocyte apoptosis and osteoclast resorption in the estrogen-deficient state. Expression of RANKL has also been demonstrated in osteocytes, which are now believed to be the largest source of RANKL [47,48]. RANKL deletion in osteocytes has been shown to prevent osteoclast-dependent bone resorption due to unloading and has also been shown to lead to an osteopetrotic phenotype [48,49]. It is plausible that the loss of estrogen may stimulate bone resorption in part by increasing osteocyte apoptosis and thereby RANKL expression [50]. Future work assessing osteocyte-related changes in this rat OVX model will include evaluation of osteocyte apoptosis.

While not directly assessed in this study, a proposed mechanism by which the lacunar-canalicular surface is altered after OVX is through periosteocytic remodeling, the process by which osteocytes may modify their immediate environment through matrix modification. The capability of osteocytes to adapt their lacunar wall under certain conditions was suggested in early studies [51,52] and then largely dismissed due to criticisms related to the methods of

measurement of lacunar size and as well as the mounting evidence that osteoclasts were responsible for bone resorption [53]. However, recent studies continue to suggest that osteocytes can remodel their local environment in response to hyperparathyroidism, limb immobilization, lactation, and parathyroid hormone administration [54-57]. While none of the early studies included detailed measurements of changes in canalicular size, likely because of the resolution of the approaches used, an increased canalicular volume has recently been documented in lactating rats [57]. There is increasing evidence that osteocytes are metabolically active cells and can modify the matrix surrounding them via production of collagen-digesting proteins such as matrix metalloproteinases that have been demonstrated to be secreted during the development of osteocyte processes and are suggested to remain active in mature osteocytes [58,59].

The assessment of canalicular distribution in this study is one of the few 3D analyses of the number of canaliculi that emanate from osteocyte lacunae. Significant branching of the primary canaliculi was found in both OVX and SHAM groups. In addition, a lower number of osteocytic processes emanating from the osteocyte cell body have been documented in other 3D confocal studies [60], which may be due to differences in species, animal age, and type of bones analyzed. Nonetheless, the number of primary canaliculi per lacuna reported here is in the range (41- 115) previously estimated for different species [61].

Contradictory results have been reported concerning osteocyte lacunar density differences in osteoporotic bone. While some studies have shown significantly higher lacunar density in human osteoporotic bone [62], other reports demonstrate lower lacunar density in osteoporotic females compared to healthy females [63]. In our study, we did not find differences in lacunar densities between SHAM and OVX rats. In addition, the average distance between two osteocyte lacunae found in the present study (~25 μm) is very similar to a previous 3D

confocal study in chicks [60]. Similarly, lacunar volumes are in agreement with previously reported values of osteocyte volume for different species using confocal microscopy [60,64]. While a reduced lacunar area has been reported in human osteoporotic samples [62], our study showed no significant lacunar volume differences between SHAM and OVX groups.

It should be noted that the confocal microscopy analyses present a limitation related to overestimation of porosity due to resolution and distortion effects. The diameter of canaliculi is of the same order of magnitude as the resolution of confocal microscopy (~ 200 nm), which causes confocal images to overestimate the canalicular porosity due to partial volume effects. This overestimation only applies to the measurement of the canaliculi and not the lacunae because the lacunar size (order 10 μm) is well-characterized at a resolution of 200 nm. In addition, a mismatch in the index of refraction between the immersion oil and mounting media can result in z-axis geometrical distortion in confocal images. We have not accounted for any elongation along the z-axis because we estimate this distortion will affect all the measurements similarly since canaliculi weave in and out of all three dimensions and the lacunae analyzed were not oriented in any preferential direction. The SEM and TEM studies were designed to quantify the canalicular diameter and to assess the amount of overestimation of canalicular size occurring in confocal images, since EM has a higher resolution than confocal microscopy. The SEM analysis gave an average canalicular diameter approximately 30% smaller than that measured with confocal microscopy, whereas the TEM analysis gave an average canalicular diameter approximately 50% smaller than that measured with confocal microscopy. The difference between measurements using the two methodologies may arise because SEM samples go through minimal processing and topographical images are obtained, while TEM samples are dehydrated and embedded in a resin prior to obtaining very thin sections. Another important step needed to

calculate lacunar-canalicular microporosities was the image thresholding. Much investigation went into the choice of threshold, and the standard method chosen (Otsu's method [30]) is appropriate for this application, since we have emphasized the relative changes in microporosities between ovariectomized and control animals without focusing on the actual porosity values.

Other limitations of this study relate to the animal model used. While the ovariectomized rat model is not exactly equivalent to postmenopausal osteoporosis in humans, it has characteristics similar to that of postmenopausal bone loss, including increased bone turnover with resorption greater than formation, more trabecular than cortical bone loss, and an initially rapid loss of bone followed by a slower loss of bone [12,27,28]. Twenty-week-old rats were used to avoid the rapid growth stage that produces significant bone turnover in the proximal tibia [25,26]. While some studies show that the rat tibia continues to grow until approximately 26 weeks of age, with a slower rate in the last several weeks, other studies have demonstrated that beyond 20 weeks of age tibial growth has essentially stopped, even though the growth plate remains open [65,66]. Another limitation of the rat ovariectomy model was that despite pair feeding, the body weight of the OVX group was greater than the controls six weeks post-ovariectomy. It has been shown that pair feeding reduces ovariectomy-induced weight gain in the rat, but it does not prevent increased weight gain compared to age-matched controls [67]. The weight gain in OVX rats has been suggested to counteract some of the effects of bone loss due to loss of ovarian function.

The physiological implications of having a more permeable lacunar-canalicular wall around the osteocyte in the estrogen-deficient state relate to the potential altering of the effects of interstitial fluid flow due to mechanical loading [24]. An increased permeability of the lacunar-

canalicular wall may alter both solute transport and interstitial fluid velocities around osteocytes during mechanical loading. It is also possible that alterations in the surface of the lacunar-canalicular network could disrupt the connections of the osteocyte process to the canalicular wall, impairing the capability of the osteocyte to perceive mechanical stimuli and potentially affecting the viability of the osteocyte [68,69]. If the connections between osteocytes and the surrounding matrix are diminished due to ovariectomy, postmenopausal osteoporosis could be a remodeling response to reduced perceived loading in the presence of actual continued loading, where the bone cells cannot process strain-related information as effectively [68]. Further work to identify the mechanisms by which the osteocyte microenvironment is altered in estrogen-deficient rats as well as to investigate how the alterations in the osteocyte microenvironment affect interstitial fluid flow around osteocytes is warranted and is underway.

Table 2.1 Osteocyte lacunar area and canalicular diameter measured using 2D confocal microscopy images of cortical and cancellous bone from the tibial metaphysis. Values expressed as mean ± standard deviation. CTRL: control (n=6); OVX: ovariectomized (n=6).

	Lacunar area (μm^2)		**Canalicular diameter (nm)**	
	CTRL	**OVX**	**CTRL**	**OVX**
Cortical bone: metaphysis				
trabecular remnants	49.4 ± 4.5	50.4 ± 5.9	520 ± 42	542 ± 33
lamellar region	49.2 ± 7.0	51.1 ± 5.2	553 ± 33	697 ± 51[a]
Cancellous bone: metaphysis	60.9 ± 6.9	67.5 ± 13	483 ± 24	714 ± 82[a]

[a] $p < 0.05$ versus CTRL

Table 2.2. Lacunar-canalicular network parameters measured using 3D confocal microscopy images of cortical bone from the tibial metaphysis. Values expressed as mean ± standard deviation. SHAM: sham-operated (n=6); OVX: ovariectomized (n=6).

	SHAM	**OVX**
Osteocyte lacunar density (#/ mm^3)	$6.73x10^4 \pm 1.4x10^4$	$7.70x10^4 \pm 2.5x10^4$
Side length (L) of cubic volume surrounding one osteocyte lacuna (μm)	24.8 ± 1.7	23.9 ± 2.1
Osteocyte lacunar volume (μm^3)	352 ± 30	393 ± 92
Number of primary canaliculi per lacuna	83.9 ± 14	89.7 ± 15
Number of secondary canaliculi per lacuna	387 ± 34	365 ± 40

[a] $p < 0.05$ versus SHAM

Figure Captions

Fig. 2.1 (a) A typical tibial diaphysis section from an OVX rat created from approximately 50 montaged confocal images; scale bar = 300 μm. (b) Enlarged image of square region in (a), which demonstrates the high resolution of the images; scale bar = 50 μm. (c) Enlarged image of the square region in (b), further illustrating the details of the lacunar-canalicular network; scale bar = 10 μm. Osteocyte lacunae (short arrows), and canaliculi (long arrows) are indicated in (b) and (c).

Fig. 2.2 (a) A montaged light micrograph of the proximal rat tibia showing the cancellous regions sampled with 375 μm x 375 μm field of view images from the metaphysis (dashed line boxes) and the epiphysis (solid line boxes); scale bar = 800 μm. Typical metaphysis (b) and epiphysis (c) confocal images; osteocyte lacunae (short arrows) are indicated; scale bars = 50 μm.

Fig. 2.3 SEM images of cancellous bone from the tibial metaphysis for (a) a CTRL specimen and (b) an OVX specimen showing canalicular openings (white arrows); loose collagen fibers are visible in the OVX specimen (black arrow). Canalicular diameter was measured as the smallest dimension of the opening (black lines). (c) TEM image of cancellous bone from the tibial metaphysis from SHAM showing canalicular cross-sections and measurement of canalicular diameter (black lines). TEM sections were counterstained with uranyl acetate for 40 minutes and lead citrate for 5 minutes.

Fig. 2.4 (a) Schematic of cubic volume of bone (average side length L) surrounding one osteocyte lacuna. Secondary canaliculi intersect the faces of the cube. (b) Confocal scan of cubic volume of bone tissue centered on one osteocyte lacuna demonstrating the canalicular network spanning in all directions; scale bar = 5 μm. (c) Confocal scan of a 25 μm x 25 μm x 25 μm cubic volume surrounding one osteocyte lacuna with only secondary canaliculi rendered viewable on all six faces of the cube; scale bar = 5 μm. (d) Cropped scan from (c) showing primary canaliculi emanating directly from the osteocyte lacuna; scale bar = 3 μm. (e) Isolated osteocyte lacuna from same scan constructed in Mimics software; scale bar = 2 μm. (f) Higher resolution scan of canaliculi taken between two osteocytes; scale bar = 2 μm.

Fig. 2.5 Relative lacunar-canalicular porosities measured using 2D confocal microscopy for (a) cortical diaphysis and cortical metaphysis cross-sections and (b) cancellous bone from the epiphysis and metaphysis of the proximal tibia. All measurements were scaled to the CTRL mean for each porosity; bars represent mean values ± standard deviations; *statistical difference between CTRL (n=6) and OVX (n=6) ($p < 0.05$).

Fig. 2.6 (a) Confocal reconstructed image of a typical OVX tibial metaphysis cross-section (cancellous bone in the medullary region was not preserved in these unembedded sections); scale bar = 400 μm. (b) Confocal and (c) backscattered electron images of the rectangular region indicated in (a); the region of trabecular remnants is enclosed within the yellow lines and lamellar bone is marked with red asterisks. Scale bar in (c) = 200 μm. (d) Confocal and (e) backscattered electron images of the same portion of a CTRL tibial diaphysis section; a red line

traces the same pathway in each image. Areas with an absent or disconnected canalicular network (black regions surrounding osteocyte lacunae in the confocal images) correspond to higher mineralization (whiter regions in the backscattered electron images), whereas greater canalicular density areas correspond to areas of lower mineralization. Scale bar in (e) = 200 μm.

Fig. 2.7 Box plots showing 3D confocal microscopy measurements of canalicular volume (%) from cortical bone from the proximal tibial metaphysis. + indicates the mean of each group. A significant difference (34% increase) in canalicular volume was found between SHAM (n=6) and OVX (n=6) (*$p < 0.05$).

Fig. 2.8 TEM images of cancellous bone from the tibial metaphysis showing (a) smooth surfaces in a SHAM osteocyte lacuna (red arrows) and (b) collagen fibers in an OVX lacuna giving the border a rough appearance (yellow arrow). (c) Smooth SHAM canaliculi (red arrow); scale bar = 500 nm and (d) OVX canaliculus with collagen fibers at the surface (yellow arrow); scale bar = 500 nm.

Fig. 2.1

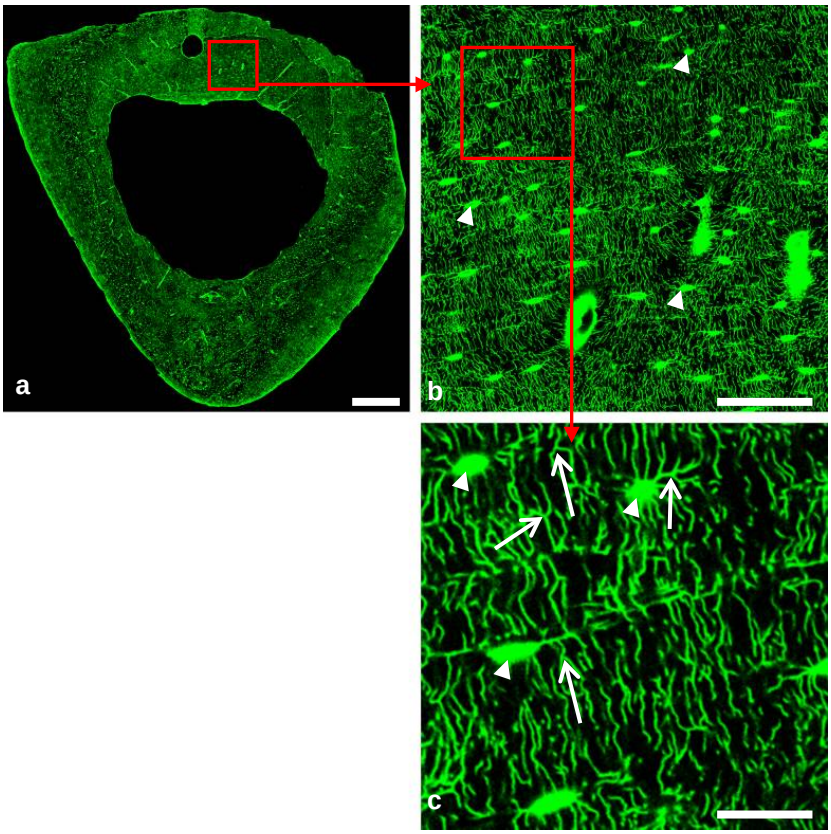

Fig. 2.2

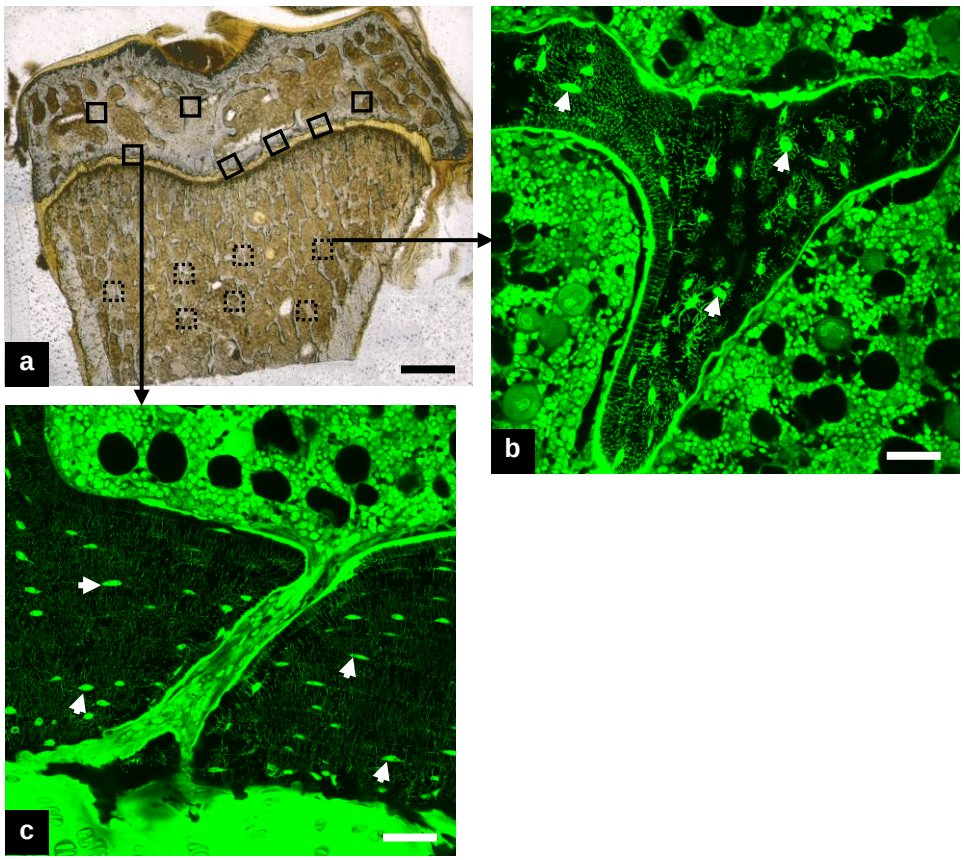

Fig. 2.3

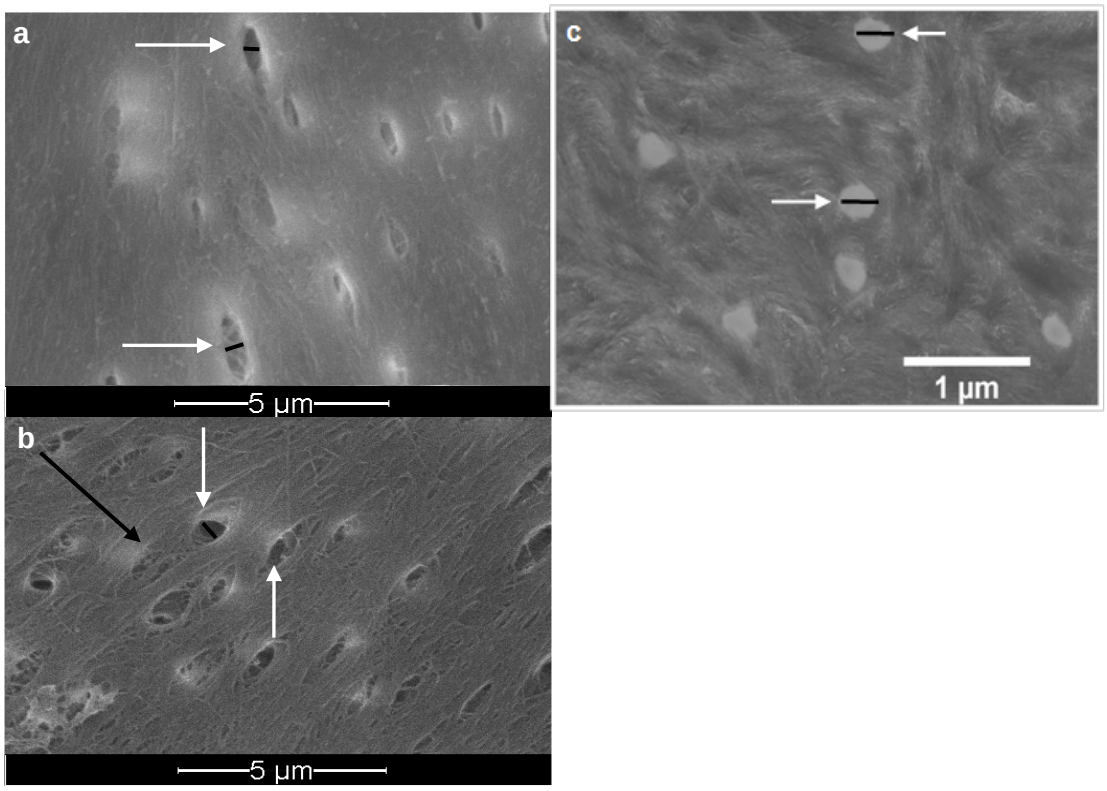

Fig. 2.4

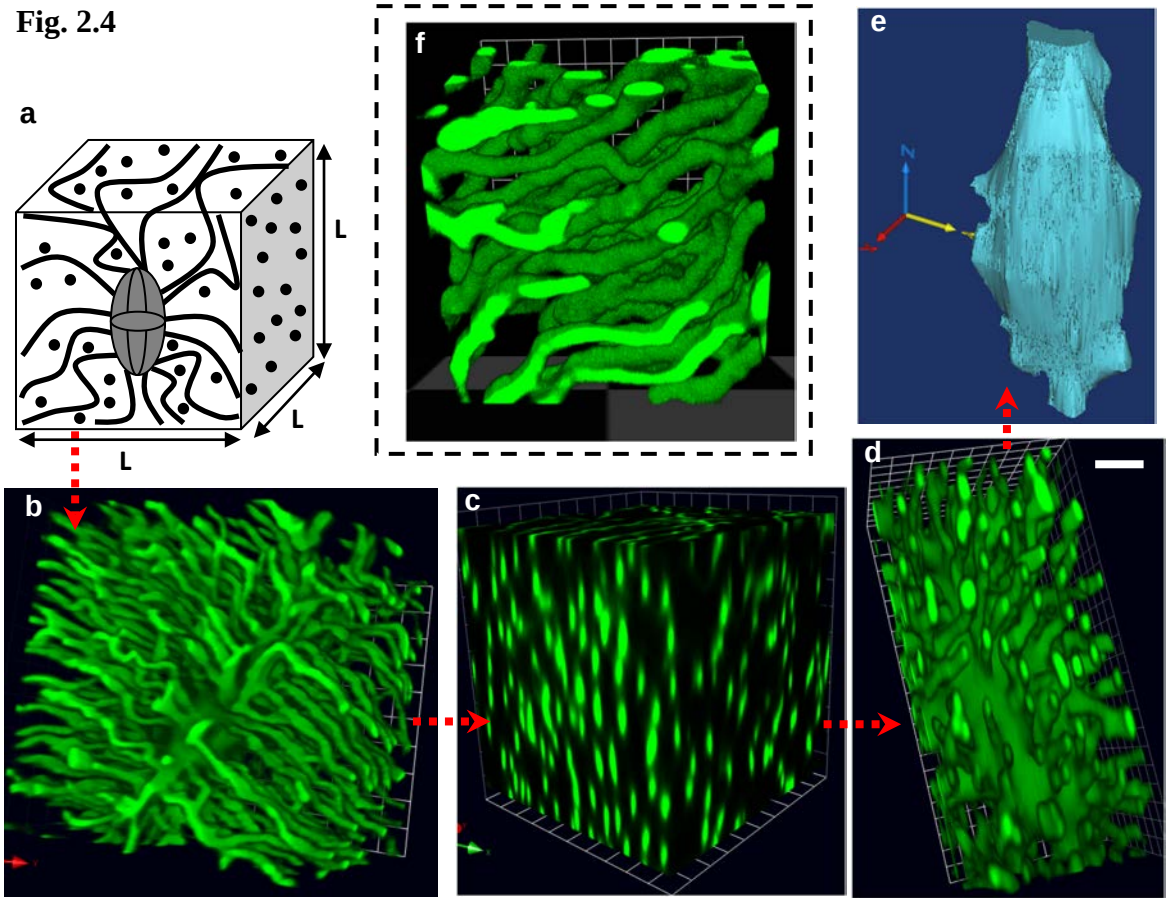

Fig. 2.5

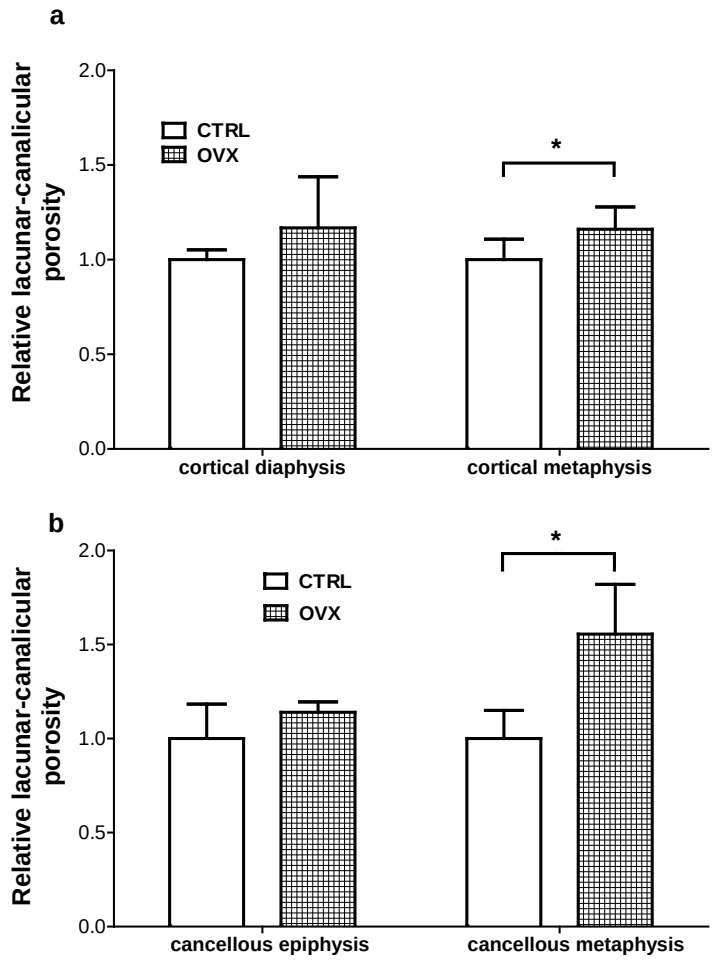
a
Relative lacunar-canalicular porosity
2.0
1.5
1.0
0.5
0.0
CTRL
OVX
*
cortical diaphysis
cortical metaphysis
b
Relative lacunar-canalicular porosity
2.0
1.5
1.0
0.5
0.0
CTRL
OVX
*
cancellous epiphysis
cancellous metaphysis

Fig. 2.6

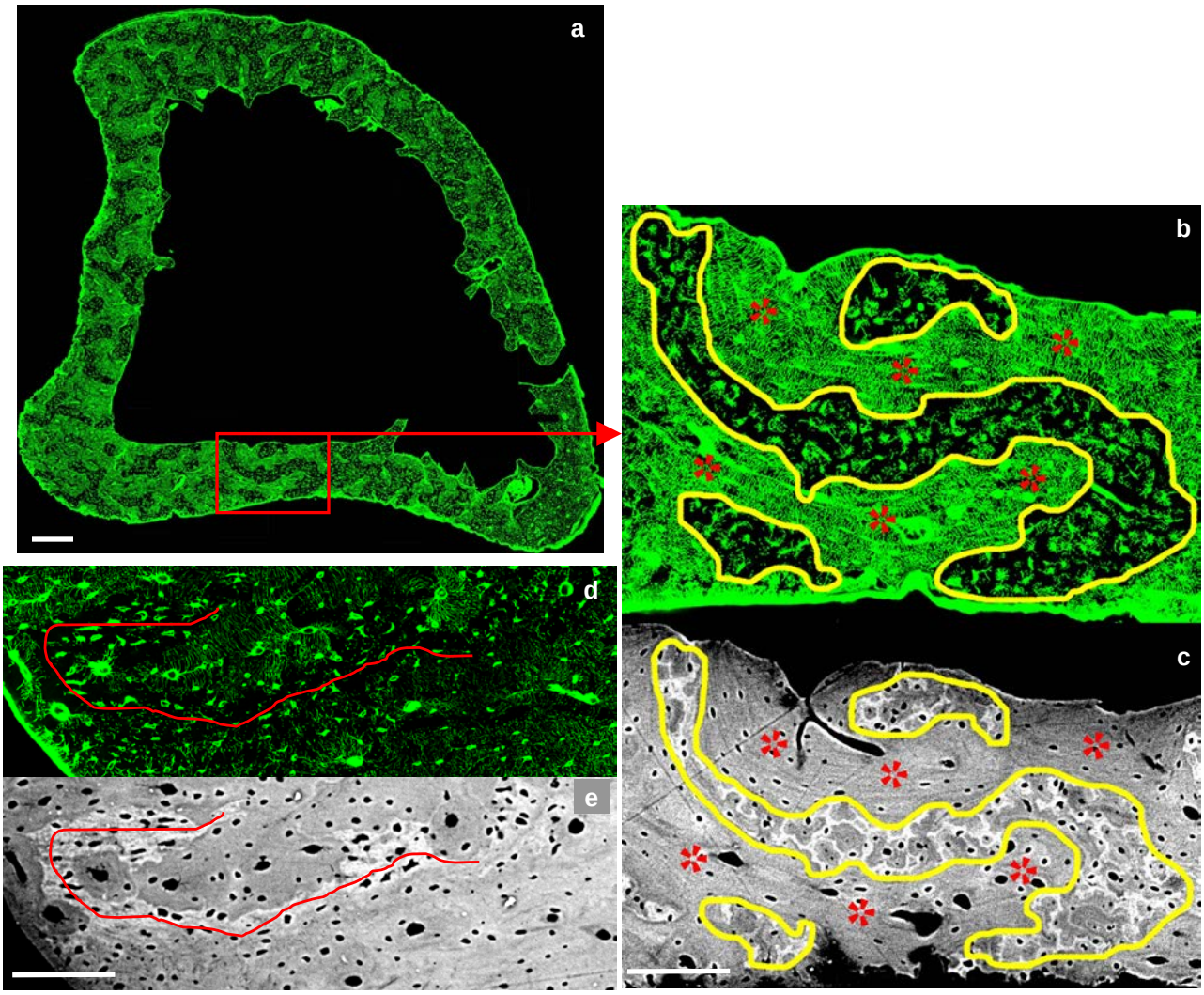

Fig. 2.7

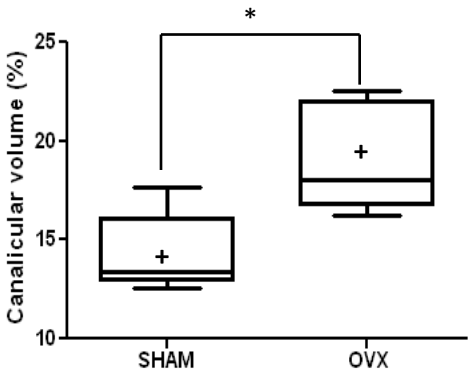

Fig. 2.8

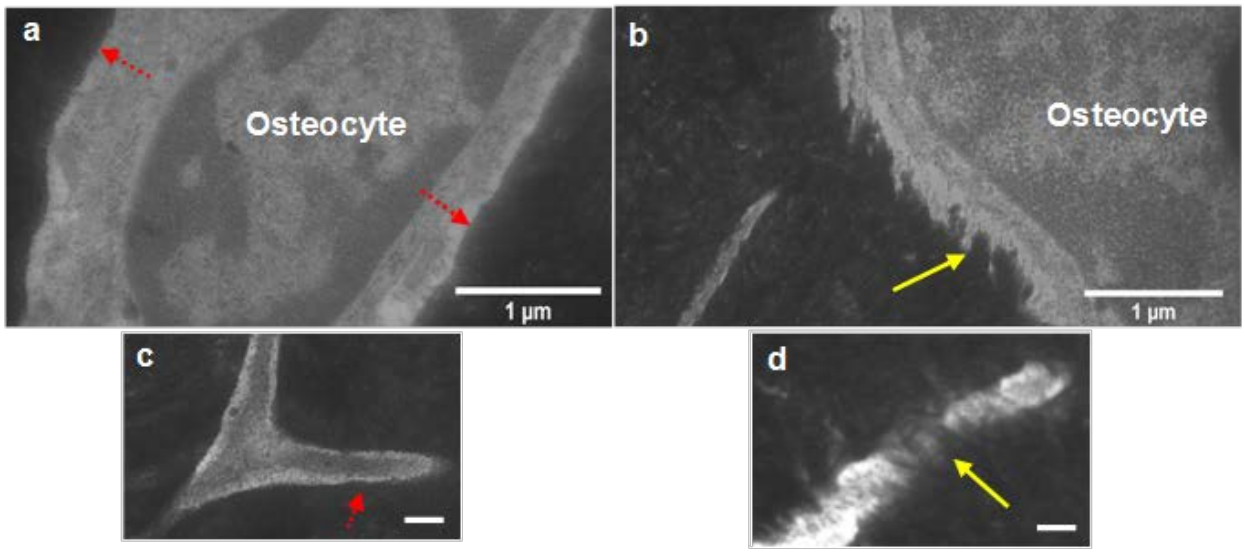

CHAPTER 3

DISTRIBUTION OF APOPTOTIC OSTEOCYTES, MMP-2, AND MMP-3 IN THE OSTEOCYTE LACUNAR-CANALICULAR NETWORK OF ESTROGEN-DEFICIENT RATS

Abstract

Postmenopausal bone loss is associated with estrogen loss, increased bone remodeling and increased osteocyte apoptosis. Previous work from our laboratory has demonstrated that estrogen-deficient rats had a larger effective lacunar-canalicular porosity surrounding osteocytes in cortical bone from the proximal tibial metaphysis, with the effective canalicular size increased due to estrogen deficiency as measured using a small molecular weight tracer. Increase in effective canalicular size coincided with nanostructural matrix-mineral level surfaces changes in the osteocyte lacunae and canaliculi as assessed by electron microscopy. In the current study, twenty-week-old female Sprague Dawley rats were ovariectomized (OVX) to determine the effects of estrogen loss on osteocyte apoptosis, and matrix metalloproteinases MMP-2 and MMP-3 were tested as potential candidates of bone degradation in the osteocyte lacunar-canalicular network. Using immunohistochemistry approaches, we quantified temporal and spatial patterns of osteocyte apoptosis in cortical bone of the proximal tibial metaphysis. Osteocyte apoptosis, as measured by cleaved caspase-3 activity, increased in estrogen-deficient rats at 1 and 2 weeks post-surgery and returned to control levels at 6 weeks. Furthermore, apoptotic osteocytes were observed to be uniformly distributed across the width of the proximal tibial cortex. Significant changes were not observed in MMP-2 and MMP-3 presence between SHAM and OVX groups at any time point. MMP-2 levels decreased significantly in SHAM rats over time, and remained unchanged in OVX rats, although a non-significant trend of increased MMP-2 was observed in OVX rats at 6 weeks post-surgery. An increase in MMP-3 levels was seen in both SHAM and OVX groups over time. These results demonstrate that MMP-2 and MMP-3 are not primary candidates of bone degradation that may create nanostructural matrix changes in the osteocyte lacunar-canalicular environment in estrogen-deficient rats. The precise mechanism by which osteocyte viability is altered is not known; however, it is postulated that

fluid flow may have a role in preventing apoptosis. Continued studies in our laboratory will explore other potential candidates of bone degradation that may be causing nanostructural changes in the osteocyte lacunar-canalicular microenvironment that have the potential to cause impaired cell mechanotransduction in conditions like postmenopausal osteoporosis.

1. Introduction

Osteocytes are the non-proliferative cells encased in bone matrix that can regulate bone remodeling processes in response to mechanical or environmental changes [1,2]. Studies support the idea that osteocytes are metabolically active cells that orchestrate the remodeling process via signaling to the other bone cell types. Osteocytes antagonize osteoblast activity by producing sclerostin and can influence osteoclast activity by producing RANKL/OPG [3,4]. Other evidence suggesting the ability of osteocytes to remodel their surroundings is given by enlarged lacunae and canaliculi in lactating and glucocorticoid-treated mice [5-7]. The motivation of this study comes from our recent findings demonstrating that estrogen-deficient rats have a larger effective lacunar-canalicular porosity surrounding osteocytes as measured by a small molecular weight tracer, with the change in effective canalicular size coinciding with nanostructural matrix-mineral level changes in the osteocyte lacunar-canalicular porosity [8]. This study was designed to further assess the changes in osteocyte viability and to test potential candidates causing bone degradation in the lacunar-canalicular network in estrogen-deficient rats.

Osteocyte apoptosis has been documented in microdamage, aging, disuse, and estrogen deficiency [9-14]. Osteocytes located near the sites of microdamage undergo apoptosis, which has been correlated with increased bone remodeling due to enhanced RANKL production [4, 10,15]. Cardoso et al. [10] showed that osteocyte apoptosis is necessary for microdamge removal, as inhibiting fatigue-induced apoptosis prevented activation of osteoclast resorption. With aging there is also an increase in osteocyte apoptosis, along with an increase in empty and hypermineralized lacunae [11,16]. Osteocytes have also been shown to die by apoptosis in the absence of loading [12]. Estrogen reduction studies have shown that osteocytes die in human cancellous and cortical bone and in OVX rat bone [13,14]. It has been proposed that osteocyte

apoptosis seen after estrogen loss, glucocorticoids and disuse is a non-targeted process [14,17]. However, Emerton et al. [9] demonstrated that osteocyte apoptosis occurs non-uniformly in cortical bone of ovariectomized (OVX) mice, with increased apoptotic osteocytes in regions that are subsequently resorbed and consist of an irregular canalicular network, demonstrating that osteocyte apoptosis caused by estrogen reduction may be a targeted process. Impaired fluid flow due to the presence of an irregular canalicular network may perhaps be the cause of increased osteocyte death.

The precise mechanism by which osteocyte viability is altered is not known; however, it is postulated that fluid flow may have a role in preventing apoptosis. Bones of osteoporotic patients have demonstrated that regions with low osteocyte density correspond to areas that sustain fractures [18]. It has also been suggested that estrogen might have the ability to alter the equilibrium strain set point of bone such that the response to strain levels and rates are dampened or not felt by osteocytes in the absence of estrogen [19]. The three most likely possibilities of how osteocyte cell viability may be altered due to estrogen deficiency are: 1) By the loss of protective estrogen's antioxidant effect, 2) By downregulation of estrogen receptor proteins, which have been shown to be stimulated by fluid flow, and 3) By altered or diminished number of tethering elements caused by microstructural alterations in the osteocyte lacunar-canalicular network [8,20].

The ability of matrix metalloproteinases (MMPs) to degrade matrix proteins in the osteocyte lacunar-canalicular network of estrogen-deficient rats has not yet been explored. Osteocytes express several MMPs; of these, MMP-2 and MMP-3 can cleave substrates similar to those present in the osteocyte lacunar-canalicular microenvironment, including osteopontin, perlecan, fibronectin, vitronectin, aggrecan and bone sialoprotein [21-26]. MMP-2 and MMP-3

are initially synthesized as inactive zymogens with a pro-peptide domain that are removed before the enzyme becomes active. MMP-2 degrades collagens type I, IV, V, VII, X, and XI, fibronectin, elastin, laminin, vitronectin, and tenascin [24]. It is the most abundant enzyme in the MMP family that is secreted by osteoblasts and osteocytes and is known to play a crucial role in forming and maintaining the osteocytic canalicular network in growing animals [22,27,28]. Cancellous bone tissue extracts from 9-month-old estrogen-deficient rats have shown significantly increased MMP-2 levels (both pro and active forms) as detected by gel zymography [29]. Serum MMP-2 levels have been shown to be significantly higher in postmenopausal women [30]. MMP-3, on the other hand, degrades aggrecan, fibronectin, vitronectin, perlecan, decorin and laminin [24,31]. Active MMP-3 expression has also been detected in osteocytes of neonatal rib bone and the matrix surrounding osteocytic lacunae [32]; and osteoblasts, the predecessors of osteocytes, have been shown to upregulate MMP-3 synthesis following estrogen withdrawal [33]. Commonalities in substrate cleavage by MMPs and those present in the osteocytic network, and their upregulation in osteocytes and osteoblasts due to estrogen-deficiency make them likely candidates causing alterations in the osteocyte lacunar-canalicular network.

The goals of this study were to assess the effects of estrogen reduction on osteocyte apoptosis and to test matrix metalloproteinases MMP-2 and MMP-3 as potential candidates of bone degradation in the osteocyte lacunar-canalicular network using a rat ovariectomy (OVX) model of postmenopausal osteoporosis. Temporal and spatial patterns of osteocyte apoptosis, as measured by cleaved caspase-3, and MMP-2 and MMP-3 were quantified in the osteocyte lacunar-canalicular network. Increased osteocyte apoptosis has the potential to alter fluid flow in the osteocyte lacunar-canalicular network, and since MMP-2 and MMP-3 are secreted by

osteocytes and osteoblasts and their activity is modulated following estrogen deficiency, it makes them likely candidates for bone degradation in the osteocyte lacunar-canalicular network.

2. Material and Methods

2.1 Osteoporosis model and experimental design

The ovariectomized (OVX) rat was used as a model for postmenopausal osteoporosis to study bone loss due to estrogen deficiency [34,35]. Twenty-week-old rats were used to avoid the modeling effects on the rat skeleton caused by rapid growth that produces significant bone turnover in the proximal tibia [36,37]. The study was approved by the Institutional Animal Care and Use Committee at the Hospital for Special Surgery.

Fifty-four female Sprague Dawley rats (Harlan Laboratories) were divided into two groups, with one group undergoing ovariectomy (OVX, n=27) and the other group acting as control (SHAM, n=27). The ovaries were surgically removed in the OVX group and the SHAM group underwent sham surgery where the ovaries were exposed but not removed. Nine animals from both groups were sacrificed at three different time points: one, two and six weeks post-surgery. These particular time points were used to examine bone turnover at the early osteoclastic resorptive stage (1 week), at the peak of bone resorption during estrogen-deficiency (2 weeks), and when bone turnover has plateaued (6 weeks) as seen in 3-month-old rats [38]. Animals sacrificed at the first time point were acclimatized one week after surgery and fed ad libitum. The OVX groups sacrificed 2- and 6-weeks post-surgery were pair-fed to the average food intake of the SHAM group. Uterine horns were weighed to confirm ovariectomy at sacrifice. Animal weights were also recorded at sacrifice.

The work was divided into two studies that examined the osteocyte lacunar-canalicular network: quantification of MMP-2 and MMP-3, OVX n=6, SHAM n=6 per time point (1, 2 and 6 weeks post-surgery) and quantification of osteocyte apoptosis, OVX n=3, SHAM n=3 per time point (1, 2 and 6 weeks post-surgery).

2.2 Sample preparation

The analysis was focused on the proximal tibia, where significant bone loss is seen in the proximal tibia following OVX [39,40] and where changes in the osteocytic network were observed [8]. The tibiae of each rat were harvested, cleaned of soft tissue, cut ~2 mm below the growth plate, and immediately placed in zinc-buffered formalin for 72 hours at 4^{o}C. After fixation, samples were decalcified in formic acid for 4 days, and embedded in paraffin wax or methylmethacrylate (MMA) resin for the osteocyte apoptosis or MMP analysis, respectively. 5 μm paraffin-embedded or 4 μm MMA-embedded cross sections were cut from the cortical tibial metaphysis and adhered to glass slides (Fig. 3.1). MMA resin enabled better preservation of the osteocyte lacunar-canalicular morphology, which was crucial for visualizing MMP staining in canaliculi. MMA-embedded sections were adhered to glass slides using Haupt's adhesive solution.

2.3 Immunohistochemistry protocols for cleaved caspase-3, MMP-2, and MMP-3

Immunohistochemistry protocols were used to quantify osteocyte apoptosis and MMPs in the osteocyte lacunar-canalicular network. Sections were deparaffinized or deplasticized, rehydrated and treated with 3% hydrogen peroxide to inhibit endogenous peroxidase activity, and blocked for 30 minutes afterward. Nonspecific tissue binding was inhibited by incubating tissue sections in protein block (Dako and/or Rodent Block R, Biocare Medical, CA) for 30 minutes at room temperature. Specimens were incubated in a humidified chamber overnight at 4º C with either MMP-2 (1:500), MMP-3 (1:50) (ab37150 & ab52915 respectively, Abcam, Cambridge MA), or cleaved caspase-3 primary (1:1000) (Cell Signaling #9116, Carpinteria, CA)

antibody. Osteocyte apoptosis was quantified via the cleaved caspase-3 pathway. Caspase-3 is the last effector caspase that is activated for cell destruction [41] and has been used in many studies as an endpoint for apoptotic cell death [9,10]. Detection was performed using secondary antibody (HRP polymer, Biocare Medical) and developed with DAB substrate chromogen system (Vector Laboratories, Burlingame, CA). Sections were counterstained with toluidine blue, dehydrated and coverslipped with mounting medium. Optimal dilution for the primary antibody was determined using internal positive control tissues (growth plate or articular cartilage). Negative staining controls were established by applying rabbit serum without the primary antibody in each immunostaining protocol.

For qualitative analysis of MMP signal within the canaliculus, a fluorescent secondary antibody (Alexa Probes, 488nm) was also used. This was preformed to assess if MMPs were present in the osteocyte canaliculi that can degrade matrix proteins in the immediate environment of the osteocyte processes. Using a confocal microscope system (Leica TCS SP2), scans were taken with a 63x oil immersion lens (1.4 numerical aperture, -1 offset, pinhole set at 1 Airy unit) and wavelength excitation of 488 nm. Confocal images were taken at a resolution of 2048 x 2048 pixels with a field view of 375 µm x 375 µm.

2.4 Quantification of cleaved caspase-3, and MMP-2 and MMP-3

To assess spatial differences in osteocyte apoptosis and MMP presence, the cortical metaphysis sections were divided into four anatomical locations and three regions of interest (ROI): endocortical (E), intracortical (I) and periosteal (P), through the cortical width (Fig. 3.1). Each sampled ROI was 87.5 µm x 77.5 µm. For both SHAM and OVX groups, stained and non-stained osteocytes were counted under brightfield microscopy at 40X magnification. Cleaved

caspase-3 or MMP positively stained osteocytes (casp+ Ot, MMP 2+ Ot or MMP 3+ Ot) appeared as brown-colored cells, and non-stained cells were colored blue by the toluidine counterstain. Cell bodies that were 50% or more inside the ROI were counted. Three sections per animal, at least 16 μm apart, were used to quantify cleaved caspase-3 or MMP positive osteocytes using this approach, such that approximately 100 osteocytes were assessed per rat.

2.5 Statistical analysis

For the cleaved caspase-3 and MMP analyses, the percent cleaved caspase-3 positive osteocytes (% casp+ Ot) and the percent MMP-2 and -3 positive osteocytes (% MMP 2+ Ot and % MMP3+ Ot) were analyzed. Spatial differences in cleaved caspase-3 and MMP presence in the endocortical (E), intracortical (I) and periosteal (Pe) regions were assessed at each of the three time points (1, 2 and 6-weeks surgery) using two-way repeated-measures ANOVA with Bonferroni post-hoc tests for the two factors: treatment (OVX and SHAM) and location (E, I and Pe). Pooled whole cross-sectional analysis was performed for cleaved caspase-3 and MMP presence using two-way ANOVA with Bonferroni post-hoc t-tests for the two factors: treatment (OVX and SHAM) and time (1, 2 and 6 weeks post-surgery). All the statistical analyses were performed with the Prism 5 statistics software package (GraphPad Software Inc.).The normality of all data sets was confirmed before using parametric tests, and the significance level was set at $p < 0.05$.

3. Results

The effectiveness of ovariectomy was verified by the absence of ovaries. Uterine horn weights were significantly less at all time points in OVX rats compared to SHAM. Despite pair-feeding, the OVX rats weighed significantly more than SHAM rats at 2 and 6 weeks post-surgery (Table 3.1).

3.1 Quantification of cleaved caspase-3 in osteocyte lacunae

Cleaved caspase-3 positive cells were clearly visualized in the osteocyte lacunae in the chromogenic stained sections (Fig. 3.2). Ovariectomy caused an approximately 4-fold increase in overall osteocyte apoptosis within the tibial metaphyseal cortex at 1 and 2 weeks post-surgery, while at 6 weeks post-surgery, osteocyte apoptosis was not significantly different in OVX compared to SHAM controls (Fig. 3.3a). There were no differences in cleaved caspase-3 in the four anatomical regions analyzed (A, P, M, L) (data not shown).

Spatial differences in osteocyte apoptosis of the four anatomical locations (A, P, M, L) were not observed in the endocortical (E), intracortical (I) and periosteal (Pe) regions. Apoptotic activity was significantly increased in the endocortical, intracortical, and periosteal regions of OVX rats at 1 and 2 weeks post-surgery compared to SHAM, while no significant differences were observed between OVX and SHAM in any of three regions at 6-weeks post-surgery (Fig. 3.3 b-d).

3.2 Quantification of MMP-2 and MMP-3 in osteocyte lacunae

MMP-2 positive osteocytes were clearly visualized in the osteocyte lacunae and canaliculi in both chromogenic and fluorescently stained sections (Figs. 3.4 & 3.5). While MMP-2 staining was not significantly different between SHAM and OVX at any time point, MMP-2 activity was significantly decreased in SHAM at 6-weeks compared to the 1-week time point, such that the presence of MMP-2 6 weeks post-surgery was almost larger in OVX compared to SHAM ($p=0.0582$). In the estrogen-deficient animals, MMP-2 presence remained close to baseline levels in the osteocyte lacunar-canalicular network over time (Fig. 3.6a).

MMP-3 stained osteocyte lacunae were observed, but no staining was seen inside the canalicular network. No significant differences were observed in MMP-3 staining between SHAM and OVX at any time point. However, MMP-3 activity was significantly increased at 6 weeks post-surgery in both SHAM and OVX (Fig. 3.6b).

4. Discussion

The results of this study demonstrate that osteocyte viability is altered due to estrogen deficiency, and MMP-2 and MMP-3 are not primary candidates of bone degradation that may create nanostructural matrix changes in the osteocyte lacunar-canalicular environment in estrogen-deficient rats. Osteocyte apoptosis, as measured by cleaved caspase-3 activity, increased in estrogen-deficient rats at 1 and 2 weeks post-surgery and returned to control levels at 6 weeks. Furthermore, this activity was observed to be distributed throughout the cortical width. The MMP analysis demonstrated that significant differences were not found in MMP-2 and MMP-3 presence between SHAM and OVX groups at the time points analyzed, although a non-significant increased trend was observed in MMP-2 in OVX rats at 6-weeks post-surgery.

Parfitt [17] proposed that bone remodeling was a ‘stochastic’ or ‘targeted’ process. Targeted remodeling has been shown in studies of microdamage and estrogen loss. Verborgt et al. [42] demonstrated that bone areas that show increased osteocyte death due to microdamage was subsequently resorbed. Other studies suggest a relationship between cell death and bone turnover. Spatial and temporal associations of osteocyte apoptosis have been demonstrated following estrogen withdrawal in humans and animals [9,43,44]. Noble et al. [44] found that there was a non-uniform distribution of apoptotic osteocytes in human cancellous bone. Hedgecock et al. [43] showed in rabbit cortex that remodeling occurred in areas where osteocytes died. Emerton et al. [9] demonstrated that osteocyte apoptosis occurred in a non-random manner; areas that exhibited increased osteocyte apoptosis were the same regions that were resorbed at a subsequent time point. In our study osteocyte apoptosis increased in estrogen-deficient rats at 1 and 2 weeks post-surgery and returned to control levels at 6 weeks following estrogen withdrawal, and osteocyte apoptosis did not increase in any preferential region. Similar temporal increases in osteocyte apoptosis have been shown to occur after immediate loss of estrogen that fall to control levels later on [9].

A role of reactive oxygen species in increasing osteocyte apoptosis is suggested in several aging studies. Osteocyte death due to aging is thought to be caused by loss of estrogen and accumulation of reactive oxygen species (ROS) in women [45]. ROS has been shown to stimulate osteoclast differentiation, formation, and activity [11,46]. Increased ROS levels have been demonstrated in the bone marrow of OVX mice and the introduction of antioxidants has shown to decrease the OVX-induced bone loss [46]. Estrogen is an antioxidant and the absence of it creates oxidative stress in cells. Administering animals with estrogens prevents H_2O_2-induced oxidative damage [47]. Therefore, the increased osteocyte apoptosis following estrogen

loss in our study may be a result of increased oxidative stress to the osteocytes. Other factors for increased apoptosis besides age-related stress include microstructural alterations as seen by microfractures. Osteocytes are bathed in interstitial fluid that enables transport of molecules in the lacunar-canalicular network by dynamic mechanical loading. Microdamage has the potential to sever the osteocyte canalicular network, which could alter cell viability by causing diminished fluid flow.

It is postulated that there are two ways that osteocytes may sense the fluid flow in vivo: by strains experienced by tethering attachment sites as fluid flows through the canaliculus [23], or by receptor proteins like ERalpha, which may be triggered by shear stresses caused by the fluid flow over the osteocyte processes. Cell viability may then be altered either by a diminished number of tethering elements caused by microstructural alterations or by a decreased number of cell surface receptor proteins, which are shown to be down-regulated in the absence of estrogen [20]. Future studies are being designed to study whether tethering connections are altered in estrogen-deficient rats possibly due to the nanostructural matrix-mineral level changes in the lacunar-canalicular network, which may elicit a direct relation between structural changes of the osteocyte microenvironment and osteocyte apoptosis.

Limitations of this study are related to the type of fixative used and the immunohistochemistry techniques. The measured cleaved caspase-3 levels are higher than previous reports for controls (~5% casp+ Ot), which may be due to the zinc-fixative used for tissue fixation, as it has been shown to increase antigenicity [48]. The higher caspase levels compared to the previous studies may also be due to the difference in anatomical site; the cortical proximal tibial metaphysis was analyzed in this study. Immunohistochemistry techniques have limitations with regard to commercially available antibodies. Although immunohistochemistry

demonstrates the quantity of MMP protein, the approach is restricted by currently available antibodies that do not differentiate between latent and proteolytically active forms of the enzyme. Electrophoretic techniques such as zymography that require tissue homogenization or in situ approaches that use fluorescent markers can be used to demonstrate active MMP quantities, but are restricted to how the sample is prepared as well as low signal strengths [29]. Despite these limitations, identifying MMP presence specifically in the osteocyte lacunar-canalicular network makes immunohistochemistry the best technique because it clearly demarcates the response from osteocytes and is not limited by signal strength.

While this study found no significant differences in MMP-2 and MMP-3 levels in estrogen-deficient rats, it is possible that other MMPs besides MMP-2 and MMP-3 need to be studied in future experiments. Continued work in our laboratory will test other MMP candidates such as MMP-13 and MMP-14. MMP-13 has recently been shown to be necessary for lactation-induced osteocyte perilacunar remodeling [49], and MMP-14 has recently been shown to modulate mechanosensitivity affecting bone mass [50]. MMP-14 levels are also shown to be affected by estrogen deficiency [51,52]. Thus, there may be a link between other MMPs and bone matrix degradation around the osteocyte lacunar-canalicular network that needs to be further tested. Additional studies that identify the exact mechanisms by which degradation occurs in the osteocyte microenvironment and how it contributes to diminished bone quality after estrogen withdrawal will help in the design of approaches to treat and potentially prevent postmenopausal osteoporosis.

Table 3.1. Uterine horn and animal weights for the three time points analyzed. Values expressed as mean ± standard deviation. SHAM: control (n=9 per time point); OVX: ovariectomized (n=9 per time point).

	1 week		2 weeks		6 weeks	
	SHAM	**OVX**	**SHAM**	**OVX**	**SHAM**	**OVX**
Uterine horns (g)	0.49 ± 0.06	0.25 ± 0.03*	0.53 ± 0.10	0.19 ± 0.04*	0.72 ± 0.23	0.14 ± 0.03*
Body weights (g)	224 ± 5.2	235 ± 8.0	231 ± 21	262 ± 8.3*	238 ± 11	290 ± 14*

* Different from SHAM at same time point ($p < 0.05$)

Figure Captions

Fig. 3.1 (a) A schematic of the rat tibia showing the metaphysis region where cross sections were analyzed for MMP and cleaved caspase-3 staining. (b) Schematic of a cortical tibia metaphysis cross section showing the four anatomical locations (**A** = anterior, **P** = posterior, **M** = medial, **L** = lateral) analyzed. The three regions of interest analyzed (Endocortical (E), Intracortical (I), Periosteal (Pe)) are also indicated.

Fig. 3.2 (a) Hypertrophic chondrocytes and (b) osteocytes positively stained for cleaved caspase-3; Black arrows indicate positively stained cells; scale bars = 20 μm.

Fig. 3.3 (a) Osteocyte apoptosis over the time-course of the experiment. Data pooled for all anatomical locations (A, P, M, L). Osteocyte apoptosis was significantly increased 1 week post-ovariectomy (OVX) and remained elevated at 2-weeks post-surgery (*$p < 0.05$); osteocyte apoptosis was not significantly different from SHAM controls at 6 weeks. Osteocyte apoptosis across the cortical width in the endocortical (E), intracortical (I) and periosteal (P) regions at (b) 1 week, (c) 2-weeks, and (d) 6-weeks post-surgery (*$p < 0.05$).

Fig. 3.4 (a) Hypertrophic chondrocytes and (b) osteocytes positively stained for MMP-2, and (c) articular cartilage chondrocytes and (d) osteocytes positively stained for MMP-3. Arrows indicate positively stained cells; scale bars = 50 μm.

Fig. 3.5 (a) Image taken with confocal microscopy of fluorescently-labeled osteocyte lacunae and canaliculi, and (b) chromogenic-labeled osteocyte canaliculi showing positive staining for MMP-2; positive staining (yellow arrows) are indicated; scale bars = 10 μm.

Fig. 3.6 Matrix metalloproteinase (MMP) changes over time between SHAM operated and ovariectomized (OVX) rats (a) % positive MMP-2 osteocytes (% MMP 2+Ot), and, (b) % positive MMP-3 osteocytes (% MMP 3+Ot) over the time-course of the experiment (*$p < 0.05$).

Fig. 3.1

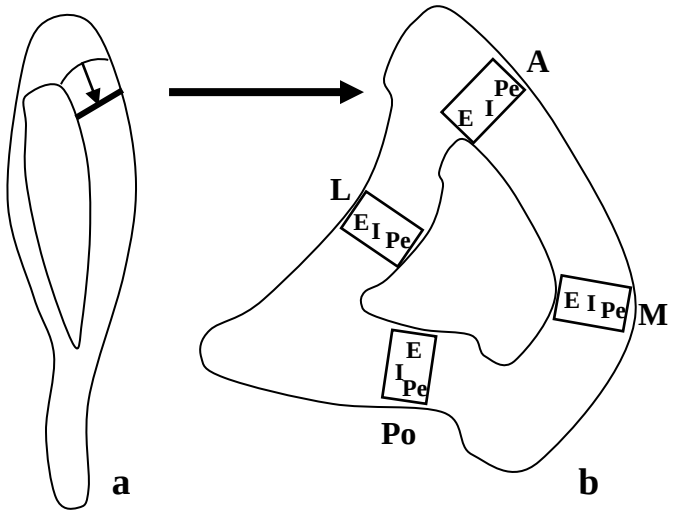

Fig. 3.2

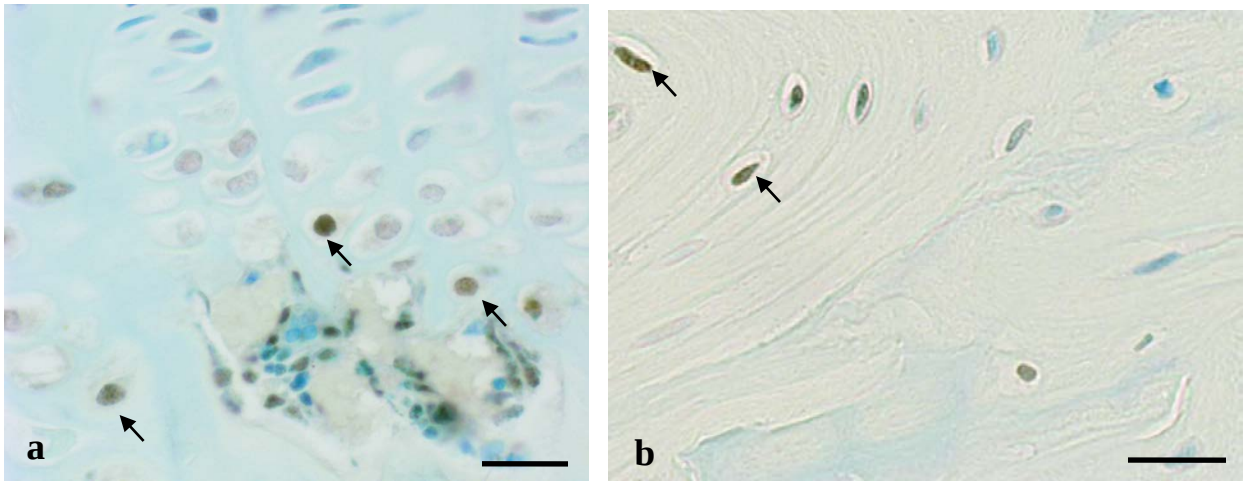

Fig. 3.3

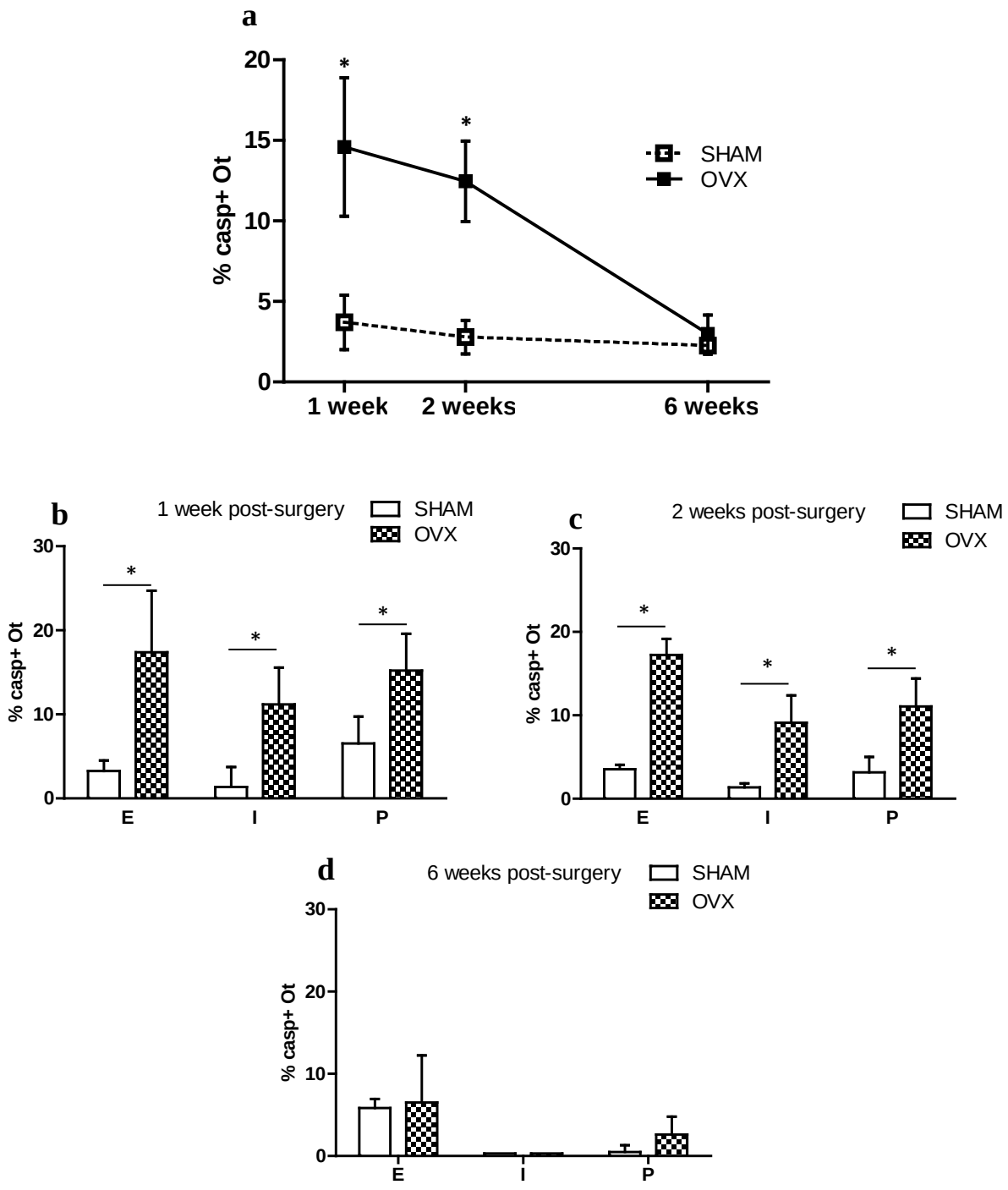
a
% casp+ Ot
20
15
10
5
0
*
*
SHAM
OVX
1 week
2 weeks
6 weeks
b
1 week post-surgery
SHAM
OVX
% casp+ Ot
30
20
10
0
*
*
*
E
I
P
c
2 weeks post-surgery
SHAM
OVX
% casp+ Ot
30
20
10
0
*
*
*
E
I
P
d
6 weeks post-surgery
SHAM
OVX
% casp+ Ot
30
20
10
0
E
I
P

Fig. 3.4

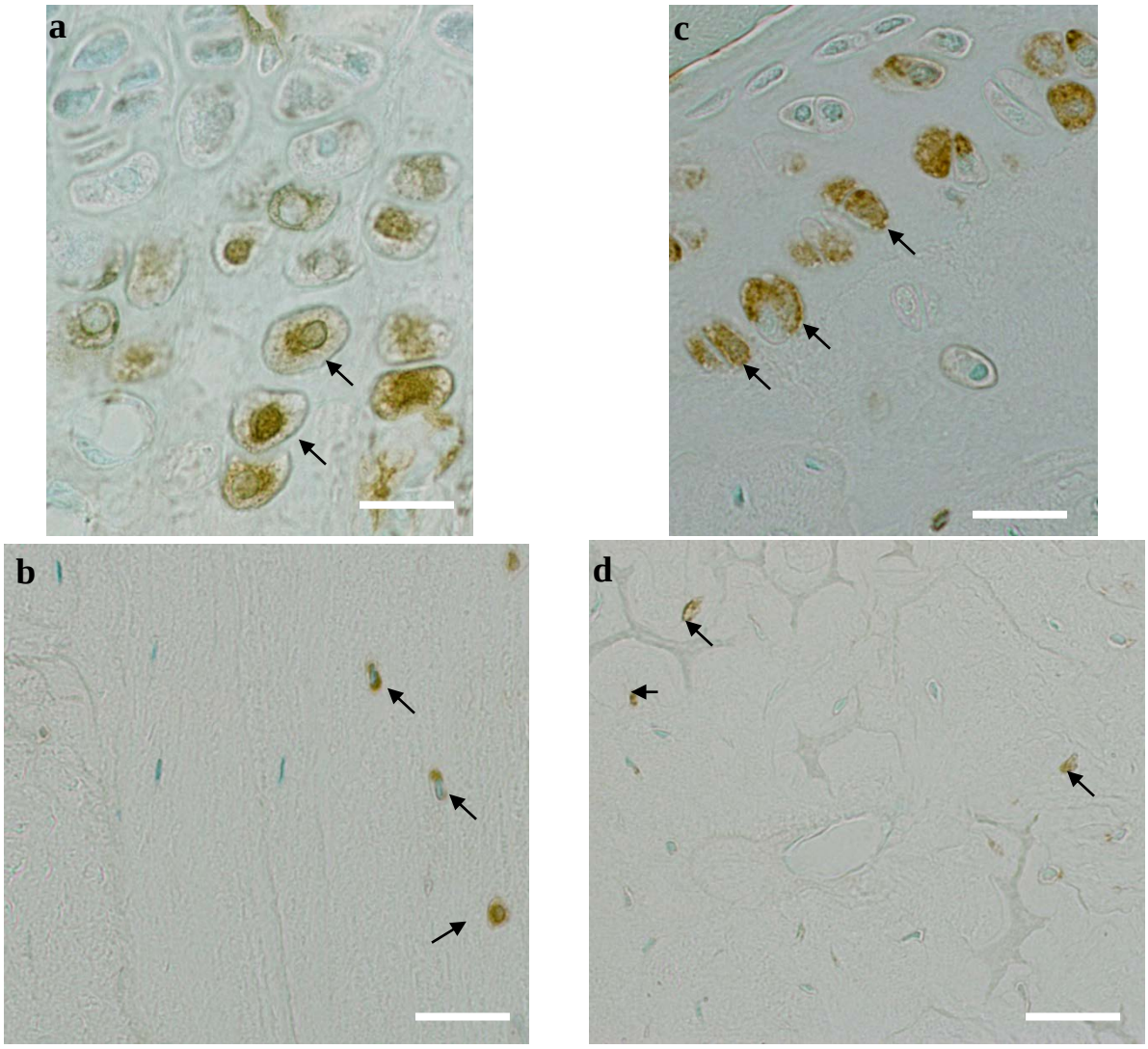

Fig. 3.5

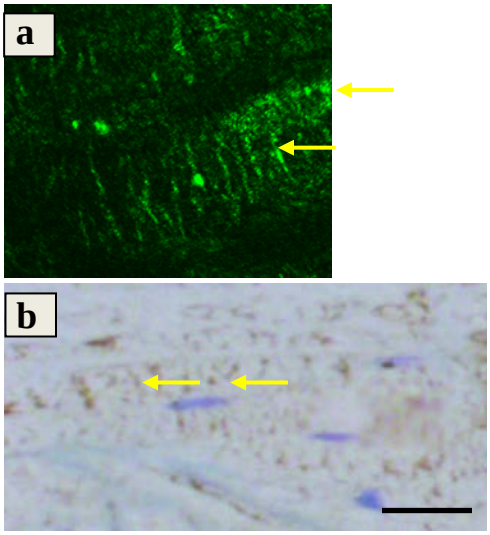

Fig. 3.6

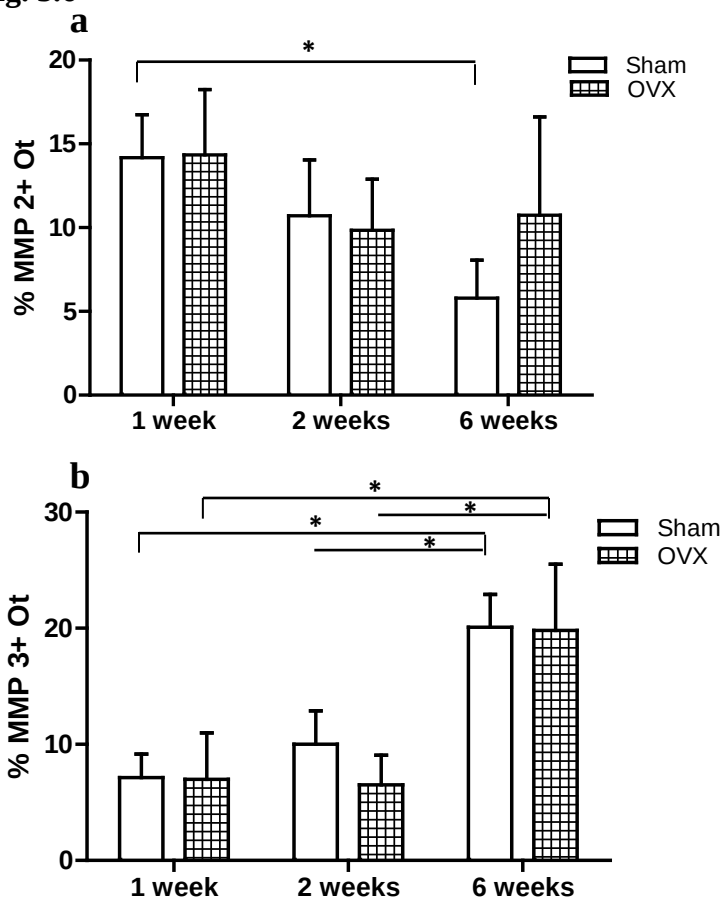
a
*
Sham
OVX
% MMP 2+ Ot
20
15
10
5
0
1 week
2 weeks
6 weeks
b
*
*
*
*
Sham
OVX
% MMP 3+ Ot
30
20
10
0
1 week
2 weeks
6 weeks

CHAPTER 4

ASSESSING BONE TURNOVER IN ESTROGEN-DEFICIENT RATS USING FLUORESCENT BONE LABELING AND NANOINDENTATION

Abstract

Increased bone turnover during postmenopausal osteoporosis contributes to bone loss and decreased mechanical integrity of bone tissue. Previous work from our laboratory using the rat ovariectomy (OVX) model of postmenopausal osteoporosis demonstrated that a larger effective canalicular size and nanostructural matrix-mineral level changes occurred in the osteocyte lacunar-canalicular porosity of estrogen-deficient rats. In the current study, bone turnover and mineral changes were studied in OVX rats using fluorescent bone labels and nanoindentation. Twenty-week-old female Sprague Dawley rats were ovariectomized to study bone remodeling changes occurring 6-weeks post-surgery in the proximal tibial metaphysis, where significant bone loss occurs after estrogen loss. Rats were given calcein and xylenol orange, dynamic labels of bone formation and mineralizing surfaces, at day 11 and 3 before sacrifice, respectively. To assess alterations in the degree of mineralization of the matrix surrounding the osteocytes of estrogen-deficient rats, changes in elastic modulus and hardness were determined by nanoindentation. Mineral apposition and bone formation rates increased at the endocortical surfaces in OVX rats, while no changes were seen in percent mineralizing surfaces on the periosteal surface. A non-significant trend of increasing percent mineralizing vascular pores was also seen in OVX. The elastic modulus (SHAM: 23.3 ± 1.19 GPa; OVX: 22.6 ± 1.88 GPa) and hardness (SHAM: 0.78 ± 0.04 GPa; OVX: 0.79 ± 0.05 GPa) were unaltered due to estrogen deficiency. Together, the bone labeling and nanoindenatation results suggest that the nanostructural matrix-mineral level changes in the osteocyte lacunar-canalicular porosity of estrogen-deficient rats demonstrated in our previous work are indeed due to alterations occurring on the local surfaces of the osteocyte lacunae and canaliculi, and not because of bone matrix changes occurring by a change in mineralization of OVX tissue due to bone turnover.

1. Introduction

Postmenopausal osteoporosis occurs after the sharp reduction in estrogen after menopause, and is characterized by an increase in bone remodeling, leading to decreased bone mass, decreased strength, and increased fracture risk [1, 2]. Several parameters, such as bone porosities, trabecular and cortical architecture, and mineral-matrix content and organization determine bone strength [3-5]. The deteriorating effects of estrogen loss on the architecture and mechanics of bone are becoming increasingly well understood in terms of altered bone macro-structure and a decrease in bone mineral density (BMD) [5-7]. However, the role that altered nanostructural elements play in the pathophysiology of osteoporosis still needs to be better understood.

Previous work from our laboratory using high-resolution techniques demonstrated alterations in the osteocyte microenvironment in the rat ovariectomy (OVX) model of osteoporosis. Confocal microscopy analyses demonstrated that OVX increased the effective lacunar-canalicular porosity surrounding osteocytes in cortical and cancellous bone from the rat tibia metaphysis, with the increase in porosity largely explained by increased canalicular diameter, as measured by penetration of a small molecular weight dye. Furthermore, electron microscopy analyses indicated nanostructural matrix-mineral level surface changes in the osteocyte lacunae and canaliculi in OVX rats [8]. These changes were better characterized in this study using bone labels and nanoindentation.

Several studies have used bone labels to identify histomorphometric indices of mineral apposition and bone formation to study the high bone turnover that takes place following estrogen withdrawal. Wronski et al. [9,10] used fluorochrome labels to show that rats ovariectomized at 3 months had a marked increase in cancellous bone formation for several

months after surgery compared to controls. Rats ovariectomized at 7 months of age showed increased periosteal and endocortical bone formation rates in the cortical bone of the tibial diaphysis 12 weeks after surgery [11]. Higher bone turnover experienced by OVX rats can increase bone formation rates and the amount of newly deposited bone that would first go through a phase of rapid primary mineralization and a slower secondary mineralization phase [9,10,12,13]. For this reason, it becomes important to differentiate between newer, lower-mineralized bone versus older, higher-mineralized bone.

Nanoindentation helps characterize the mechanical behavior of bone at the submicrostructural level and has been used to study changes occurring due to estrogen deficiency [14-16]. Using nanoindentation, mechanical properties of structural units such as lamellae and interlamellae in cortical bone [17-19] and trabecular bone in different locations [14,19-21] have been characterized. This technique has the advantage that it can measure mechanical properties of mineral and mineral organization [14,15,20]. Nanoindentation has the potential to detect submicron level changes in bone quality parameters like elastic modulus and hardness of both dry and wet bone tissue with a high spatial resolution (~1μm or less) [22]. Microscopic and nanoscopic studies have assessed the effects of estrogen withdrawal on the arrangement of the submicron building blocks of bone. Using electron microscopic imaging it has been shown that collagen fibers and mineral crystal may change due to estrogen withdrawal [23-25]. Nanoindentation of cancellous bone from ovariectomized rat vertebrae and proximal tibiae shows that estrogen deficiency causes a loss of bone mass but the elastic and hardness properties of the remaining bone tissue are unchanged [26-30]. Other studies have also shown that estrogen deficiency decreases elastic modulus in OVX sheep compared to controls, while there is no change in hardness in cancellous bone [20].

In the current study we assessed mineral changes in rats that underwent overiectomy at 20 weeks of age to better determine dynamic indices of mineralization and bone formation post-surgery since data do not exist on animals of this age. Fluorescent labels were used to determine mineral apposition and bone formation rates at the whole tissue level. Nanoindentation was also used to examine variations in the submicron properties of the mineralized matrix around the osteocytes in estrogen-deficient rats. These two methodologies together helped determine whether the nanostructural alterations observed in our previous work [8] were an effect of higher bone turnover experienced by estrogen-deficient rats.

2. Materials and methods

2.1 Ovariectomized (OVX) rat model

The ovariectomized rat was used as a model for postmenopausal osteoporosis [31]. Twenty-week-old rats were used to avoid the early, rapid growth stage that produces significant bone turnover in the proximal tibia [32,33]. Twenty-four female Sprague Dawley rats (Harlan Laboratories) were used of which twelve rats underwent ovariectomy (OVX, n=12) and were fed ad libitum for one week after surgery. The OVX rats were then pair-fed to the average food intake of control rats (20 g standard rat chow per day) for the remainder of the study. The control group (SHAM, n=12) underwent sham surgery where the ovaries were exposed but not removed. Six weeks post-surgery (at 26 weeks of age) rats from both groups (SHAM and OVX) were sacrificed because this duration of ovariectomy has previously been shown to produce significant bone loss in the proximal tibia similar to postmenopausal osteoporosis [9,34]. Uterine horn weights were also recorded to assess the effectiveness of ovariectomy. Twelve of the animals used in this study (SHAM n=6, OVX n=6) were also used in the studies described in Chapter 3.

Both the SHAM and OVX groups received two bone formation markers via the intraperitoneal (IP) cavity at 11 and 3 days before sacrifice (15 mg/kg calcein and 90 mg/kg xylenol orange, respectively) to assess histomorphometric indices of bone formation rate, mineral apposition rate and percent mineralizing surfaces. Bones from a subset of twelve animals (OVX, n=6; SHAM, n=6) were used for the nanoindentation study. All procedures were approved by the Institutional Animal Care and Use Committee at the Hospital for Special Surgery.

2.2 Sample preparation for histomorphometric and nanoindentation analyses

For cortical bone histomorphometric analysis, the right tibiae were fixed in phosphate-buffered formalin for 72 hours at 4^{o}C and remained undecalcified. Bones were embedded in PMMA and cortical cross sections (120 μm thickness) were cut from the proximal metaphysis at ~2 mm distal to the growth plate using a sawing microtome (Leica Instruments, Nussloch, Germany), polished to a final thickness of 70 μm, and then coverslipped.

For nanoindentation testing, the left tibiae were collected at the time of necropsy and tissue was kept frozen at -20 ^{o}C. Prior to embedding bones were thawed and cut using a diamond blade saw (Buehler) at the proximal metaphysis ~2 mm distal to the growth plate. Specimens were then placed in peel-away molds and filled with an epoxy resin (Loctite Medical Epoxy, M-21HP, Hysol), which does not infiltrate the tissue but merely holds it in place. The embedded specimens were polished first using silicon carbide abrasive papers of decreasing grit sizes (600, 800, and 1200 grit) under deionized water, then with 0.5 and 0.25 μm diamond bead suspension solution and sonicated between each polishing step to remove debris. Samples were then dehydrated overnight at room temperature before testing.

2.3 Mineral apposition and bone formation rates

Histomorphometric bone parameters were measured using a bone-specific image analysis semi-automated system, Osteomeasure software (OsteoMetrics Inc., Atlanta, GA). To assess bone formation rates, the following parameters were measured and calculated: double-labeled surface (dLS/BS, %); single-labeled surface (sLS/BS, %); mineralizing surface (MS/BS, %); mineral apposition rate (MAR, μm/day), calculated as the distance between double labels divided by interval labeling time; and bone formation rate (BFR/BS, $\mu m^3/\mu m^2$/day), calculated as MAR×MS/BS. For surfaces displaying a single label, the MS/BS value was recorded, while for those displaying double labels, MAR and BFR values were documented. Mineralizing vascular pores were quantified by counting fluorescently labeled vascular pores throughout the tibial cortex. Pores with 50% or more of their parameter labeled with the calcein label were considered to be stained and were divided by the total number of vascular pores to obtain the percent mineralizing vascular pores.

2.4 Nanoindentation testing

Load-control nanoindentation tests were performed on dry specimens using a Triboindenter^{TM} (Hysitron, MN) nanoindenter. A Berkovich diamond tip (a pyramidal-shaped indenter), with a defined elastic modulus of 1141 GPa and Poisson's ratio of 0.07, was calibrated using fused quartz crystals prior to testing. Load was applied at a constant rate by driving the indenter into the bone specimen. The maximum load (P_{max}) was held on the sample for 10 seconds, to minimize effects of viscoelastic deformation of the specimen. The indenter was unloaded at the same rate used in the loading step (Fig. 4.1). The loading creates a complex combination of elastic and post-yield deformation. When the load on the tip is released, the

elastic response of the material is detected. The slope at the point of initial unloading is used to derive the elastic properties of the sample. The indenter was held on the surface of the specimen for approximately 100 seconds to establish thermal drift before proceeding to the next indent.

For each tibia specimen, two matrices of 25 indents, 5 μm apart, were made in the anterior and posterior regions of the cortical proximal metaphysis (Fig. 4.2). The indents were each ~800 nm wide. The elastic modulus (E) and hardness (H) were measured in an osteocyte-rich area, which was identified using the optical microscope installed in the nanoindenter system. Identifying an osteocyte-rich area was important because the changes observed in our previous study were only in lamellar bone regions that can be identified as an area with a dense osteocyte lacunar-canalicular network [8]. The endocortical and periosteal regions were excluded for nanoindentation.

The load-displacement data from each indentation were used to calculate the elastic modulus (E) and hardness (H) using the Oliver and Pharr method [16]. The load can be expressed according to a power-law relationship, which is valid for the upper portion of the unloading curve (Fig. 4.3). This relation is of the form:

$$P = \alpha (h - h_f)^n \quad (1)$$

where α and n are the power-law fitting constants. Equation (1) is then differentiated at the maximum contact depth (h_{max}), with the initial slope of the unloading curve used to determine the elastic constant stiffness (S) (Fig. 4.3):

$$S = (dP/dh) \quad (2)$$

The contact stiffness (S) is used to calculate the reduced elastic modulus (E_r) using the Oliver and Pharr method [16]. The elastic modulus, E, is then calculated using

$$\frac{1}{E_r} = \frac{(1 - v_i^2)}{E_i} + \frac{(1 - v^2)}{E} \quad (3)$$

where E_i and v_i are the modulus and Poisson's ratio of the indenter, respectively. The Poisson's ratio of bone, v, is taken to be 0.3 [15,19]. Contact hardness (H) is defined as the hardness (H) at peak load (P_{max}).

$$H = P_{max} / A \quad (4)$$

2.5 Statistical analyses

Unpaired, two-tailed t-tests were used to assess differences between the SHAM and OVX groups for uterine horn weight, body weight, endocortical bone formation rates (Ec.BFR), endocortical mineral formation rates (Ec.MAR), periosteal mineralizing surface (Ps.MS/BS), percent mineralizing vascular pores, elastic modulus (E), and hardness (H). All the statistical analyses were performed with the Prism 5 statistics software package (GraphPad Software Inc.). The normality of all data sets was confirmed before using parametric tests, and the significance level was set at $p < 0.05$.

3. Results

3.1 Effectiveness of ovariectomy (OVX)

The effectiveness of ovariectomy was verified by the reduced weight of the uterine horns in the OVX rats (0.14 ± 0.02g) compared to SHAM (0.84 ± 0.34g). Despite pair-feeding, at 26 weeks of age the OVX rats weighed significantly more than the SHAM-operated control rats: OVX (n=12): 291 ± 18 g; SHAM (n=12): 239 ± 11 g.

3.2 Mineral apposition and bone formation rates

Animals that did not successfully receive the IP injections of calcein or xylenol orange were eliminated from the analysis. Thus, 6 SHAM rats and 7 OVX rats were analyzed for mineral apposition and bone formation rates, while percent mineralizing vascular pores (calcein label only) was analyzed in 9 SHAM and rats and 8 OVX rats.

Dynamic fluorochrome-based parameters indicated that bone formation rate and mineral apposition rate increased by 54% and 71%, respectively, on the endocortical surface in the OVX group. No significant bone formation was found on the periosteal surface of OVX. A non-significant trend was observed for percent mineralizing vascular pores in estrogen-deficient rats ($p = 0.072$) (Fig. 4.4, Table 4.1).

3.3 Analysis of material properties using nanoindentation

The results were pooled from the two anatomical locations analyzed (anterior and posterior) since no differences were observed within groups in the two locations. The elastic modulus (SHAM: 23.3 ± 1.19 GPa; OVX: 22.6 ± 1.88 GPa) and hardness (SHAM: 0.78 ± 0.04 GPa; OVX: 0.79 ± 0.05 GPa) in the proximal cortical tibial metaphysis did not change in the OVX group (Fig. 4.5a). The distributions of values were also similar between SHAM and OVX for E and H (Fig. 4.5b).

4. Discussion

The present study used bone labeling and nanoindentation techniques to determine dynamic bone changes of the mineralized matrix of estrogen-deficient rats that may occur due to higher bone remodeling. Previous work from our laboratory demonstrated that OVX increased

the effective lacunar-canalicular porosity surrounding osteocytes in cortical bone from the rat tibia metaphysis, with the increase in porosity largely explained by increased effective canalicular porosity, as measured by penetration of a small molecular weight dye [8]. Further analysis with electron microscopy demonstrated that the larger effective canalicular size in the estrogen-deficient state was due to nanostructural matrix-mineral level differences around the osteocyte canaliculi, and surface matrix changes were observed on lacunar surfaces [8]. Mineral apposition and bone formation rates were increased in OVX rats at the endocortical surfaces 6-weeks post-surgery, while no changes were seen in mineralizing surfaces on the periosteal surface. A non-significant trend of increasing percent mineralizing vascular pores was also seen in OVX rats. The nanoindentation analysis demonstrated that the elastic modulus and hardness were not altered due to estrogen deficiency. Since the degree of mineralization of bone tissue has been shown to be related to the mechanical properties of hardness and elastic modulus [14, 35] and no changes were observed in these parameters, the results suggests that the nanostructural matrix-mineral level changes observed in our previous study are indeed matrix-mineral changes occurring in the local surfaces of the osteocyte lacunae and canaliculi, and not because of a change in degree of mineralization of OVX tissue due to bone remodeling. A local mineral change in the immediate environment of the osteocytes suggests that these cells may play a role in mineral mobilization in diseased conditions like postmenopausal osteoporosis.

Nanoindentation helps identify differences in mechanical properties of bone tissue without homogenizing the bone tissue. Techniques that determine mineral differences at the microstructural level, e.g. x-ray diffraction, require powdering of the bone tissue, which makes it impossible to find local gradients in mineral characteristics. Other techniques like Fourier Transform Infrared Spectroscopy (FTIR) and micro-computed tomography (μCT) do not give

the resolution needed to assess nano-level mineral changes. Nanoindentation has been instrumental in identifying differences in mineralization of older and higher mineralized interstitial lamellar bone versus newer bone as in osteons [19]. It has also successfully shown that osteons have a mineralization and age gradient [36]. Future work will be done using quantitative backscattered electron imaging (qBSE), which helps assess mineral differences by giving high resolution (~1 μm) images. Thus, alterations of local surface minerals of the osteocyte lacunae in estrogen-deficient animals can be better detected by qBSE.

The values of elastic modulus and hardness found in the present study are similar to those found previously for human and rat bone tissue [22,29,37,38]. Trabecular bone from a 92-year-old female cadaver showed a mean elastic modulus of 20.8 GPa and mean hardness of 0.8 GPa [37]. Human cortical tibial osteons showed an elastic modulus of 22.4 GPa and hardness of 0.62 GPa and interstitial lamellae exhibited an elastic modulus of 25.7 GPa and hardness of 0.74 GPa values, respectively [15]. A few studies have examined the material properties of osteoporotic bone using nanoindentation. Lane et al. [29] showed that trabecular bone from OVX rat tibia exhibited elastic moduli ranging from 20 to 27 GPa and hardness values from 0.7 to 1.3 GPa. Hengsburger et al. [38] showed that the vertebral body cortex had an elastic modulus that ranged from 15 to 21 GPa and hardness 0.7 to 1 GPa.

Dehydration of bone tissue has been shown to affect its material properties. The dehydration process has been shown to increase tissue stiffness up to 22.6% [30]. An increased elastic modulus in osteonal and interstitial lamellae tissue (15% and 10%, respectively) and hardness (18% and 12%, respectively) have been documented in dehydrated bovine bone tissue [15]. It has also been postulated that drying of bone tissue contracts the individual fibrils, with contraction depending on the level of mineralization of the tissue [15]. As noted, dehydration of

bone may increase the material properties of elastic modulus and hardness; however, in our study this would occur similarly in both SHAM and OVX.

The observations from our previous work showing altered matrix-mineral nanostructural properties in the osteocyte lacunar-canalicular network of estrogen-deficient rats in combination with the current work imply that the nanostructural alterations seen in the ovariectomized rats are occurring in the immediate local environment of the osteocytes: the osteocyte lacunae and annular spaces of the canaliculi. Previous studies have implicated that osteocytes are metabolically active cells and may also have the capability to adapt to environmental changes [39,40]. Studies have shown that renal calcium absorption is substantially impaired in postmenopausal patients [41,42], and if an increased global demand of calcium ion can arises, mobilization of mineral ions from the osteocyte lacunar-canalicular network may be required. Future studies need to investigate whether mineral is being mobilized from the osteocytic network or whether matrix degradation is occurring in the osteocyte lacunar-canalicular porosity.

Table 4.1. Bone histomorphometric indices measured (mineral apposition and bone formation rates along with percent mineralizing surfaces). Values expressed as mean ± standard deviation. SHAM: control; OVX: ovariectomized.

	SHAM	**OVX**
Endocortical bone formation rate (Ec.BFR) ($\mu m^3/\mu m^2$/day)	0.68 ± 0.20	1.27 ± 0.32*
Endocortical mineral apposition rate (Ec.MAR) (μm/day)	1.62 ± 0.27	2.29 ± 0.44*
Periosteal mineralizing surface / bone surface (Ps.MS/BS) (%)	19.6 ± 6.5	22.5 ± 7.1
Mineralizing vascular pores (%)	16.3 ± 7.0	25.2 ± 12

* Different from SHAM ($p < 0.05$ vs. OVX)

Figure captions

Fig. 4.1 Loading profile used for the nanoindentation tests.

Fig. 4.2 A schematic representation of the rat tibia showing the regions analyzed. Cross sections at the proximal metaphysis (**M**) were analyzed for mineral apposition and bone formation rates as well as for nanoindentation. A matrix of 25 nanoindents 5 μm apart, was made in the anterior and posterior regions (**A** = anterior, **P** = posterior) of the cortical tibial metaphysis in an osteocyte-rich area.

Fig. 4.3 A representative load-displacement curve for a nanoindent made during one cycle of loading and unloading, showing quantities [peak load (P_{max}), the maximum displacement (h_{max}), and the initial loading stiffness (S)] used to determine elastic modulus and hardness properties.

Fig. 4.4 Calcein and xylenol orange labels in an OVX rat demonstrate double labels on the endocortical surface and single label in the vascular pore. Yellow dashed box shows a vascular pore labled with calcein in the cortical bone; scale bars = 100 μm

Fig. 4.5 The elastic modulus (E) and hardness (H) derived using nanoindentation of bone matrix surrounding osteocytes in the cortical proximal tibial metaphysis. (a) There were no significant differences in E and H between SHAM and OVX. Values expressed as mean ± standard deviation. (b) Box plots of E and H values showing the distribution of the 300 indents (50 indents per animal) in SHAM (n=6) and OVX (n=6).

Fig. 4.1

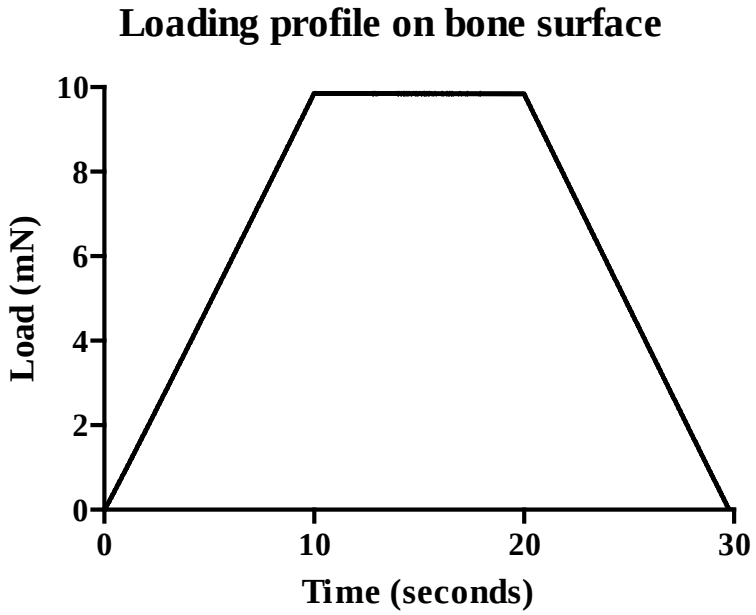
Loading profile on bone surface
Load (mN)
10
8
6
4
2
0
0
10
20
30
Time (seconds)

Fig. 4.2

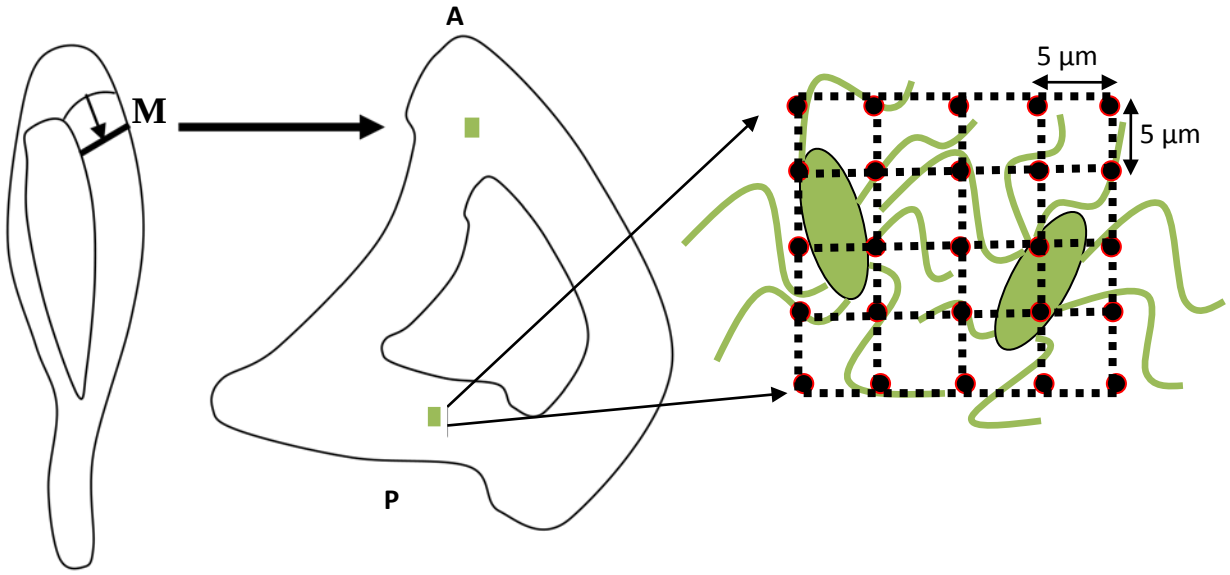

Fig. 4.3

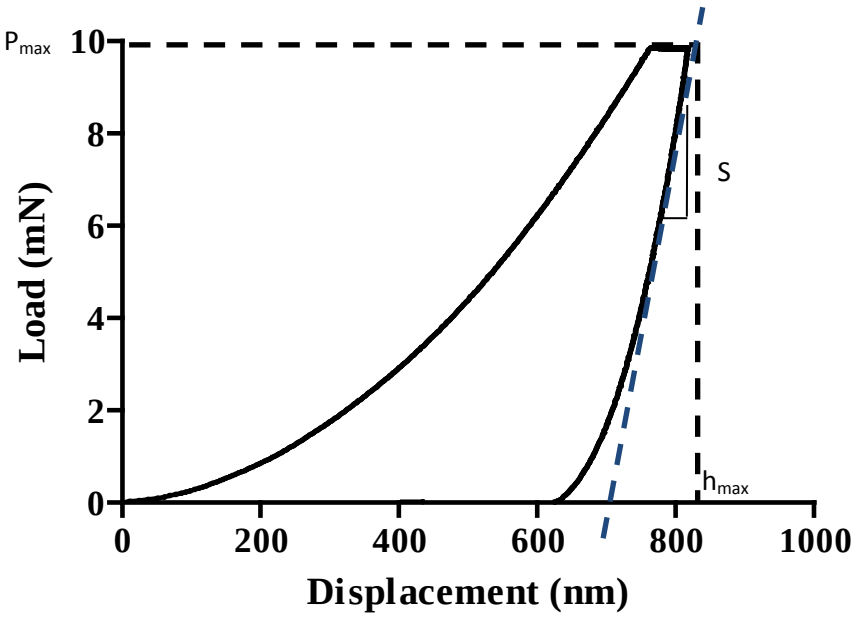
P_{max}
10
8
6
4
2
0
Load (mN)
S
h_{max}
0
200
400
600
800
1000
Displacement (nm)

Fig. 4.4

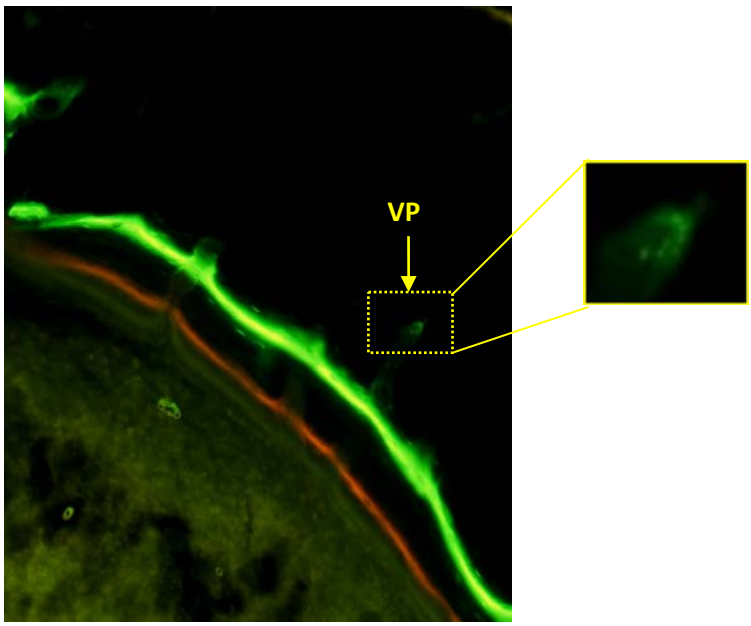

Fig. 4.5

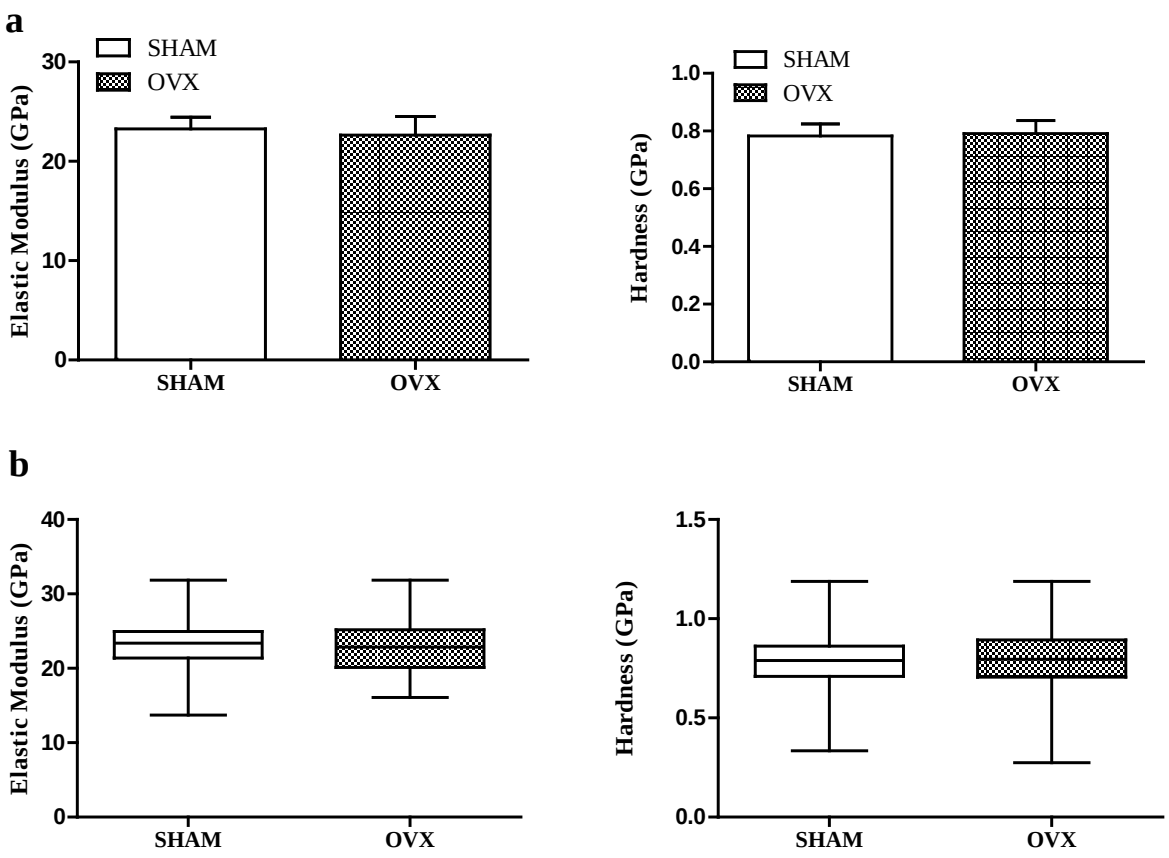
a
SHAM
OVX
Elastic Modulus (GPa)
30
20
10
0
SHAM
OVX
SHAM
OVX
Hardness (GPa)
1.0
0.8
0.6
0.4
0.2
0.0
SHAM
OVX
b
Elastic Modulus (GPa)
40
30
20
10
0
SHAM
OVX
Hardness (GPa)
1.5
1.0
0.5
0.0
SHAM
OVX

CHAPTER 5

GENERAL CONCLUSIONS AND FUTURE WORK

GENERAL CONCLUSIONS AND FUTURE WORK

The goal of this dissertation was to better understand bone degradation that occurs during postmenopausal osteoporosis by investigating how the osteocyte mechanical environment is altered in the estrogen-deficient state. The ovariectomized (OVX) rat was used as a model for postmenopausal osteoporosis, and the analysis focused on the proximal tibial metaphysis, where significant bone loss occurs during osteoporosis [1-3].

While it has been previously shown that osteoporosis causes bone macroarchitecture changes via a decrease in bone volume fraction, there is little analysis in the literature related to changes in the lacunar-canalicular porosity that houses the osteocytes. Studies in Chapter 2 determined whether the osteocyte lacunar-canalicular network is altered after loss of estrogen. To investigate alterations in the osteocyte microenvironment we utilized high-resolution microscopy techniques to assess several aspects of the osteocyte lacunar-canalicular network, including lacunar-canalicular porosity, lacunar area and volume, canalicular diameter and volume, and number of canaliculi per lacuna using the rat ovariectomy model of osteoporosis.

Results from Chapter 2 using confocal microscopy analyses indicated that OVX rats have a larger effective lacunar-canalicular porosity surrounding osteocytes in both cortical and cancellous bones from the proximal tibial metaphysis, with little change in cortical bone from the diaphysis or cancellous bone from the epiphysis. The increase in the effective lacunar-canalicular porosity in the tibial metaphysis was not due to changes in osteocyte lacunar density, lacunar size, or the number of canaliculi per lacuna. Instead, the effective canalicular size measured using a small molecular weight tracer was larger in OVX rats compared to controls. Further analysis using scanning and transmission electron microscopy demonstrated that the larger effective canalicular size in the estrogen-deficient state was due to nanostructural matrix-mineral

level differences like loose collagen surrounding osteocyte canaliculi. These matrix-mineral differences were also found in osteocyte lacunae in OVX, but the small surface changes did not significantly increase the effective lacunar size. This study is the first to perform a 3D characterization of the osteocyte lacunar-canalicular porosity in estrogen-deficient rats.

The results from Chapter 2 suggest that the changes occurring in the osteocyte lacunar-canalicular microenvironment are making the lacunar-canalicular surfaces more permeable, which could affect interstitial fluid flow around osteocytes during mechanical loading. An increased permeability of the lacunar-canalicular wall may alter both solute transport and interstitial fluid velocities around osteocytes during mechanical loading. It is also possible that alterations in the surface of the lacunar-canalicular network could disrupt the connections of the osteocyte process to the canalicular wall, impairing the capability of the osteocyte to perceive mechanical stimuli and potentially affecting the viability of the osteocyte. If the connections between osteocytes and the surrounding matrix are diminished due to ovariectomy, bone loss during postmenopausal osteoporosis could then be a remodeling response caused by reduced perceived loading in the presence of actual continued loading, where the bone cells may not be able to process the strain-related information effectively.

To build upon the findings of Chapter 2, future work needs to investigate whether the tethering connections between the osteocyte and the canalicular wall are altered in the estrogen-deficient state. Previous studies analyzing the tethering connections in control animals have used the mouse as the experimental model because perfusing mouse bone with electron microscopy fixative to preserve the proteoglycan components in the lacunar-canalicular network is relatively easier than in rats because mice are much smaller [4]. Thus, to study the tethering connections during estrogen deficiency it is recommended that ovariectomized mice are used. Additional

experiments could also be designed to assess the changes in lacunar-canalicular permeability due to OVX. An in vivo injection of two tracers, one that freely passes through the lacunar-canalicular porosity (e.g., albumin) along with a larger molecular tracer that has been shown to be excluded from the lacunar-canalicular pores (e.g., ferritin) [5] could be used to demonstrate an increase in permeability around osteocytes due to OVX.

Chapter 3 had two aims: to assess osteocyte apoptosis and to test potential candidates of bone degradation around the osteocyte in the estrogen-deficient state. The fist aim of Chapter 3 used an immunohistochemistry approach to quantify temporal and spatial patterns of osteocyte apoptosis in the cortical bone of the proximal tibial metaphysis in estrogen-deficient rats at 1-, 2-, and 6-weeks post-OVX. Results indicated that osteocyte apoptosis, as measured by cleaved caspase-3 activity, increased in estrogen-deficient rats at 1- and 2-weeks post-surgery and returned to control levels at 6 weeks. Furthermore, apoptotic osteocytes were observed to be uniformly distributed across the width of the tibial cortical bone. The role of osteoclast activity may need to be tested in future studies along with including trabecular bone from the tibial metaphysis in the analysis, in order to elucidate bone resorption and spatial and temporal patterns of apoptosis that may exist in the cancellous compartment, which goes through a high remodeling phase following estrogen loss [1-3].

The precise mechanism by which osteocyte viability is altered is not known; however, it is postulated that fluid flow may have a role in preventing apoptosis. Estrogen deficiency is postulated to affect osteocyte viability by the loss of protective estrogen's antioxidant effect, and by downregulation of estrogen receptor proteins, which have been shown to be stimulated by fluid flow. Cellular debris from dead and fragmented osteocytes could inhibit fluid flow by obstructing the lacunar-canalicular pathway and later possibly by hypermineralization of the

lacuna. Altered or diminished number of tethering elements that may occur due to the nanostructural alterations seen in Chapter 2 may also increase osteocyte apoptosis due to estrogen deficiency.

The second aim of Chapter 3 was to test for the presence of molecules that would have the capability to cause the nanostructural changes in the bone matrix surrounding osteocytes that was demonstrated in Chapter 2. The potential candidates tested were metalloproteinases MMP-2 and MMP-3, both of which have been shown to cleave substrates similar to those present in the osteocyte lacunar-canalicular microenvironment; in addition, their activity has been shown to be regulated by estrogens [6,7]. Temporal changes in MMP-2 and MMP-3 were assessed in the osteocyte lacunar-canalicular network in estrogen-deficient rats and no significant differences were found between SHAM and OVX at any time point. While MMP-2 levels decreased significantly in SHAM rats over time, they remained unchanged in OVX rats, although a non-significant trend of increased MMP-2 was seen in estrogen-deficient rats at 6-weeks post-surgery. This non-significant increase may be due to the activity of newly formed osteocytes on the endocortical surfaces or by the activity of older osteocytes present in the cortical bone. This difference needs to be further assessed in future studies. In addition, an increase in MMP-3 levels was seen in both SHAM and OVX groups over time. The increase of MMP-3 presence in controls may be due to periosteocytic remodeling of the non-collagenous proteins after the animal has surpassed its peak skeletal bone growth.

Because MMP-2 and MMP-3 levels were relatively unmodulated in the lacunar-canalicular network in the OVX rat model, it appears that these two MMPs do not play a critical role in bone degradation around osteocytes after estrogen withdrawal. Future work should test other matrix metalloproteinases, such as MMP-13 and MMP-14, to see whether they may be

involved in this process. MMP-13 has recently been shown to be necessary for lactation-induced osteocyte perilacunar remodeling [8], and MMP-14 has recently been shown to modulate mechanosensitivity, affecting bone mass [9]. Other potential candidates that could cause nanostructural degradation in the osteocyte pericellular region are ADAMTS (A disintegrin and metalloprotease with thrombospondin motifs), proteases that can cleave proteoglycans such as aggrecan, versican, and brevican, and have been shown to be present in osteoblasts and osteocytes during rat tooth eruption [10]. Additional proteinases that could be investigated are cathepsin B and dipeptidyl peptidase I & II, which have also been associated with osteoblasts and osteocytes [11]. The work presented in Chapter 3 has effectively eliminated two candidate proteinases that do not seem to cause changes in the osteocytic environment, although it should be noted that a closer analysis of MMP-2 may be warranted since a non-significant trend of increased MMP-2 at the 6-week time point could be further investigated with a higher power experiment using an increased number of rats per group. Identification of the MMP(s) or other proteases responsible for degrading matrix in the osteocyte lacunar-canalicular network can help to develop appropriate drug regimes, e.g., MMP inhibitors, for effective osteoporosis treatments.

Because MMPs cleave non-collagenous proteins, the concentration of chondroitin sulphates was also tested as part of this work (see Appendix), and was found to remain unchanged in OVX tissue. Because changes in noncollagenous proteins have also been shown in osteoporotic bone [12], it is likely that other non-collagenous proteins may be altered during estrogen deficiency. Thus, changes in heparan sulphate proteoglycans (e.g., perlecan) [13] in the osteocyte lacunar-canalicular network of estrogen-deficient rats can be tested in future studies.

Bone remodeling by osteocytes, also called periosteocytic remodeling, in estrogen-deficient rats has not been previously shown, but indications of this process were observed in

Chapter 2. Thus, it becomes vital to determine if the nanostructural mineral-matrix changes in estrogen-deficient rats may be due to a bone remodeling process that may create new, less mineralized bone after OVX. Our final objective, which was summarized in Chapter 4, was to assess bone remodeling differences that may arise due to new bone formed in OVX tissue, using fluorescent bone labels and nanoindentation.

Results from Chapter 4 indicated that mineral apposition and bone formation rates were increased at the endocortical surfaces in OVX rats, but no changes were seen in percent mineralizing surfaces on the periosteal surfaces. A non-significant trend of increased percent mineralizing surfaces of the vascular porosity was seen in OVX rats as well. The elastic modulus and hardness were found unaltered due to estrogen deficiency. Together the bone labeling and nanoindentation results suggest that the nanostructural matrix-mineral level changes in the estrogen-deficient rats seen in Chapter 2 are indeed alterations occurring in the local environment of the osteocyte lacunar-canalicular network, and not global bone matrix changes caused by a change in mineralization of OVX tissue due to increased bone turnover.

Future work needs to study bone mineral density distribution (BMDD) and tissue mineral density (TMD) of the cortical tibial metaphysis of estrogen-deficient rats using quantitative backscattered electron imaging (qBSE) and micro-computed tomography (μCT). qBSE, using a field-emission gun, will enable taking high resolution images (~1μm) to help determine if surface mineral changes are occurring in the osteocyte environment of estrogen-deficient rats. TMD studies will further strengthen the findings of the fluorescent labels that were used in Chapter 4 and would determine whether global mineral changes are occurring in estrogen-deficient rats. Geometric changes in the cortical tibial metaphysis could also be assessed using μCT imaging.

To further investigate changes in the osteocyte microenvironment in the estrogen-deficient state, the role of fibroblast growth factor-23 (FGF-23) should also be investigated. FGF-23 regulates serum phosphate concentration by affecting renal function. FGF-23 synthesis by osteocytes coincides with a regularly distributed osteocyte lacunar-canalicular network [14]. The role of this molecule needs to be tested in estrogen-deficient animals to see whether osteocytes may be remodeling and regulating local phosphate ions from the lacunar-canalicular surfaces via the FGF-23 pathway and also inhibiting osteoblast activity through the sclerostin-estrogen link. Osteocytes may be intimately involved in mineral mobilization in conditions like osteoporosis perhaps due to the demand of calcium that arises by impaired calcium absorption in the kidney that has been shown in some studies [15,16], which could contribute to the altered matrix-mineral level changes seen the osteocyte lacunar-canalicular network of OVX rats. Serum levels of calcium and phosphate share an inverse relationship, and modulated levels of FGF-23 in osteocytes of OVX animals would suggest that osteocytes may be controlling the renal ion concentrations during estrogen deficiency.

Together, the results of this dissertation have demonstrated micro- and nano-structural changes that occur in the osteocyte microenvironment after estrogen withdrawal and have assessed how these changes may be occurring. By understanding the relationship between microarchitectural changes in the osteocyte lacunar-canalicular environment, temporal and spatial patterns of osteocyte apoptosis, the role of MMPs as candidates of bone degradation, and bone remodeling changes in estrogen-deficient animals, we have advanced the understanding of the role osteocytes play in postmenopausal osteoporosis. Additional studies that identify the exact mechanisms by which osteocyte degradation occurs and contributes to diminished bone

quality after estrogen withdrawal will help in the design of approaches to treat, and potentially prevent, postmenopausal osteoporosis.

APPENDIX

A.1. Assessing Changes in Chondroitin Sulphate Proteoglycans in Estrogen-Deficient Rats

Purpose

To assess changes in chondrotin sulphate proteoglycans in the cortical metaphysis of the proximal tibia in estrogen-deficient rats.

Methods

Osteoporosis Model

Ten female Sprague Dawley rats (Harlan Laboratories) were divided into two groups, with one group undergoing ovariectomy (OVX, n=5) and the other group acting as control (SHAM, n=5). The right tibiae were harvested from the 6-weeks time point from the animals used in the study described in Chapter 3.

Sample preparation

Right tibiae of each rat were harvested, cleaned of soft tissue, cut ~2 mm below the growth plate, and immediately placed in phosphate-buffered formalin for 72 hours at 4^{o}C. After fixation, samples were decalcified in ethylenediaminetetraacetic acid (EDTA) for 2 weeks, and embedded in paraffin wax. 5 µm paraffin-embedded longitudinal sections were cut from the cortical tibial metaphysis and adhered to glass slides to stain for chondroitin sulphate proteoglycans.

Immunohistochemistry protocol

An immunohistochemistry protocol was developed to quantify chondroitin sulphate proteoglycans like aggrecan, versican, brevican etc., around the osteocyte lacunae. Sections were deparaffinized, rehydrated and treated with 3% hydrogen peroxide to inhibit endogenous peroxidase activity and blocked for 30 minutes afterwards. Nonspecific tissue binding was blocked by incubating tissue sections in protein block (Dako) for 30 minutes at room temperature. Specimens were incubated in a humidified chamber overnight at 4º C with chondroitin sulphate (1:200) (C8035, Sigma-Aldrich) antibody. Detection was performed using secondary antibody (VECTASTAIN ABC Systems, Vector laboratories, CA) and developed with DAB substrate chromogen system. Sections were counterstained with Weigert's hematoxylin, dehydrated and coverslipped with mounting medium. Optimal dilution for the primary antibody was determined using internal positive control tissues (growth plate). Appropriate negative staining controls were examined.

Quantification of chondroitin sulphate around osteocyte lacunae

Stained (CS+ Ot) and non-stained osteocytes were counted under brightfield microscopy at 40X magnification. Stained osteocytes were counted in three regions of interest (ROI 87.5 µm x 77.5 µm) per anatomical location (anterior and posterior) through the cortical width. Stained cells were identified as brown-colored cells and non-stained cells were stained purple. Cell bodies that were 50% or more inside the ROI were considered to be part of the quantification. Three longitudinal sections per animal from the cortical tibial metaphysis, at least 16 µm apart, were used to quantify chondroitin sulphate positive osteocytes (Fig. A.1).

Statistical Analysis

Whole cross-sectional analysis was performed by pooling all data from the three ROIs and two quadrants because no statistical differences were observed within the quadrants. Unpaired, two-tailed t-tests were used to assess differences between the SHAM and OVX groups for the chondroitin sulphate stained osteocytes (CS+ Ot). Quantification was performed by pooling data from the anterior and posterior quadrants on the longitudinal sections. All the statistical analyses were performed using the Prism 5 statistics software package (GraphPad Software Inc.).The normality of all data sets was confirmed before using parametric tests, and the significance level was set at $p < 0.05$.

Results

Quantification of chondroitin sulphate staining around osteocyte lacunae

Only ~ 5% of osteocytes stained positively for chondroitin sulphate proteoglycans (CS+ Ot) at 6-weeks post-surgery in both SHAM and OVX groups. This amount was not significantly different between SHAM and OVX animals at this time point (Fig. A.2).

Fig. A.1 Osteocytes stained for chondroitin sulphate proteoglycans; Black arrows indicate positively stained cells; scale bars = 100 μm.

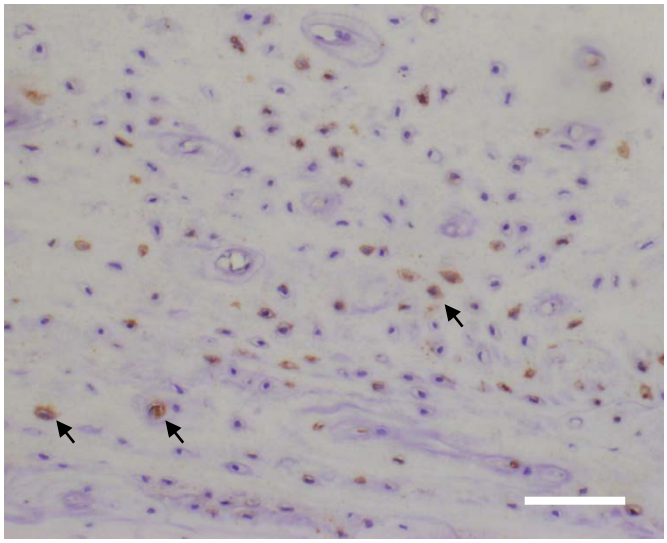

Fig. A.2 Box plots showing chondroitin sulphate (%) positive osteocytes from cortical bone from the proximal tibial metaphysis. + indicates the mean of each group. No significant differences were found between SHAM and OVX.

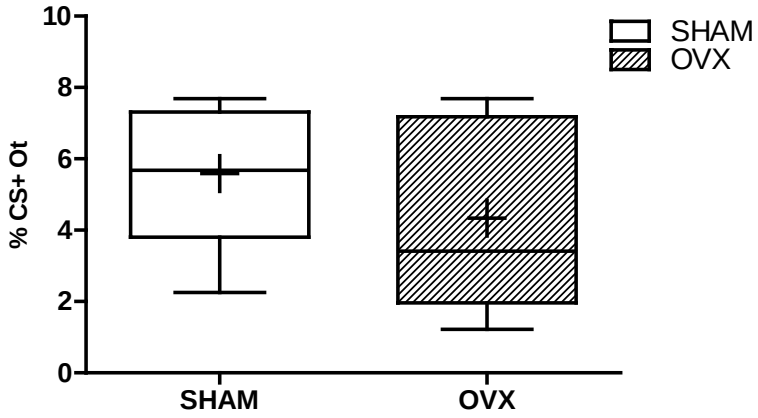

BIBLIOGRAPHY

INTRODUCTION

[1] Cowin S.C., Doty S.B. Tissue Mechanics, Springer 2007, XVI, Chapter 11, 682-690

[2] Martin R. B., Burr D.B. and Sharkey N.A. Skeletal Tissue Mechanics; Springer 1998, Chapter 1, 15-23

[3] Majeska, R.J., Cell biology of bone. Bone Mechanics Handbook, 2001, Cowin SC editor, New York, CRC Press, Chapter 2, 3-23

[4] You LD, Weinbaum S, Cowin SC, Schaffler MB. Ultrastructure of the osteocyte process and its pericellular matrix. Anat Rec A Discov Mol Cell Evol Biol. 2004;278(2):505-13

[5] Wang Y, McNamara LM, Schaffler MB, Weinbaum S. A model for the role of integrins in flow induced mechanotransduction in osteocytes. Proc Natl Acad Sci USA 2007; 104:15941-15946

[6] Doty SB. Morphological evidence of gap junctions between bone cells. Calcif Tissue Int. 1981;33(5):509-12

[7] Bonewald L. Osteocytes as multifunctional cells. J Musculoskelet Neuronal Interact. 2006; 6(4):331-3

[8] Frost HM. The mechanostat: a proposed pathogenic mechanism of osteoporoses and the bone mass effects of mechanical and nonmechanical agents. Bone Miner. 1987;2(2):73-85

[9] Frost, H. Presence of Microscopic Cracks In Vivo In Bone. Henry Ford Hospital Medical Bulletin 1960;8:25-35

[10] Parfitt, A. M. Osteonal and hemi-osteonal remodeling: the spatial and temporal framework for signal traffic in adult human bone. J Cell Biochem 1994;55(3): 273-86

[11] Verborgt O, Gibson GJ, Schaffler MB. Loss of osteocyte integrity in association with microdamage and bone remodeling after fatigue in vivo. J Bone Miner Res 2000; 15(1): 60-7

[12] Cardoso L, Herman BC, Verborgt O, Laudier D, Majeska RJ, Schaffler MB. Osteocyte apoptosis controls activation of intracortical resorption in response to bone fatigue. J Bone Miner Res. 2009;24(4):597-605

[13] Qing H, Ardeshirpour L, Pajevic PD, Dusevich V, Jähn K, Kato S, Wysolmerski J, Bonewald LF. Demonstration of osteocytic perilacunar/canalicular remodeling in mice during lactation. J Bone Miner Res. 2012. doi: 10.1002/jbmr.1567

[14] Bakker A, Klein-Nulend J, Burger E. Shear stress inhibits while disuse promotes osteocyte apoptosis. Biochem Biophys Res Commun. 2004;320(4):1163-8

[15] Tomkinson A, Reeve J, Shaw RW, Noble BS. The death of osteocytes via apoptosis accompanies estrogen withdrawal in human bone. J Clin Endocrinol Metab. 1997;82(9):3128-35

[16] Emerton KB, Hu B, Woo AA, Sinofsky A, Hernandez C, Majeska RJ, Jepsen KJ, Schaffler MB. Osteocyte apoptosis and control of bone resorption following ovariectomy in mice. Bone 2010;46(3):577-83

[17] Jee, W. Integrated Bone Tissue Physiology: Anatomy and Physiology. Bone Mechanics 2001; New York, CRC Press LLC. 1: 1-56

[18] Piekarski K, Munro M. Transport mechanism operating between blood supply and osteocytes in long bones. Nature 1977;269: 80-2

[19] Wang L, Ciani C, Doty SB, Fritton SP. Delineating bone's interstitial fluid pathway in vivo. Bone 2004; 34:499-509

[20] Kufahl RH, Saha S. A theoretical model for stress-generated fluid flow in the canaliculi-lacunae network in bone tissue. J Biomech 1990;23: 171-80

[21] Nyman JS, Roy A, Shen X, Acuna RL, Tyler JH, Wang X. The influence of water removal on the strength and toughness of cortical bone. J Biomech 2006;39:931-938

[22] Fritton SP, Weinbaum S. Fluid and Solute Transport in Bone: Flow-Induced Mechanotransduction. Annu Rev Fluid Mech. 2009;41:347-374

[23] Weinbaum S, Cowin SC, Zeng Y. A model for the excitation of osteocytes by mechanical loading-induced bone fluid shear stresses. J Biomech. 1994;27(3):339-60

[24] Knothe Tate ML, Niederer P, Knothe U. In vivo tracer transport through the lacunocanalicular system of rat bone in an environment devoid of mechanical loading. Bone 1998;22:107-117

[25] Knothe Tate ML, Steck R, Forwood MR, Niederer P. In vivo demonstration of load-induced fluid flow in the rat tibia and its potential implications for processes associated with functional adaptation. J Exp Biol 2000;203:2737-2745

[26] Ajubi NE, Klein-Nulend J, Nijweide PJ, Vrijheid-Lammers T, Alblas MJ, Burger EH. Pulsating fluid flow increases prostaglandin production by cultured chicken osteocytes--a cytoskeleton-dependent process. Biochem Biophys Res Commun 1996;225: 62-8

[27] Donahue SW, Jacobs CR, Donahue HJ. Flow-induced calcium oscillations in rat osteoblasts are age, loading frequency, and shear stress dependent. Am J Physiol Cell Physiol 2001;281: C1635-41

[28] Klein-Nulend J, Semeins CM, Ajubi NE, Nijweide PJ, Burger EH. Pulsating fluid flow increases nitric oxide (NO) synthesis by osteocytes but not periosteal fibroblasts--correlation with prostaglandin upregulation. Biochem Biophys Res Commun 1995;217: 640-8

[29] Ajubi NE, Klein-Nulend J, Alblas MJ, Burger EH, Nijweide PJ. Signal transduction pathways involved in fluid flow-induced PGE2 production by cultured osteocytes. Am J Physiol 1999;276: E171-8

[30] Genetos DC, Kephart CJ, Zhang Y, Yellowley CE, Donahue HJ. Oscillating fluid flow activation of gap junction hemichannels induces ATP release from MLO-Y4 osteocytes. J Cell Physiol 2007;212: 207-14

[31] Adachi T, Aonuma Y, Tanaka M, Hojo M, Takano-Yamamoto T, Kamioka H. Calcium response in single osteocytes to locally applied mechanical stimulus: differences in cell process and cell body. J Biomech. 2009;42(12):1989-95

[32] Kaiser J, Lemaire T, Naili S, Sansalone V, Komarova SV. Do calcium fluxes within cortical bone affect osteocyte mechanosensitivity? J Theor Biol. 2012;303:75-86

[33] Wang Y, McNamara LM, Schaffler MB, Weinbaum S. Strain amplification and integrin based signaling in osteocytes. J Musculoskelet Neuronal Interact. 2008;8(4):332-4

[34] McNamara LM, Majeska RJ, Weinbaum S, Friedrich V, Schaffler MB. Attachment of osteocyte cell processes to the bone matrix. Anat Rec (Hoboken). 2009;292(3):355-63

[35] Han Y, Cowin SC, Schaffler MB, Weinbaum S. Mechanotransduction and strain amplification in osteocyte cell processes. Proc Natl Acad Sci U S A. 2004;101(47):16689-94

[36] Wang Y, McNamara LM, Schaffler MB, Weinbaum S. A model for the role of integrins in flow induced mechanotransduction in osteocytes. Proc Natl Acad Sci USA 2007; 104:15941-15946

[37] You J, Yellowley CE, Donahue HJ, Zhang Y, Chen Q, Jacobs CR. Substrate deformation levels associated with routine physical activity are less stimulatory to bone cells relative to loading-induced oscillatory fluid flow. J Biomech Eng 2000;122: 387-93

[38] Lanyon LE. Using functional loading to influence bone mass and architecture: objectives, mechanisms, and relationship with estrogen of the mechanically adaptive process in bone. Bone. 1996;18(1 Suppl):37S-43S

[39] Jacobs CR, Temiyasathit S, Castillo AB. Osteocyte mechanobiology and pericellular mechanics. Annu Rev Biomed Eng. 2010;12:369-400

[40] Praetorius HA, Spring KR. Removal of the MDCK cell primary cilium abolishes flow sensing. J. Membr. Biol. 2003; 191:69–76

[41] Mosley JR. Osteoporosis and bone functional adaptation: mechanobiological regulation of bone architecture in growing and adult bone, areview. J Rehabil Res Dev. 2000;37(2):189-99

[42] Martin, R. B. Toward a unifying theory of bone remodeling. Bone 2000; 26(1):1-6

[43] Rubin CT, McLeod KJ, Lanyon LE. Prevention of osteoporosis by pulsed electromagnetic fields. J Bone Joint Surg Am. 1989;71(3):411-7

[44] Turner CH. Three rules for bone adaptation to mechanical stimuli. Bone. 1998;23(5):399-407

[45] Srinivasan S, Weimer DA, Agans SC, Bain SD, Gross TS. Low-magnitude mechanical loading becomes osteogenic when rest is inserted between each load cycle. J Bone Miner Res. 2002; 17(9):1613-20

[46] van der Meulen MC, Morgan TG, Yang X, Baldini TH, Myers ER, Wright TM, Bostrom MP. Cancellous bone adaptation to in vivo loading in a rabbit model. Bone. 2006;38(6):871-7

[47] Bonnet N, Laroche N, Beaupied H, Vico L, Dolleans E, Benhamou CL, Courteix D. Doping dose of salbutamol and exercise training: impact on the skeleton of ovariectomized rats. J Appl Physiol. 2007;103(2):524-33

[48] Honda A, Sogo N, Nagasawa S, Shimizu T, Umemura Y. High-impact exercise strengthens bone in osteopenic ovariectomized rats with the same outcome as Sham rats. J Appl Physiol. 2003 ;95(3):1032-7

[49] Fonseca H, Moreira-Gonçalves D, Esteves JL, Viriato N, Vaz M, Mota MP, Duarte JA Voluntary exercise has long-term in vivo protective effects on osteocyte viability and bone strength following ovariectomy. Calcif Tissue Int. 2011;88(6):443-54

[50] National Foundation of Osteoporosis. www.nof.org, accessed 5-12-12

[51] World Health Organization. www.who.org, accessed 5-16-12

[52] Mödder UI, Roforth MM, Hoey K, McCready LK, Peterson JM, Monroe DG, Oursler MJ, Khosla S. Effects of estrogen on osteoprogenitor cells and cytokines/bone-regulatory factors in postmenopausal women. Bone. 2011;49(2):202-7

[53] Oursler MJ. Estrogen regulation of gene expression in osteoblasts and osteoclasts. Crit Rev Eukaryot Gene Expr. 1998;8(2):125-40

[54] Birkedal-Hansen H. Role of cytokines and inflammatory mediators in tissue destruction. J Periodontal Res. 1993;28(6 Pt 2):500-10

[55] Poole KE, van Bezooijen RL, Loveridge N, Hamersma H, Papapoulos SE, Löwik CW, Reeve J. Sclerostin is a delayed secreted product of osteocytes that inhibits bone formation. FASEB J 2005;19(13): 1842-4

[56] Kalu DN. The ovariectomized rat model of postmenopausal bone loss. Bone Miner 1991;15(3):175-91

[57] Wronski TJ, Lowry PL, Walsh CC, Ignaszewski LA. Skeletal alterations in ovariectomized rats. Calcif Tissue Int. 1985;37(3):324-8

[58] Wronski TJ, Walsh CC, Ignaszewski LA . Histologic evidence for osteopenia and increased bone turnover in ovariectomized rats. Bone; 1986; 7(2):119-23

[59] Wronski TJ, Cintrón M, Dann LM. Temporal relationship between bone loss and increased bone turnover in ovariectomized rats. Calcif Tissue Int; 1988; 43(3):179-83

[60] Yamaura M, Nakamura T, Tsurukami H, Hijioka A, Narusawa K, Ohnishi H, Ohta T, Hosoda K. Local bone turnover in the Metaphysis of the proximal tibia and the lumbar vertebra during the early periods after ovariectomy in rats. Calcif Tissue Int 1996;58(1):52-9

[61] Boyd SK, Davison P, Müller R, Gasser JA. Monitoring individual morphological changes over time in ovariectomized rats by in vivo micro-computed tomography. Bone 2006; 39(4):854-62

[62] Horton JA, Bariteau JT, Loomis RM, Strauss JA, Damron TA. Ontogeny of skeletal maturation in the juvenile rat. Anat Rec (Hoboken) 2008;291(3):283-92

[63] Roach HI, Mehta G, Oreffo RO, Clarke NM, Cooper C.Temporal analysis of rat growth plates: cessation of growth with age despite presence of a physis. J Histochem Cytochem. 2003;51(3):373-83

[64] Thompson DD, Simmons HA, Pirie CM, Ke HZ. FDA Guidelines and animal models for osteoporosis. Bone. 1995;17:125S-133S

[65] Frost HM, Jee WS. On the rat model of human osteopenias and osteoporoses. Bone Miner 1992;18(3):227-36

[66] Westerlind KC, Wronski TJ, Ritman EL, Luo ZP, An KN, Bell NH, Turner RT. Estrogen regulates the rate of bone turnover but bone balance in ovariectomized rats is modulated by prevailing mechanical strain. Proc Natl Acad Sci U S A. 1997;94(8):4199-204

[67] Gadeleta SJ, Boskey AL, Paschalis E, Carlson C, Menschik F, Baldini T, Peterson M, Rimnac CM. A physical, chemical, and mechanical study of lumbar vertebrae from normal, ovariectomized, and nandrolone decanoate-treated cynomolgus monkeys (Macaca fascicularis). Bone 2000;27(4):541-50

[68] Kneissel M, Boyde A, Gasser JA. Bone tissue and its mineralization in aged estrogen-depleted rats after long-term intermittent treatment with parathyroid hormone (PTH) analog SDZ PTS 893 or human PTH(1-34). Bone 2001;28:237-50

[69] Cheng Z, Yao W, Zimmermann EA, Busse C, Ritchie RO, Lane NE. Prolonged treatments with antiresorptive agents and PTH have different effects on bone strength and the degree of mineralization in old estrogen-deficient osteoporotic rats. J Bone Miner Res 2009; 24:209-20

[70] Li B, Aspden RM. Material properties of bone from the femoral neck and calcar femorale of patients with osteoporosis or osteoarthritis. Osteoporos Int 1997;7:450-6

[71] Guo XE, Goldstein SA.Vertebral trabecular bone microscopic tissue elastic modulus and hardness do not change in ovariectomized rats. J Orthop Res. 2000;18(2):333-6

[72] Boyde A, Compston JE, Reeve J, Bell KL, Noble BS, Jones SJ, Loveridge N. Effect of estrogen suppression on the mineralization density of iliac crest biopsies in young women as assessed by backscattered electron imaging. Bone 1998;22(3):241-50

[73] McNamara LM, Ederveen AG, Lyons CG, Price C, Schaffler MB, Weinans H, Prendergast PJ. Strength of cancellous bone trabecular tissue from normal, ovariectomized and drug-treated rats over the course of ageing. Bone 2006;39:392-400

[74] Bailey AJ, Wotton SF, Sims TJ, Thompson PW. Biochemical changes in the collagen of human osteoporotic bone matrix. Connect Tissue Res 1995; 29(2):119-32

[75] Kafantari H, Kounadi E, Fatouros M, Milonakis M, Tzaphlidou M. Structural alterations in rat skin and bone collagen fibrils induced by ovariectomy. Bone 2000;26(4):349-53

[76] Wallace JM, Erickson B, Les CM, Orr BG, Banaszak Holl MM. Distribution of type I collagen morphologies in bone: relation to estrogen depletion. Bone 2010;46(5):1349-54

[77] Ferris BD, Klenerman L, Dodds RA, Bitensky L, Chayen J. Altered organization of non-collagenous bone matrix in osteoporosis. Bone 1987; 8(5):285-8

[78] Krane SM, Inada M. Matrix metalloproteinases and bone. Bone 2008;43(1):7-18

[79] Aiken A, Khokha R. Unraveling metalloproteinase function in skeletal biology and disease using genetically altered mice. Biochim Biophys Acta 2010;1803(1):121-32

[80] Sternlicht MD, Werb Z. How matrix metalloproteinases regulate cell behavior. Annu Rev Cell Dev Biol. 2001;17:463-516

[81] Page-McCaw A, Ewald AJ, Werb Z. Matrix metalloproteinases and the regulation of tissue remodelling. Nat Rev Mol Cell Biol 2007;8(3):221-33

[82] Inoue K, Mikuni-Takagaki Y, Oikawa K, Itoh T, Inada M, Noguchi T, Park JS, Onodera T, Krane SM, Noda M, Itohara S. A crucial role for matrix metalloproteinase 2 in osteocytic canalicular formation and bone metabolism. J Biol Chem. 2006;281(44):33814-24

[83] Holmbeck K, Bianco P, Caterina J, Yamada S, Kromer M, et al. 1999. MT1-MMP-deficient mice develop dwarfism, osteopenia, arthritis, and connective tissue disease due to inadequate collagen turnover. Cell 99:81–92

[84] Mansell JP, Tarlton JF, Bailey AJ. Expression of gelatinases within the trabecular bone compartment of ovariectomized and parathyroidectomized adult female rats. Bone. 1997;20(6):533-8

[85] Guo LJ, Luo XH, Wu XP, Shan PF, Zhang H, Cao XZ, Xie H, Liao EY. Serum concentrations of MMP-1, MMP-2, and TIMP-1 in Chinese women: age-related changes, and the relationships with bone biochemical markers, bone mineral density. Clin Chim Acta. 2006; 371:137-42

[86] Bord S, Horner A, Hembry RM, Compston JE. Stromelysin-1 (MMP-3) and stromelysin-2 (MMP-10) expression in developing human bone: potential roles in skeletal development. Bone. 1998;23(1):7-12

[87] Breckon JJ, Papaioannou S, Kon LW, Tumber A, Hembry RM, Murphy G, Reynolds JJ, Meikle MC. Stromelysin (MMP-3) synthesis is up-regulated in estrogen-deficient mouse osteoblasts in vivo and in vitro. J Bone Miner Res. 1999;14(11):1880-90

[88] Geoffroy V, Marty-Morieux C, Le Goupil N, Clement-Lacroix P, Terraz C, Frain M, Roux S, Rossert J, de Vernejoul MC. In vivo inhibition of osteoblastic metalloproteinases leads to increased trabecular bone mass. J Bone Miner Res. 2004;19(5):811-22

[89] Cowles EA, DeRome ME, Pastizzo G, Brailey LL, Gronowicz GA. Mineralization and the expression of matrix proteins during in vivo bone development. Calcif Tissue Int. 1998; 62:74-82

[90] Shibata S, Baba O, Oda T, Yokohama-Tamaki T, Qin C, Butler WT, Sakakura Y, Takano Y. An immunohistochemical and ultrastructural study of the pericellular matrix of uneroded hypertrophic chondrocytes in the mandibular condyle of aged c-src-deficient mice. Arch Oral Biol. 2008; 53:220-30

[91] Thompson WR, Modla S, Grindel BJ, Czymmek KJ, Kirn-Safran CB, Wang L, Duncan RL, Farach-Carson MC. Perlecan/Hspg2 deficiency alters the pericellular space of the lacunocanalicular system surrounding osteocytic processes in cortical bone. J Bone Miner Res. 201;26:618-29

[92] Xiong J, Onal M, Jilka RL, Weinstein RS, Manolagas SC, O'Brien CA. Matrix-embedded cells control osteoclast formation. Nat Med. 2011;17(10):1235-41

[93] Mueller RJ, Richards RG. Immunohistological identification of receptor activator of NF-kappaB ligand (RANKL) in human, ovine and bovine bone tissues. J Mater Sci Mater Med 2004;15:367–72

[94] Vinatier D, Dufour P, Subtil D. Apoptosis: a programmed cell death involved in ovarian and uterine physiology. Eur J Obstet Gynecol Reprod Biol. 1996;67(2):85-102

[95] Boatright KM, Salvesen GS. Mechanisms of caspase activation. Curr Opin Cell Biol. 2003;15(6):725-31

[96] Noble B. Microdamage and apoptosis. Eur J Morphol. 2005;42(1-2):91-8

[97] Tomkinson A, Reeve J, Shaw RW, Noble BS. The death of osteocytes via apoptosis accompanies estrogen withdrawal in human bone. J Clin Endocrinol Metab.1997;82(9):3128-35

[98] Tomkinson A, Gevers EF, Wit JM, Reeve J, Noble BS. The role of estrogen in the control of rat osteocyte apoptosis. J Bone Miner Res. 1998;13(8):1243-50

[99] Almeida M, Han L, Martin-Millan M, Plotkin LI, Stewart SA, Roberson PK, Kousteni S, O'Brien CA, Bellido T, Parfitt AM, Weinstein RS, Jilka RL, Manolagas SC. Skeletal

involution by age-associated oxidative stress and its acceleration by loss of sex steroids. J Biol Chem. 2007; 282(37):27285-97

[100] Aguirre JI, Plotkin LI, Stewart SA, Weinstein RS, Parfitt AM, Manolagas SC, Bellido T. Osteocyte apoptosis is induced by weightlessness in mice and precedes osteoclast recruitment and bone loss. J Bone Miner Res 2006;21(4): 605-15

[101] Bakker A, Klein-Nulend J, Burger E. Shear stress inhibits while disuse promotes osteocyte apoptosis. Biochem Biophys Res Commun. 2004;320(4):1163-8

[102] Tatsumi S, Ishii K, Amizuka N, Li M, Kobayashi T, Kohno K, Ito M, Takeshita S, Ikeda K. Targeted ablation of osteocytes induces osteoporosis with defective mechanotransduction. Cell Metab. 2007;5(6):464-75

[103] Schöneich C. Reactive oxygen species and biological aging: a mechanistic approach. Exp Gerontol. 1999;34(1):19-34

[104] Rikans, LE and Hornbrook KR. Lipid peroxidation, antioxidant protection and aging. Biochim Biophys Acta 1997;1362(2-3): 116-27

[105] Hamada Y, Kitazawa S, Kitazawa R, Fujii H, Kasuga M, Fukagawa M. Histomorphometric analysis of diabetic osteopenia in streptozotocin-induced diabetic mice: a possible role of oxidative stress. Bone 2007; 40(5): 1408-14

[106] Finkel, T and NJ Holbrook. Oxidants,oxidative stress and the biology of ageing. Nature 2000; 408(6809): 239-47

[107] Kanda N, Watanabe S. 17beta-estradiol inhibits oxidative stress-induced apoptosis in keratinocytes by promoting Bcl-2 expression. J Invest Dermatol. 2003;121(6):1500-9

[108] Grassi F, Tell G, Robbie-Ryan M, Gao Y, Terauchi M, Yang X, Romanello M, Jones DP, Weitzmann MN, Pacifici R. Oxidative stress causes bone loss in estrogen deficient mice through enhanced bone marrow dendritic cell activation. Proc Natl Acad Sci U S A 2007; 104(38): 15087-92

[109] Zaman G, Jessop HL, Muzylak M, De Souza RL, Pitsillides AA, Price JS, Lanyon LL. Osteocytes use estrogen receptor alpha to respond to strain but their ERalpha content is regulated by estrogen. J Bone Miner Res. 2006;21(8):1297-306

[110] Mueller RJ, Richards RG. Immunohistological identification of receptor activator of NF-kappaB ligand (RANKL) in human, ovine and bovine bone tissues. J Mater Sci Mater Med 2004;15:367–72

[111] Martin A, Liu S, David V, Li H, Karydis A, Feng JQ, Quarles LD. Bone proteins PHEX and DMP1 regulate fibroblastic growth factor Fgf23 expression inosteocytes through a common pathway involving FGF receptor (FGFR) signaling. FASEB J. 2011;25(8):2551-62

[112] Ubaidus S, Li M, Sultana S, de Freitas PH, Oda K, Maeda T, Takagi R, Amizuka N. FGF23 is mainly synthesized by osteocytes in the regularly distributed osteocytic lacunar

canalicular system established after physiological bone remodeling. J Electron Microsc (Tokyo). 2009;58(6):381-92

[113] Mosekilde L, Melsen F. A tetracycline-based histomorphometric evaluation of bone resorption and bone turnover in hyperthyroidism and hyperparathyroidism. Acta Med. Scand 1978; 204:97–102

[114] Teti A, Zallone A. Do osteocytes contribute to bone mineral homeostasis? Osteocytic osteolysis revisited. Bone. 2009;44(1):11-6

[115] Lane NE, Yao W, Balooch M, Nalla RK, Balooch G, Habelitz S, Kinney JH, Bonewald LF. Glucocorticoid-treated mice have localized changes in trabecular bone material properties and osteocyte lacunar size that are not observed in placebo-treated or estrogen-deficient mice. J Bone Miner Res. 2006;21(3):466-76

[116] Talmage DW, Talmage RV. Calcium homeostasis: how bone solubility relates to all aspects of bone physiology. J Musculoskelet Neuronal Interact 2007;7:108–12

[117] Jande SS, Bélanger LF. Electron microscopy of osteocytes and the pericellular matrix in rat trabecular bone. Calcif Tissue Res 1971;6:280–9

[118] Jande SS, Bélanger LF. The life cycle of the osteocyte. Clin Orthop Relat Res 1973; 94: 281–305

[119] Tazawa K, Hoshi K, Kawamoto S, Tanaka M, Ejiri S, Ozawa H. Osteocytic osteolysis observed in rats to which parathyroid hormone was continuously administered. J Bone Miner Metab 2004;22:524–9

[120] McKee MD, Nanci A. Osteopontin at mineralized tissue interfaces in bone, teeth, and osseointegrated implants: ultrastructural distribution and implications for mineralized tissue formation, turnover, and repair. Microsc Res Tech 1996;33(2):141–64

[121] Rubin C, Sun YQ, Hadjiargyrou M, McLeod K. Increased expression of matrix metalloproteinase-1 in osteocytes precedes bone resorption as stimulated by disuse: evidence for autoregulation of the cell's mechanical environment? J Orthop Res. 1999;17(3):354-61

CHAPTER 2

[1] McNamara LM, Majeska RJ, Weinbaum S, Friedrich V, Schaffler MB. Attachment of osteocyte cell processes to the bone matrix. Anat Rec (Hoboken) 2009;292:355-63

[2] Burger EH, Klein-Nulend J. Mechanotransduction in bone--role of the lacuno-canalicular network. FASEB J 1999; 13 Suppl:S101-12

[3] Bonewald LF. Osteocytes as dynamic multifunctional cells. Ann N Y Acad Sci 2007; 1116:281–290

[4] Fritton SP, Weinbaum S. Fluid and solute transport in bone: flow-induced mechanotransduction. Annu Rev Fluid Mech 2009;41:347-74

[5] Han Y, Cowin SC, Schaffler MB, Weinbaum S. Mechanotransduction and strain amplification in osteocyte cell processes. Proc Natl Acad Sci U S A 2004;101:16689-94

[6] Wang Y, McNamara LM, Schaffler MB, Weinbaum S. A model for the role of integrins in flow induced mechanotransduction in osteocytes. Proc Natl Acad Sci U S A 2007; 104: 15941-6

[7] Piekarski K, Munro M. Transport mechanism operating between blood supply and osteocytes in long bones. Nature 1977;269:80-2

[8] Knothe Tate ML, Knothe U, Niederer P. Experimental elucidation of mechanical load-induced fluid flow and its potential role in bone metabolism and functional adaptation. Am J Med Sci 1998;316:189-95

[9] Wang L, Cowin SC, Weinbaum S, Fritton SP. Modeling tracer transport in an osteon under cyclic loading. Ann Biomed Eng 2000;28:1200-9

[10] Tami AE, Schaffler MB, Knothe Tate ML. Probing the tissue to subcellular level structure underlying bone's molecular sieving function. Biorheology 2003;40:577-90

[11] Wang L, Ciani C, Doty SB, Fritton SP. Delineating bone's interstitial fluid pathway in vivo. Bone 2004;34:499-509

[12] Frost HM, Jee WS. On the rat model of human osteopenias and osteoporoses. Bone Miner 1992;18:227-36

[13] Wronski TJ, Lowry PL, Walsh CC, Ignaszewski LA. Skeletal alterations in ovariectomized rats. Calcif Tissue Int 1985;37:324-8

[14] Tomkinson A, Reeve J, Shaw RW, Noble BS. The death of osteocytes via apoptosis accompanies estrogen withdrawal in human bone. J Clin Endocrinol Metab 1997;82:3128-35

[15] Miller SC, Bowman BM, Miller MA, Bagi CM. Calcium absorption and osseous organ-, tissue-, and envelope-specific changes following ovariectomy in rats. Bone 1991;12:439-46

[16] Westerlind KC, Wronski TJ, Ritman EL, Luo ZP, An KN, Bell NH, Turner RT. Estrogen regulates the rate of bone turnover but bone balance in ovariectomized rats is modulated by prevailing mechanical strain. Proc Natl Acad Sci U S A 1997;94:4199-204

[17] Brouwers JE, Lambers FM, van Rietbergen B, Ito K, Huiskes R. Comparison of bone loss induced by ovariectomy and neurectomy in rats analyzed by in vivo micro-CT. J Orthop Res 2009;27:1521-7

[18] Tomkinson A, Gevers EF, Wit JM, Reeve J, Noble BS. The role of estrogen in the control of rat osteocyte apoptosis. J Bone Miner Res 1998;13:1243-50

[19] Knothe Tate ML, Adamson JR, Tami AE, Bauer TW. The osteocyte. Int J Biochem Cell Biol 2004;36:1-8

[20] Almeida M, Han L, Martin-Millan M, Plotkin LI, Stewart SA, Roberson PK, Kousteni S, O'Brien CA, Bellido T, Parfitt AM, Weinstein RS, Jilka RL, Manolagas SC. Skeletal involution by age-associated oxidative stress and its acceleration by loss of sex steroids. J Biol Chem 2007;282:27285-97

[21] Kafantari H, Kounadi E, Fatouros M, Milonakis M, Tzaphlidou M. Structural alterations in rat skin and bone collagen fibrils induced by ovariectomy. Bone 2000;26:349-53

[22] Francisco JI, Yu Y, Oliver RA, Walsh WR. Relationship between age, skeletal site, and time post-ovariectomy on bone mineral and trabecular microarchitecture in rats. J Orthop Res 2011; 29:189-96

[23] Weinstein RS, Manolagas SC. Apoptosis and osteoporosis. Am J Med 2000;108:153-64

[24] Klein-Nulend J, Nijweide PJ, Burger EH. Osteocyte and bone structure. Curr Osteoporos Rep 2003;1:5-10

[25] Turner RT. Cancellous bone turnover in growing rats: time-dependent changes in association between calcein label and osteoblasts. J Bone Miner Res 1994;9:1419-24

[26] Erben RG. Trabecular and endocortical bone surfaces in the rat: modeling or remodeling? Anat Rec 1996;246:39-46

[27] Wronski TJ, Dann LM, Scott KS, Cintron M. Long-term effects of ovariectomy and aging on the rat skeleton. Calcif Tissue Int 1989;45:360-6

[28] Kalu DN. The ovariectomized rat model of postmenopausal bone loss. Bone Miner 1991;15:175-91

[29] Ciani C, Doty SB, Fritton SP. An effective histological staining process to visualize bone interstitial fluid space using confocal microscopy. Bone 2009;44:1015-7

[30] Otsu N. A threshold selection method from gray-level histograms. IEEE Trans Sys Man Cyber 1979;9:62–6

[31] Enlow DH. Principles of Bone Remodeling. Springfield, IL: Charles C. Thomas; 1963

[32] Jande SS, Bélanger LF. Electron microscopy of osteocytes and the pericellular matrix in rat trabecular bone. Calcif Tissue Res 1971;6:280-9

[33] Wassermann F, Yaeger JA. Fine structure of the osteocyte capsule and of the wall of the lacunae in bone. Zeitschrift für Zellforschung 1965;67:636-652

[34] Gadeleta SJ, Boskey AL, Paschalis E, Carlson C, Menschik F, Baldini T, Peterson M, Rimnac CM. A physical, chemical, and mechanical study of lumbar vertebrae from normal, ovariectomized, and nandrolone decanoate-treated cynomolgus monkeys (Macaca fascicularis). Bone 2000; 27:541-50

[35] Kneissel M, Boyde A, Gasser JA. Bone tissue and its mineralization in aged estrogen-depleted rats after long-term intermittent treatment with parathyroid hormone (PTH) analog SDZ PTS 893 or human PTH(1-34). Bone 2001;28:237-50

[36] Cheng Z, Yao W, Zimmermann EA, Busse C, Ritchie RO, Lane NE. Prolonged treatments with antiresorptive agents and PTH have different effects on bone strength and the degree of mineralization in old estrogen-deficient osteoporotic rats. J Bone Miner Res 2009; 24:209-20

[37] Li B, Aspden RM. Material properties of bone from the femoral neck and calcar femorale of patients with osteoporosis or osteoarthritis. Osteoporos Int 1997;7:450-6

[38] Boyde A, Compston JE, Reeve J, Bell KL, Noble BS, Jones SJ, Loveridge N. Effect of estrogen suppression on the mineralization density of iliac crest biopsies in young women as assessed by backscattered electron imaging. Bone 1998;22:241-50

[39] McNamara LM, Ederveen AG, Lyons CG, Price C, Schaffler MB, Weinans H, Prendergast PJ. Strength of cancellous bone trabecular tissue from normal, ovariectomized and drug-treated rats over the course of ageing. Bone 2006;39:392-400

[40] Valenta A, Roschger P, Fratzl-Zelman N, Kostenuik PJ, Dunstan CR, Fratzl P, Klaushofer K. Combined treatment with PTH (1-34) and OPG increases bone volume and uniformity of mineralization in aged ovariectomized rats. Bone 2005;37:87-95

[41] Bailey AJ, Wotton SF, Sims TJ, Thompson PW. Biochemical changes in the collagen of human osteoporotic bone matrix. Connect Tissue Res 1995; 29:119-32

[42] Wallace JM, Erickson B, Les CM, Orr BG, Banaszak Holl MM. Distribution of type I collagen morphologies in bone: relation to estrogen depletion. Bone 2010;46:1349-54

[43] Ferris BD, Klenerman L, Dodds RA, Bitensky L, Chayen J. Altered organization of non-collagenous bone matrix in osteoporosis. Bone 1987;8:285-8

[44] Ikeda T, Yamaguchi A, Yokose S, Nagai Y, Yamato H, Nakamura T, Tsurukami H, Tanizawa T, Yoshiki S. Changes in biological activity of bone cells in ovariectomized rats revealed by in situ hybridization. J Bone Miner Res 1996;11:780-8

[45] Emerton KB, Hu B, Woo AA, Sinofsky A, Hernandez C, Majeska RJ, Jepsen KJ, Schaffler MB. Osteocyte apoptosis and control of bone resorption following ovariectomy in mice. Bone 2010;46:577-83

[46] Atkins GJ, Findlay DM. Osteocyte regulation of bone mineral: a little give and take. Osteoporos Int 2012, doi: 10.1007/s00198-012-1915-z

[47] Mueller RJ, Richards RG. Immunohistological identification of receptor activator of NF-kappaB ligand (RANKL) in human, ovine and bovine bone tissues. J Mater Sci Mater Med. 2004;15:367-72

[48] Nakashima T, Hayashi M, Fukunaga T, Kurata K, Oh-Hora M, Feng JQ, Bonewald LF, Kodama T, Wutz A, Wagner EF, Penninger JM, Takayanagi H. Evidence for osteocyte regulation of bone homeostasis through RANKL expression. Nat Med 2011;17:1231-4

[49] Xiong J, Onal M, Jilka RL, Weinstein RS, Manolagas SC, O'Brien CA. Matrix embedded cells control osteoclast formation. Nat Med 2011;17:1235-41

[50] Xiong J, O'Brien CA. Osteocyte RANKL: New insights into the control of bone remodeling. J Bone Miner Res 2012;27:499-505

[51] Belanger LF. Osteocytic osteolysis. Calcif Tissue Res 1969;4:1-12

[52] Wright PH, Jowsey JO, Robb RA. Osteocyte lacunar area in normal bone, hyperparathyroidism, renal disease, and osteoporosis. Surg Forum 1978;29:558-9

[53] Parfitt AM. The cellular basis of bone turnover and bone loss: a rebuttal of the osteocytic resorption--bone flow theory. Clin Orthop Relat Res 1977:236-47

[54] Teti A, Zallone A. Do osteocytes contribute to bone mineral homeostasis? Osteocytic osteolysis revisited. Bone 2009;44:11-6

[55] Tazawa K, Hoshi K, Kawamoto S, Tanaka M, Ejiri S, Ozawa H. Osteocytic osteolysis observed in rats to which parathyroid hormone was continuously administered. J Bone Miner Metab 2004;22:524-9

[56] Lane NE, Yao W, Balooch M, Nalla RK, Balooch G, Habelitz S, Kinney JH, Bonewald LF. Glucocorticoid-treated mice have localized changes in trabecular bone material properties and osteocyte lacunar size that are not observed in placebo-treated or estrogen-deficient mice. J Bone Miner Res 2006;21:466-76

[57] Qing H, Ardeshirpour L, Pajevic PD, Dusevich V, Jähn K, Kato S, Wysolmerski J, Bonewald LF. Demonstration of osteocytic perilacunar/canalicular remodeling in mice during lactation. J Bone Miner Res 2012. doi: 10.1002/jbmr.1567

[58] Holmbeck K, Bianco P, Pidoux I, Inoue S, Billinghurst RC, Wu W, Chrysovergis K, Yamada S, Birkedal-Hansen H, Poole AR. The metalloproteinase MT1-MMP is required for normal development and maintenance of osteocyte processes in bone. J Cell Sci 2005;118:147-56

[59] Inoue K, Mikuni-Takagaki Y, Oikawa K, Itoh T, Inada M, Noguchi T, Park JS, Onodera T, Krane SM, Noda M, Itohara S. A crucial role for matrix metalloproteinase 2 in osteocytic canalicular formation and bone metabolism. J Biol Chem 2006;281:33814-24

[60] Sugawara Y, Kamioka H, Honjo T, Tezuka K, Takano-Yamamoto T. Three-dimensional reconstruction of chick calvarial osteocytes and their cell processes using confocal microscopy. Bone 2005;36:877-83

[61] Beno T, Yoon YJ, Cowin SC, Fritton SP. Estimation of bone permeability using accurate microstructural measurements. J Biomech 2006;39:2378-87

[62] Mullender MG, van der Meer DD, Huiskes R, Lips P. Osteocyte density changes in aging and osteoporosis. Bone 1996;18:109-13

[63] Mullender MG, Tan SD, Vico L, Alexandre C, Klein-Nulend J. Differences in osteocyte density and bone histomorphometry between men and women and between healthy and osteoporotic subjects. Calcif Tissue Int 2005;77:291-6

[64] Vatsa A, Breuls RG, Semeins CM, Salmon PL, Smit TH, Klein-Nulend J. Osteocyte morphology in fibula and calvaria - is there a role for mechanosensing? Bone 2008;43:452-8

[65] Roach HI, Mehta G, Oreffo RO, Clarke NM, Cooper C. Temporal analysis of rat growth plates: cessation of growth with age despite presence of a physis. J Histochem Cytochem 2003;51:373-83

[66] Horton JA, Bariteau JT, Loomis RM, Strauss JA, Damron TA. Ontogeny of skeletal maturation in the juvenile rat. Anat Rec (Hoboken) 2008;291:283-92

[67] Wronski TJ, Schenck PA, Cintron M, Walsh CC. Effect of body weight on osteopenia in ovariectomized rats. Calcif Tissue Int 1987;40:155-9

[68] Lanyon L, Skerry T. Postmenopausal osteoporosis as a failure of bone's adaptation to functional loading: a hypothesis. J Bone Miner Res 2001;16:1937-47

[69] Plotkin LI, Mathov I, Aguirre JI, Parfitt AM, Manolagas SC, Bellido T. Mechanical stimulation prevents osteocyte apoptosis: requirement of integrins, Src kinases, and ERKs. Am J Physiol Cell Physiol 2005;289:C633-43

CHAPTER 3

[1] Bonewald LF. Osteocytes as dynamic multifunctional cells. Ann N Y Acad Sci 2007; 1116:281–290

[2] Seeman E. Osteocytes--martyrs for integrity of bone strength. Osteoporos Int 2006; 17(10):1443-8

[3] Kennedy OD, Herman BC, Laudier DM, Majeska RJ, Sun HB, Schaffler MB. Activation of resorption in fatigue-loaded bone involves both apoptosis and active pro-osteoclastogenic signaling by distinct osteocyte populations. Bone 2012;50(5):1115-22

[4] Poole, K. E., R. L. van Bezooijen, et al. Sclerostin is a delayed secreted product of osteocytes that inhibits bone formation. FASEB J 2005;19(13): 1842-4

[5] Qing H, Ardeshirpour L, Pajevic PD, Dusevich V, Jähn K, Kato S, Wysolmerski J, Bonewald LF. Demonstration of osteocytic perilacunar/canalicular remodeling in mice during lactation. J Bone Miner Res 2012. doi: 10.1002/jbmr.1567

[6] Lane NE, Yao W, Balooch M, Nalla RK, Balooch G, Habelitz S, Kinney JH, Bonewald LF. Glucocorticoid-treated mice have localized changes in trabecular bone material properties and osteocyte lacunar size that are not observed in placebo-treated or estrogen-deficient mice. J Bone Miner Res 2006;21(3):466-76

[7] Jande SS, Bélanger LF. Electron microscopy of osteocytes and the pericellular matrix in rat trabecular bone. Calcif Tissue Res 1971;6:280–9

[8] Sharma D, Ciani C, Ramirez Marin PA, Levy JD, Doty SB, Fritton SP. Alterations in the osteocyte lacunar-canalicular microenvironment due to ovariectomy. Bone 2012, doi:10.1016/j.bone.2012.05.014

[9] Emerton KB, Hu B, Woo AA, Sinofsky A, Hernandez C, Majeska RJ, Jepsen KJ, Schaffler MB. Osteocyte apoptosis and control of bone resorption following ovariectomy in mice. Bone 2010;46:577-83

[10] Cardoso L, Herman BC, Verborgt O, Laudier D, Majeska RJ, Schaffler MB. Osteocyte apoptosis controls activation of intracortical resorption in response to bone fatigue. J Bone Miner Res 2009;24(4):597-605

[11] Almeida M, Han L, Martin-Millan M, Plotkin LI, Stewart SA, Roberson PK, Kousteni S, O'Brien CA, Bellido T, Parfitt AM, Weinstein RS, Jilka RL, Manolagas SC. Skeletal involution by age-associated oxidative stress and its acceleration by loss of sex steroids. J Biol Chem. 2007; 282(37):27285-97

[12] Aguirre JI, Plotkin LI, Stewart SA, Weinstein RS, Parfitt AM, Manolagas SC, Bellido T. Osteocyte apoptosis is induced by weightlessness in mice and precedes osteoclast recruitment and bone loss. J Bone Miner Res 2006;21(4): 605-15

[13] Tomkinson A, Reeve J, Shaw RW, Noble BS. The death of osteocytes via apoptosis accompanies estrogen withdrawal in human bone. J Clin Endocrinol Metab 1997;82(9):3128-35

[14] Tomkinson A, Gevers EF, Wit JM, Reeve J, Noble BS. The role of estrogen in the control of rat osteocyte apoptosis. J Bone Miner Res 1998;13(8):1243–50

[15] Xiong J, O'Brien CA. Osteocyte RANKL: new insights into the control of bone remodeling. J Bone Miner Res. 2012;27(3):499-505

[16] Carpentier VT, Wong J, Yeap Y, Gan C, Sutton-Smith P, Badiei A, Fazzalari NL, Kuliwaba JS. Increased proportion of hypermineralized osteocyte lacunae in osteoporotic and osteoarthritic human trabecular bone: implications for bone remodeling. Bone 2012;50(3): 688-94

[17] Parfitt, AM. Osteonal and hemi-osteonal remodeling: the spatial and temporal framework for signal traffic in adult human bone. J Cell Biochem 1994;55(3): 273-86

[18] Dunstan CR, Somers NM, Evans RA. Osteocyte death and hip fracture. Calcif Tissue Int 1993;53 Suppl 1:S113-6; S116-7

[19] Lanyon LE. Using functional loading to influence bone mass and architecture: objectives, mechanisms, and relationship with estrogen of the mechanically adaptive process in bone. Bone 1996;18(1 Suppl):37S-43S

[20] Zaman G, Jessop HL, Muzylak M, De Souza RL, Pitsillides AA, Price JS, Lanyon LL. Osteocytes use estrogen receptor alpha to respond to strain but their ERalpha content is regulated by estrogen. J Bone Miner Res 2006;21(8):1297-306

[21] Thompson WR, Modla S, Grindel BJ, Czymmek KJ, Kirn-Safran CB, Wang L, Duncan RL, Farach-Carson MC. Perlecan/Hspg2 deficiency alters the pericellular space of the lacunocanalicular system surrounding osteocytic processes in cortical bone. J Bone Miner Res 2011;26(3):618-29.

[22] Krane SM, Inada M. Matrix metalloproteinases and bone. Bone 2008;43:7-18

[23] McNamara LM, Majeska RJ, Weinbaum S, Friedrich V, Schaffler MB. Attachment of osteocyte cell processes to the bone matrix. Anat Rec (Hoboken) 2009;292(3):355-63.

[24] Sternlicht MD, Werb Z. How matrix metalloproteinases regulate cell behavior. Annu Rev Cell Dev Biol 2001;17:463-516

[25] Cowles EA, DeRome ME, Pastizzo G, Brailey LL, Gronowicz GA. Mineralization and the expression of matrix proteins during in vivo bone development. Calcif Tissue Int 1998; 62:74-82

[26] Shibata S, Baba O, Oda T, Yokohama-Tamaki T, Qin C, Butler WT, Sakakura Y, Takano Y. An immunohistochemical and ultrastructural study of the pericellular matrix of uneroded hypertrophic chondrocytes in the mandibular condyle of aged c-src-deficient mice. Arch Oral Biol 2008; 53:220-30

[27] Aiken A, Khokha R. Unraveling metalloproteinase function in skeletal biology and disease using genetically altered mice. Biochim Biophys Acta 2010; 1803:121-32

[28] Inoue K, Mikuni-Takagaki Y, Oikawa K, Itoh T, Inada M, Noguchi T, Park JS, Onodera T, Krane SM, Noda M, Itohara S.A crucial role for matrix metalloproteinase 2 in osteocytic canalicular formation and bone metabolism. J Biol Chem 2006;281:33814-24

[29] Mansell JP, Tarlton JF, Bailey AJ. Expression of gelatinases within the trabecular bone compartment of ovariectomized and parathyroidectomized adult female rats. Bone 1997; 20(6):533-8

[30] Guo LJ, Luo XH, Wu XP, Shan PF, Zhang H, Cao XZ, Xie H, Liao EY. Serum concentrations of MMP-1, MMP-2, and TIMP-1 in Chinese women: age-related changes, and the relationships with bone biochemical markers, bone mineral density. Clin Chim Acta 2006;371:137-42

[31] Whitelock JM, Murdoch AD, Iozzo RV, Underwood PA. The degradation of human endothelial cell-derived perlecan and release of bound basic fibroblast growth factor by stromelysin, collagenase, plasmin, and heparanases. J Biol Chem 1996;26;271:10079-86

[32] Bord S, Horner A, Hembry RM, Compston JE. Stromelysin-1 (MMP-3) and stromelysin-2 (MMP-10) expression in developing human bone: potential roles in skeletal development. Bone 1998;23:7-12

[33] Breckon JJ, Papaioannou S, Kon LW, Tumber A, Hembry RM, Murphy G, Reynolds JJ, Meikle MC. Stromelysin (MMP-3) synthesis is up-regulated in estrogen-deficient mouse osteoblasts in vivo and in vitro. J Bone Miner Res 1999;14:1880-90

[34] Frost HM, Jee WS. On the rat model of human osteopenias and osteoporoses. Bone Miner 1992;18:227-36

[35] Wronski TJ, Dann LM, Scott KS, Cintron M. Long-term effects of ovariectomy and aging on the rat skeleton. Calcif Tissue Int 1989;45:360-6

[36] Erben RG. Trabecular and endocortical bone surfaces in the rat: modeling or remodeling? Anat Rec 1996;246:39-46

[37] Turner RT. Cancellous bone turnover in growing rats: time-dependent changes in association between calcein label and osteoblasts. J Bone Miner Res 1994;9:1419-24

[38] Wronski TJ, Cintrón M, Dann LM. Temporal relationship between bone loss and increased bone turnover in ovariectomized rats. Calcif Tissue Int 1988;43(3):179-83

[39] Denault, JB and GS. Salvesen. Apoptotic caspase activation and activity. Methods Mol Biol 2008; 414: 191-220

[40] Wronski TJ, Cintrón M, Dann LM. Temporal relationship between bone loss and increased bone turnover in ovariectomized rats. Calcif Tissue Int 1988;43(3):179-83

[41] Vinatier D, Dufour P, Subtil D. Apoptosis: a programmed cell death involved in ovarian and uterine physiology. Eur J Obstet Gynecol Reprod Biol 1996;67(2):85-102

[42] Verborgt O, Gibson GJ, Schaffler MB. Loss of osteocyte integrity in association with microdamage and bone remodeling after fatigue in vivo. J Bone Miner Res 2000; 15(1): 60-7

[43] Hedgecock NL, Hadi T, Chen AA, Curtiss SB, Martin RB, Hazelwood SJ. Quantitative regional associations between remodeling, modeling, and osteocyte apoptosis and density in rabbit tibial midshafts. Bone 2007;40(3):627–37

[44] Noble BS, Stevens H, Loveridge N, Reeve J. Identification of apoptotic changes in osteocytes in normal and pathological human bone. Bone 1997;20(3):273-82

[45] Schöneich C. Reactive oxygen species and biological aging: a mechanistic approach. Exp Gerontol 1999;34(1):19-34

[46] Grassi F, Tell G, Robbie-Ryan M, Gao Y, Terauchi M, Yang X, Romanello M, Jones DP, Weitzmann MN, Pacifici R. Oxidative stress causes bone loss in estrogen deficient mice through enhanced bone marrow dendritic cell activation. Proc Natl Acad Sci U S A 2007; 104(38): 15087-92

[47] Kanda N, Watanabe S. 17beta-estradiol inhibits oxidative stress-induced apoptosis in keratinocytes by promoting Bcl-2 expression. J Invest Dermatol 2003;121(6):1500-9

[48] Ott SR. Confocal microscopy in large insect brains: zinc-formaldehyde fixation improves synapsin immunostaining and preservation of morphology in whole-mounts. J Neurosci Methods 2008;172:220-30

[49] Tang S, Herber RP, Ho S, Alliston T. Matrix metalloproteinase-13 is required for osteocytic perilacunar remodeling and maintains bone fracture resistance. J Bone Miner Res 2012, doi: 10.1002/jbmr.1646

[50] Kulkarni RN, Bakker AD, Gruber EV, Chae TD, Veldkamp JB, Klein-Nulend J, Everts V. MT1-MMP modulates the mechanosensitivity of osteocytes. Biochem Biophys Res Commun 2012;417(2):824-9

[51] Ren XH, Peng XD, Wu XP, Liao EY, Sun ZQ. Association between serum soluble membrane type matrix metalloproteinase-1 (MT1-MMP) levels and bone mineral density, and biochemical markers in postmenopausal women. Clin Chim Acta 2008;390:44-8

[52] Liao EY, Liao HJ, Guo LJ, Zhou HD, Wu XP, Dai RC, Luo XH. Membrane-type matrix metalloproteinase-1 (MT1-MMP) is down-regulated in estrogen-deficient rat osteoblast in vivo. J Endocrinol Invest 2004;27:1-5

CHAPTER 4

[1] Kanis JA. Diagnosis of osteoporosis and assessment of fracture risk. Lancet. 2002; 359 (9321):1929-36

[2] Riggs BL, Khosla S, Melton LJ 3rd. Sex steroids and the construction and conservation of the adult skeleton. Endocr Rev 2002;23(3):279-302

[3] Davison KS, Siminoski K, Adachi JD, Hanley DA, Goltzman D, Hodsman AB, Josse R, Kaiser S, Olszynski WP, Papaioannou A, Ste-Marie LG, Kendler DL, Tenenhouse A, Brown JP. Bone strength: the whole is greater than the sum of its parts. Semin Arthritis Rheum 2006;36(1):22-31

[4] Turner CH. Biomechanics of bone: determinants of skeletal fragility and bone quality. Osteoporos Int 2002;13(2):97-104

[5] Tommasini SM, Trinward A, Acerbo AS, De Carlo F, Miller LM, Judex S. Changes in intracortical microporosities induced by pharmaceutical treatment ofosteoporosis as detected by high resolution micro-CT. Bone 2012;50(3):596-604

[6] Bagi CM, Miller SC. Comparison of osteopenic changes in cancellous bone induced by ovariectomy and/or immobilization in adult rats. Anat Rec 1994;239:243-54

[7] Bono CM, Einhorn TA.Overview of osteoporosis: pathophysiology and determinants of bone strength. Eur Spine J 2003;12 Suppl 2:S90-6

[8] Sharma D, Ciani C, Ramirez Marin PA, Levy JD, Doty SB, Fritton SP. Alterations in the osteocyte lacunar-canalicular microenvironment due to ovariectomy Bone 2012, doi:10.1016/j.bone.2012.05.014

[9] Wronski TJ, Lowry PL, Walsh CC, Ignaszewski LA. Skeletal alterations in ovariectomized rats. Calcif Tissue Int 1985;37:324-8

[10] Wronski TJ, Dann LM, Scott KS, Cintron M. Long-term effects of ovariectomy and aging on the rat skeleton. Calcif Tissue Int 1989;45:360-6

[11] Iwamoto J, Seki A, Takeda T, Sato Y, Yamada H, Yeh JK. Therapeutic effect of risedronate on cancellous and cortical bone in ovariectomized osteopenic rats: a comparison with the effects of alfacalcidol. Exp Anim 2006;55(4):333-42

[12] Turner RT, Vandersteenhoven JJ, Bell NH. The effects of ovariectomy and 17 beta-estradiol on cortical bonehistomorphometry in growing rats. J Bone Miner Res 1987;2(2):115-22

[13] Lips P. Vitamin D deficiency and secondary hyperparathyroidism in the elderly: consequences for bone loss and fractures and therapeutic implications. Endocr Rev 2001;22(4):477-501

[14] Mulder L, Koolstra JH, den Toonder JM, van Eijden TM. Relationship between tissue stiffness and degree of mineralization of developing trabecular bone. J Biomed Mater Res A 2008;84(2):508-15

[15] Rho JY, Roy ME 2nd, Tsui TY, Pharr GM. Elastic properties of microstructural components of human bone tissue as measured by nanoindentation. J Biomed Mater Res 1999;45(1):48-54

[16] Oliver WC, Pharr GM. On the generality of the relationship among contact stiffness, contact area, and elastic modulus during indentation. J Mater Res 1992;7(3), 613-661

[17] Hoc T, Henry L, Verdier M, Aubry D, Sedel L, Meunier A.Effect of microstructure on the mechanical properties of Haversian cortical bone. Bone 2006;38(4):466-74

[18] Fan Z, Swadener JG, Rho JY, Roy ME, Pharr GM. Anisotropic properties of human tibial cortical bone as measured by nanoindentation. J Orthop Res 2002;20(4):806-10

[19] Zysset PK, Guo XE, Hoffler CE, Moore KE, Goldstein SA. Elastic modulus and hardness of cortical and trabecular bone lamellae measured by nanoindentation in the human femur. J Biomech 1999;32(10):1005-12

[20] Brennan O, Kennedy OD, Lee TC, Rackard SM, O'Brien FJ. Biomechanical properties across trabeculae from the proximal femur of normal and ovariectomised sheep. J Biomech 2009;42(4):498-503

[21] Norman J, Shapter JG, Short K, Smith LJ, Fazzalari NL. Micromechanical properties of human trabecular bone: a hierarchical investigation using nanoindentation.J Biomed Mater Res A 2008;87(1):196-202

[22] Lewis G, Nyman JS. The use of nanoindentation for characterizing the properties of mineralized hard tissues: state-of-the art review. J Biomed Mater Res B Appl Biomater 2008;87(1):286-301

[23] Rubin MA, Jasiuk I, Taylor J, Rubin J, Ganey T, Apkarian RP. TEM analysis of the nanostructure of normal and osteoporotic human trabecular bone. Bone 2003;33(3):270-82

[24] Rubin MA, Jasiuk I. The TEM characterization of the lamellar structure of osteoporotic human trabecular bone. Micron. 2005;36(7-8):653-64

[25] Suvorova EI, Petrenko PP, Buffat PA. Scanning and transmission electron microscopy for evaluation of order/disorder in bone structure. Scanning 2007;29(4):162-70

[26] Fratzl-Zelman N, Roschger P, Gourrier A, Weber M, Misof BM, Loveridge N, Reeve J, Klaushofer K, Fratzl P. Combination of nanoindentation and quantitative backscattered electron imaging revealed altered bone material properties associated with femoral neck fragility. Calcif Tissue Int. 2009;85(4):335-43

[27] Wang X, Sudhaker Rao D, Ajdelsztajn L, Ciarelli TE, Lavernia EJ, Fyhrie DP. Human iliac crest cancellous bone elastic modulus and hardness differ with bone formation rate per bone surface but not by existence of prevalent vertebral fracture. J Biomed Mater Res B Appl Biomater. 2008;85(1):68-77

[28] Lane NE, Yao W, Kinney JH, Modin G, Balooch M, Wronski TJ. Both hPTH(1-34) and bFGF increase trabecular bone mass in osteopenic rats but they have different effects on trabecular bone architecture. J Bone Miner Res 2003;18(12):2105-15

[29] Guo XE, Goldstein SA. Vertebral trabecular bone microscopic tissue elastic modulus and hardness do not change in ovariectomized rats. J Orthop Res 2000;18(2):333-6

[30] Frost HM, Jee WS. On the rat model of human osteopenias and osteoporoses. Bone Miner 1992;18:227-36

[31] Turner RT. Cancellous bone turnover in growing rats: time-dependent changes in association between calcein label and osteoblasts. J Bone Miner Res 1994;9:1419-24

[32] Hodsman AB, Kiesel M, Fraher LJ, Watson PH, Stitt LW. Comparison of the response of pelvic and proximal tibial cancellous bone in rat to ovariectomy with estrogen replacement. Bone 1998;23:267-74

[33] Kalu DN. The ovariectomized rat model of postmenopausal bone loss. Bone Miner 1991;15:175-91

[34] van der Linden JC, Birkenhäger-Frenkel DH, Verhaar JA, Weinans H. Trabecular bone's mechanical properties are affected by its non-uniform mineraldistribution. J Biomech 2001; 34(12):1573-80

[35] Burket J, Gourion-Arsiquaud S, Havill LM, Baker SP, Boskey AL, van der Meulen MC. Microstructure and nanomechanical properties in osteons relate to tissue and animal age. J Biomech 2011;44(2):277-84

[36] Donnelly E, Baker SP, Boskey AL, van der Meulen MC. Effects of surface roughness and maximum load on the mechanical properties of cancellous bone measured by nanoindentation. J Biomed Mater Res A 2006;77(2):426-35

[37] Hengsberger S, Ammann P, Legros B, Rizzoli R, Zysset P. Intrinsic bone tissue properties in adult rat vertebrae: modulation by dietary protein. Bone 2005;36(1):134-41

[38] Qing H, Ardeshirpour L, Pajevic PD, Dusevich V, Jähn K, Kato S, Wysolmerski J, Bonewald LF. Demonstration of osteocytic perilacunar/canalicular remodeling in mice during lactation. J Bone Miner Res 2012, doi: 10.1002/jbmr.1567

[39] Belanger LF. Osteocytic osteolysis. Calcif Tissue Res 1969;4:1-12

[40] Ash SL, Goldin BR. Effects of age and estrogen on renal vitamin D metabolism in the female rat. Am J Clin Nutr 1988;47(4):694-9

[41] Caniggia A, Gennari C, Bianchi V, Guiedri R. Intestinal absorption of 45Ca in senile osteoporosis. Acta Med Scand 1963;173:613-7

CHAPTER 5

[1] Kalu DN. The ovariectomized rat model of postmenopausal bone loss. Bone Miner 1991;15:175-91

[2] Thompson DD, Simmons HA, Pirie CM, Ke HZ. FDA Guidelines and animal models for osteoporosis. Bone 1995;17:125S-133S

[3] Wronski TJ, Dann LM, Scott KS, Cintron M. Long-term effects of ovariectomy and aging on the rat skeleton. Calcif Tissue Int 1989;45:360-6

[4] McNamara LM, Majeska RJ, Weinbaum S, Friedrich V, Schaffler MB. Attachment of osteocyte cell processes to the bone matrix. Anat Rec (Hoboken) 2009;292:355-63

[5] Wang L, Ciani C, Doty SB, Fritton SP. Delineating bone's interstitial fluid pathway in vivo. Bone 2004;34(3):499-509

[6] Aiken A, Khokha R. Unraveling metalloproteinase function in skeletal biology and disease using genetically altered mice. Biochim Biophys Acta 2010;1803(1):121-32

[7] Inoue K, Mikuni-Takagaki Y, Oikawa K, Itoh T, Inada M, Noguchi T, Park JS, Onodera T, Krane SM, Noda M, Itohara S. A crucial role for matrix metalloproteinase 2 in osteocytic canalicular formation and bone metabolism. J Biol Chem 2006;281(44):33814-24

[8] Tang S, Herber RP, Ho S, Alliston T. Matrix metalloproteinase-13 is required for osteocytic perilacunar remodeling and maintains bone fracture resistance. J Bone Miner Res 2012, doi: 10.1002/jbmr.1646

[9] Kulkarni RN, Bakker AD, Gruber EV, Chae TD, Veldkamp JB, Klein-Nulend J, Everts V. MT1-MMP modulates the mechanosensitivity of osteocytes. Biochem Biophys Res Commun 2012;417(2):824-9

[10] Sone S, Nakamura M, Maruya Y, Takahashi I, Mizoguchi I, Mayanagi H, Sasano Y. Expression of versican and ADAMTS during rat tooth eruption. J Mol Histol 2005;36(4): 281-8

[11] Sannes PL, Schofield BH, McDonald DF. Histochemical localization of cathepsin B, dipeptidyl peptidase I, and dipeptidyl peptidase II in rat bone. J Histochem Cytochem 1986; 34(8):983-8

[12] Ferris BD, Klenerman L, Dodds RA, Bitensky L, Chayen J. Altered organization of non-collagenous bone matrix in osteoporosis. Bone 1987; 8(5):285-8

[13] Thompson WR, Modla S, Grindel BJ, Czymmek KJ, Kirn-Safran CB, Wang L, Duncan RL, Farach-Carson MC. Perlecan/Hspg2 deficiency alters the pericellular space of the lacunocanalicular system surrounding osteocytic processes in cortical bone. J Bone Miner Res 201;26:618-29

[14] Ubaidus S, Li M, Sultana S, de Freitas PH, Oda K, Maeda T, Takagi R, Amizuka N. FGF23 is mainly synthesized by osteocytes in the regularly distributed osteocytic lacunar-canalicular system established after physiological bone remodeling. J Electron Microsc (Tokyo) 2009;58(6):381-92

[15] Ash SL, Goldin BR. Effects of age and estrogen on renal vitamin D metabolism in the female rat. Am J Clin Nutr 1988;47(4):694-9

[16] Caniggia A, Gennari C, Bianchi V, Guiedri R. Intestinal absorption of 45Ca in senile osteoporosis. Acta Med Scand 1963;173:613-7